Martin-CR-65-41 Copy No. 3

CONTRACT NO. NAS8-11794

MS-I

EXPLOSIVE FORMING OF 2219 ALUMINUM

FINAL REPORT

JUNE 1965

PREPARED FOR

NATIONAL AERONAUTICS AND SPACE ADMINISTRATION
GEORGE C. MARSHALL SPACE FLIGHT CENTER
HUNTSVILLE, ALABAMA

PREPARED BY

MARTIN COMPANY
DENVER DIVISION
DENVER, COLORADO

Martin-CR-65-41

Copy No. 19

Contract NAS8-11794

EXPLOSIVE FORMING OF 2219 ALUMINUM
FINAL REPORT

June 1965

Authors

J. T. Snyder
K. R. Agricola
H. M. Otte
L. I. Van Torne
R. I. Adler

Approved

A. A. Ezra

Dr. A. A. Ezra, Manager
Aeromechanics and Materials Research Laboratory

MARTIN COMPANY
Denver, Colorado
Aerospace Division of Martin-Marietta Corporation

FOREWORD

This report summarizes the technical work accomplished under National Aeronautics and Space Administration Contract NAS8-11794. The program was sponsored by the Manufacturing Engineering Division of the Marshall Space Flight Center, Huntsville, Alabama, with Mr. Manly Tommie serving as the contract monitor.

The contract objectives were the study of processing parameters as they influence metal springback during the explosive forming of 2219 aluminum alloy and the study of the influence of high energy rate deformation on the metallurgical behavior of 2219 aluminum. The metallurgical aspects of the program consisting primarily of electron transmission microscopy and x-ray diffraction studies were accomplished by the Orlando Division of the Martin Company under the direction of Dr. H. M. Otte.

CONTENTS

Figure

SUMMARY

A technical program was completed under the sponsorship of the National Aeronautics and Space Administration, Huntsville, Alabama in which the parameters affecting metal springback of 2219 sheet and plate during explosive forming of 1/5-scale gore segments were studied. In addition, x-ray diffraction, optical microscopy, and electron microscopy techniques were used to study metallurgical changes occuring as a result of the high energy deformation. The analytical techniques were augmented by mechanical property evaluation.

Sheet explosive was found to be superior to either bulk Cyadyn 3 or PETN in producing more uniform properties with attendant low springback. The optimum explosive standoff from the viewpoint of uniform properties and lowest springback was found to be 3.54 inches (L/D ratio of 0.142 where D equals the blank width and L is the distance from the explosive to the blank surface).

Although a low amount of springback was achieved with 2219-T42, it was not possible to obtain uniform properties across the part through the use of explosive deformation. Therefore, 2219-T31 or 2219-T351 was selected as the optimum temper for study since the material exhibited low springback with attendant uniform mechanical properties.

Springback was found to increase with decreasing thickness of 2219-T31. Lubrication of the draw radius before forming also caused an increase in metal springback.

There was little influence of die material, draw radius, or draw depth on the reduction of springback.

An evaluation of an integral blanket concept for the reduction of springback did not result in conclusive evidence. Limited preliminary data could not be adequately verified due to insufficient time and funding.

Multiple forming operations appear to significantly reduce springback when compared to a single operation.

The 2219-T37 material did not respond to heat treatment after explosive forming because of internal energy changes caused by the high energy deformation. It was found that accelerated aging by a factor of 0.5 resulted from explosive forming. Similar behavior was observed for 2219-T42 and 2219-T31 where aging times of 0.9 and 0.7 of normal heat treating times were indicated to achieve maximum mechanical properties.

Explosive forming introduces high concentrations of dislocations and an excess concentration of vacancies produced by stress-induced climb of jogs on screw dislocations. Crystallographic imperfections such as stacking faults, micro and macroscopic twins, and microcracks were not observed.

Explosive forming reduces the residual stresses present in as-received material as shown by x-ray diffraction and causes a significant reduction in lattice parameters.

I. INTRODUCTION AND BACKGROUND

A. SPRINGBACK

Metal springback is an ever-present problem in the fabrication of sheet metal components. Springback is the tendency of a part to return to its original shape after bending. In general, it can be reduced by decreasing the yield strength or increasing the amount of plastic deformation. The following techniques have been used successfully: elevating the temperature during fabrication, using thick blanks, or drawing the part deeper. Problems encountered during the explosive forming of full-scale Saturn SIC gore segments by a NASA contractor (Ref 1) prompted the NASA to instigate a research program to study the variables governing metal springback during explosive deformation and the influence of high energy forming on metallurgical behavior.

There is not a great deal of data in the literature regarding control of springback. Several studies have been made relative to the problem of compensating for springback (Ref 2 thru 4) but the accurate prediction of springback is very difficult because of inherent variations in metal behavior and forming conditions for any given process (Ref 2). In conventional forming, springback has been found to depend on the following (Ref 5 thru 8):

1) Kind of material formed;

2) Temper of material formed;

3) Sheet thickness;

4) Size of the inner bend radius;

5) Tolerances and alignment used;

6) Friction between die and part;

7) Pressure exerted during forming;

8) Contour of the part;

9) Forming parameters used.

It has been shown (Ref 9) that less springback occurs with materials of lower yield strength than with materials of higher yield strength. For the same yield strength and amount of deformation, a material possessing a high modulus of elasticity will plastically deform a greater extent than a material having a low modulus of elasticity.

In explosive forming, reduced and sometimes nonexistent springback has been reported (Ref 10 thru 14). This has been explained by Beyer (Ref 13) as being a result of proper charge placement and by Wood (Ref 15) as a result of critical forming pressures. Depending on the material, these pressures were on the order of 40 to 50,000 psi. Below this pressure range, increased springback was observed. Henriksen (Ref 16), in contrast to the above results, found that considerable springback can occur after explosive forming and learned during his studies that maximum stresses occur in flanges or in regions of a part where large variations in curvature exist.

It was the purpose of this study to determine the separate influences of explosive forming parameters on the resulting springback of 2219 aluminum with the objective of establishing forming conditions whereby metal springback can be minimized or eliminated.

B. METALLURGICAL CONSIDERATIONS

As a result of explosive deformation and/or hardening, significant metallurgical changes can be effected. Published information shows that a great deal of effort has been spent on the study of iron-based alloys. It has been found that H-11 and 25% Ni steel respond to explosive shocking with increases in tensile and yield strengths (Ref 17). The explosively shocked 25% Ni steel was shown to raise the strength after aging approximately equivalent to the strength produced after cold rolling to 50% cold reduction. The strengths of both alloys increased with shock pressure. Microstructural changes were not evident from optical and electron microscopy observations to magnifications of 20000X.

Some insight into the strengthening mechanisms of iron-based alloys was gained under an Air Force sponsored program (Ref 18). It was learned that shocked pearlitic steels showed appreciable hardening only when free ferrite was present. Martensitic steels were not strengthened to the degree that the pearlitic steels were

for the same shock intensity. Austenitic stainless steels such as 302 shock hardened with the formation of bcc martensite and hcp martensite. In age hardening stainless steels; i.e., A286, shocked specimens were found to age in less time and to higher hardnesses than did unshocked material. In addition to strengthening effects, phase transformations have also been observed after explosive shocking of iron-based alloys (Ref 19).

Some metallurgical studies have been conducted on light alloys such as aluminum and titanium. The results obtained depend primarily on the particular alloy being formed. For example, it has been observed that little influence of explosive deformation results from explosive forming 2014 aluminum (Ref 20) while explosive forming of 2219 aluminum produces significant changes in mechanical properties (Ref 21). Ti-13V-11Cr-3Aℓ exhibits increased susceptibility to aging approximately on the same order of magnitude as that produced by a 10% reduction by cold rolling (Ref 22). We have observed during the explosive forming of Ti-6Aℓ-4V that little change in hardness or strength results from deep drawing the material using sandwich forming techniques (Ref 23).

It was of interest in the study of the explosive forming of 2219 aluminum to evaluate the resulting changes in the mechanical and structural behavior of the alloy. Therefore, macroscopic properties were studied using conventional testing techniques and optical microscopy. To permit an evaluation of structural variations occurring from explosive deformation, transmission electron microscopy, and x-ray diffraction techniques were used to permit a comparison between material changes and observed springback, which aided in an understanding of the details. In addition, mechanical evaluation was necessary to establish whether enough metal stretching was occurring to modify the alloy strength to the extent that subsequent aging resulted in full design properties.

II. EXPERIMENTAL PROCEDURE

A. MATERIAL

1. Mechanical Properties

Four different starting tempers of 2219 aluminum alloy were evaluated in this program. Table 1 shows minimum mechanical properties as established by Martin Material Specification 1117*. The mechanical properties (before forming) of the material received from the National Aeronautics and Space Administration (NASA) are given in Table 2 and vary somewhat from the values in Table 1. The four starting tempers of 2219 aluminum alloy were 0 or annealed, T42, T351, and T37. The best starting temper was determined using 0.250-in. thick material. The properties of the 2219 aluminum alloy in the annealed and T42 tempers before forming show the greatest deviation from the standard values in Table 1. These materials had been annealed and the T42 material treated by NASA after delivery from the mill. The ultimate tensile strength of the annealed material averaged 3000 psi below specification minima and the tensile yield strength of the 2219-T42 material showed a spread of 7500 psi. The annealed material did not respond to solution heat treating and aging. The properties after heat treating (before forming) showed an ultimate tensile strength 6500 psi below minimum and a yield strength 8000 psi below minima in Table 1. The 2219-T42 after aging was 3500 psi below minimum in tensile strength and 6000 psi low in yield strength as can be seen in Table 2. The as-received properties exhibited by the 2219-T351 and 2219-T37 materials were much more consistent from sheet to sheet. Both of these materials responded to the required aging cycle. However, the 2219-T351 alloy was marginal in response.

2. Chemical Composition

The copper content of this alloy is close to the maximum limits for solid solubility of copper (between 5.7 and 6.3% depending on the phase diagram referred to), whereas most other commercial high strength aluminum alloys contain from 2 to 5% copper. Because of the saturation limit of copper in aluminum, structural changes occur during explosive forming. In addition to normal hardening that occurs by second phase precipitation of $CuA\ell_2$, the 2219 alloy is susceptible to additional hardening by application of external stresses. Table 3 lists the composition of material used in this program.

*Mechanical properties listed equal or exceed those in military specifications MIL-A-8920 and MIL-E-6038.

Table 1 Martin Material Specification 1117

Temper	Tensile Strength (psi)	Yield Strength at .2% Offset (psi)	% Elongation in 2 in.
0	32,000	16,000	12
T42 (T4)	45,000	17,000	15
T31 (T351)	46,000	28,000	10
T37	49,000	38,000	6
T62 (T6)	54,000	36,000	6
T81	61,000	44,000	6
T851	61,000	44,000	6
T87 (0.020 to 0.039 in.)	61,000	50,000	5
T87 (0.040 to 2.0 in.)	63,000	50,000	5

Note: The properties are taken from MMS 1117. All values given are the minimum required by military and federal specifications.

Table 2 Mechanical Properties

Sheet No.	As-Received Properties				Properties After Heat Treating			
	Temper	Ultimate (psi)	Yield (psi)	% Elongation in 2 in.	Temper	Ultimate (psi)	Yield psi	% Elongation in 2 in.
1-0-C	0	29,200	13,300	23.5	T62			
2-0-C	0	29,400	12,800	24.0	T62			
3-0-C	0	28,600	14,400	23.5	T62			
4-0-C	0	29,000	14,000	24.0	T62			
5-0-C	0	29,000	14,000	23.5	T62	47,500*	28,000	12.5
6-0-C	0	29,200	12,800	23.5	T62			
1-42-C	T42	48,200	22,000	22.5	T62	50,500	29,200	11.5
2-42-C	T42	51,800	26,700	21.5	T62			
3-42-C	T42	49,500	19,200	22.5	T62			
4-42-C	T42	49,800	25,200	25.0	T62			
5-42-C	T42	50,200	25,000	24.0	T62			
6-42-C	T42	48,200	22,600	24.0	T62			
1-351-C	T351	55,800	41,900	21.0	T851			
2-351-C	T351	54,400	37,800	23.5	T851			
3-351-C	T351	55,300	42,800	24.0	T851			
4-351-C	T351	55,300	40,900	21.0	T851	61,200	43,200	12.5
5-351-C	T351	54,100	37,000	26.0	T851			
6-351-C	T351	55,600	40,600	21.0	T851			
1-37-C	T37	58,300	42,900	16.5	T87	65,400	52,000	10.5
2-37-C	T37	59,400	44,100	16.0	T87			
3-37-C	T37	58,900	44,300	15.0	T87			
4-37-C	T37	58,300	43,800	17.0	T87			
5-37-C	T37	58,600	43,400	15.5	T87			
6-37-C	T37	58,700	43,400	16.0	T87			
7-37-C	T37	58,900	42,900	17.5	T87			

Note: 1.* Solution heat treated at 995 ± 10°F and aged.
2. The table gives the mechanical properties of as-received and as-received and heat treated material from NASA before explosive forming.

Table 3 Typical Chemical Composition

Element	Content (%)
Copper	5.8 to 6.8
Silicon	0.20 max.
Manganese	0.20 to 0.40
Magnesium	**0.02 max.**
Iron	0.30 max.
Zinc	0.10 max.
Titanium	0.02 to 0.10
Vanadium	0.05 to 0.15
Zirconium	0.10 to 0.25
Other Elements	
Each	**0.05 max.**
Total	0.15 max.
Aluminum	**Remainder**

Note: This table represents the typical chemical composition of 2219 aluminum alloy as established by military and federal specifications in Martin Material Specification 1117.

3. Microstructure

The 2219 Aℓ sheet received from NASA was sampled for microstructural characteristics. Dark field micrographs (Fig. 1) of the 2219-0 material show typical longitudinal and transverse grain structures. The 2219-T42 material varied considerably in grain size from sheet to sheet (Fig. 2 and 3). The 2219-0 and 2219-T42 materials were warped in every sheet. The grain structures of the 2219-T37 material in Fig. 4A are typical of all sheets in the as-received material. The 2219-T351 material was very consistent in grain size from sheet to sheet. A typical transverse sampling is shown in Fig. 4B.

B. EXPLOSIVE FORMING DETAILS

1. Upper Gore Die

The upper gore die, from which most of the parametric data were obtained, is a 1/5-scale model of a section of a Saturn V bulkhead. The die is constructed of SF60 meehanite, a malleable cast iron. This die was developed for use on a previous contract (Ref 24). The design of this die was well suited to evaluating springback characteristics of 2219 aluminum because of its shallow shape. As Fig. 5 shows, only about 50% of the blank, which is roughly rectangular in shape (25 x 30 in.) is restrained by the clamping plates during forming. These factors tend to greatly accentuate springback making it possible to investigate parameters controlling spingback more precisely. These parameters will be discussed in detail in Chap. III of this report. Two types of charges were evaluated for forming characteristics.

a. Central Charge Arrangement

Two types of explosvies were evaluated utilizing a centrally located cylindrical shape. A dynamite-type explosive was selected to evaluate the effects of a relatively slow burning rate. The material used for this testing was Cyadyn 3, which is a 48% nitroglycerin dynamite with a burning speed of 7000 fps manufactured by American Cyanamid. High explosive (PETN) which has a burning speed of approximately 26,000 fps was also evaluated in the cylindrical shape. The use of two different types of explosives of the same geometrical shape made it possible to establish a charge equivalency by weight. The charges were packaged in cylindrical plastic vials constructed of clear styrene with a tight fitting polyethylene screw cap. A hole was punched in the lid so that

a number six electric blasting cap would fit tightly when inserted. This prevented water leakage when the die was submerged in the explosive forming pool. A cardboard or plastic standoff was used to locate the charge. Figure 6 shows the charge arrangement used to free form 1/5-scale dome caps. Gore part forming utilized the same setup.

b. Sheet Charge Arrangement

Sheet explosive was also evaluated in this program. Material used for performing these tests was "deta sheet c" manufactured by DuPont in thicknesses ranging from 0.025 to 0.050 in. Various thicknesses were used to produce the same blank coverage in square inches when charge requirements were varied with blank thickness and blank temper. The sheet explosive that contains 68% by weight of PETN was cut in rectangles of sizes dependent upon the alloy temper being formed to correspond with the rectangular shape of the blank. Various methods of blasting cap placement were investigated to determine the best method of sheet initiation. This was found to be center initiation using caps embedded in sheet explosive glued to the primary sheet charge. The sheet explosive was mounted on a sheet of plastic to insure rigidity of the charge during submersion of the die in the forming pool. A typical charge arrangement is illustrated in Fig. 7.

2. Lower Gore Die

This die, also constructed of SF60 meehanite, is similar in shape to the upper gore die. The die cavity, however, has a smaller radius of curvature and is, therefore, much deeper than the upper gore die. At the deepest point, that occurs at the vacuum hole, the lower gore die depth measures 4.66 in. as compared with 2.06 in. maximum depth for the upper gore die. The blank required for this die measures 32" x 32". A typical test setup with blank in place and die evacuated is depicted in Fig. 8.

3. Upper Gore Die with Inserts

The upper gore die was modified by the addition of shims to the clamping area of the die. Shims of two different thicknesses were used to investigate the effects of draw depth and die entrance radii when forming shallow shapes.

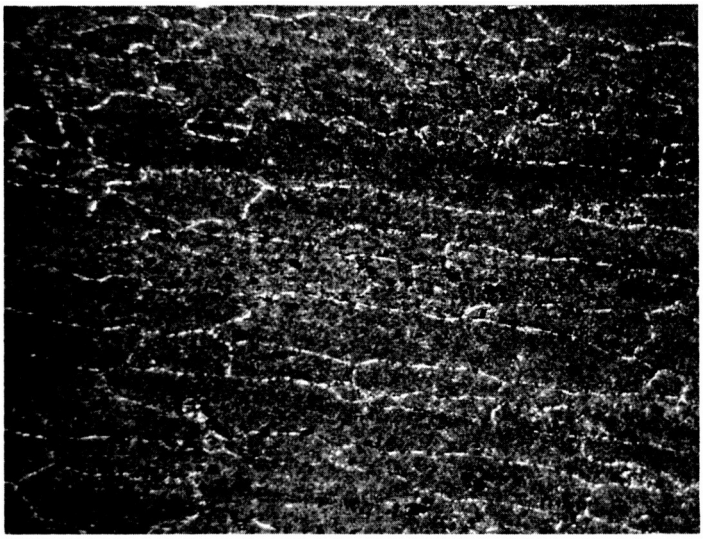

a. Longitudinal

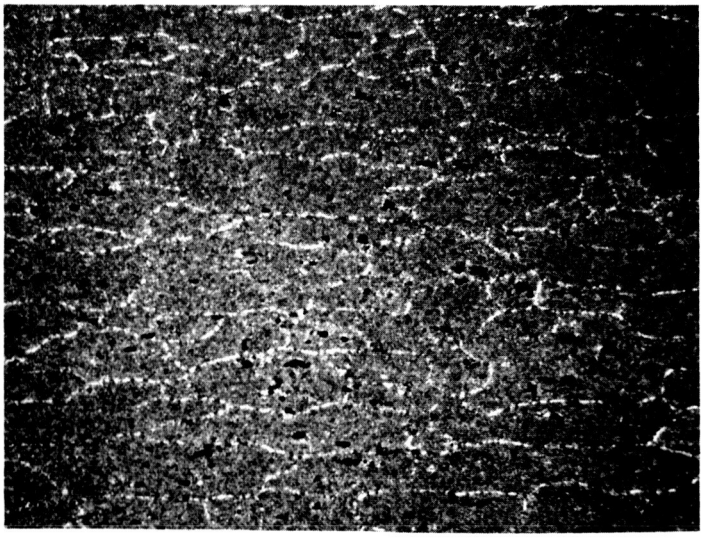

b. Transverse

Fig. 1 As-Received 2219-0 (200x micro)

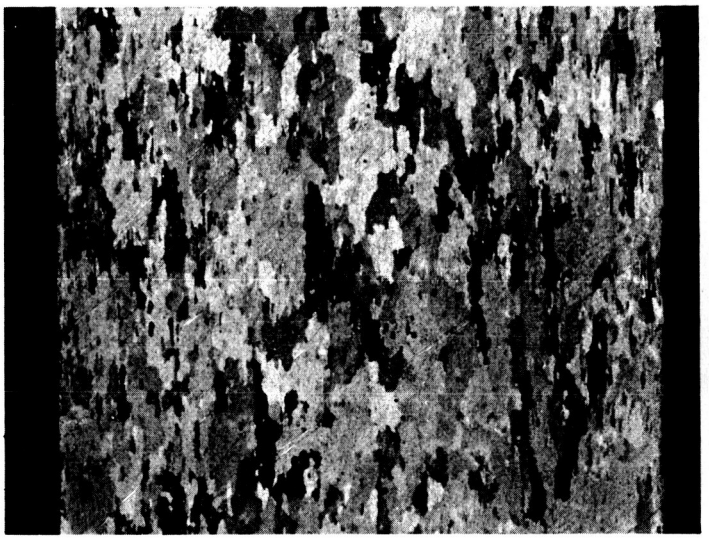

a. Specimen 3-42

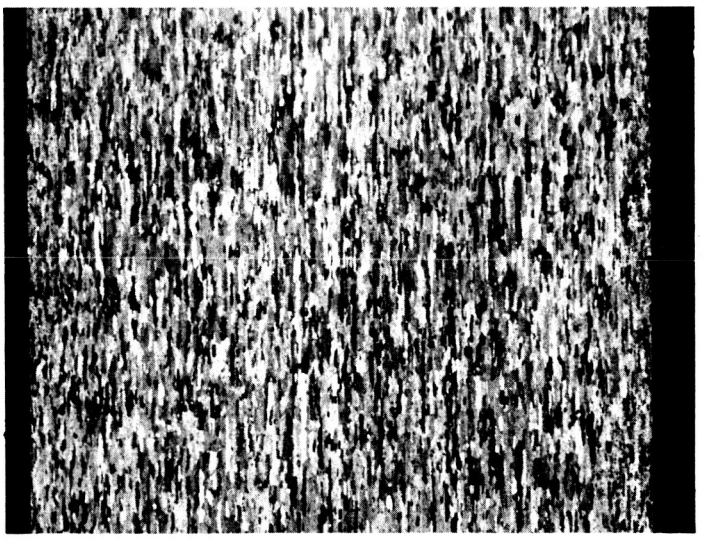

b. Specimen 4-42

Fig. 2 As-Received Longitudinal 2219-T42
(13x macro)

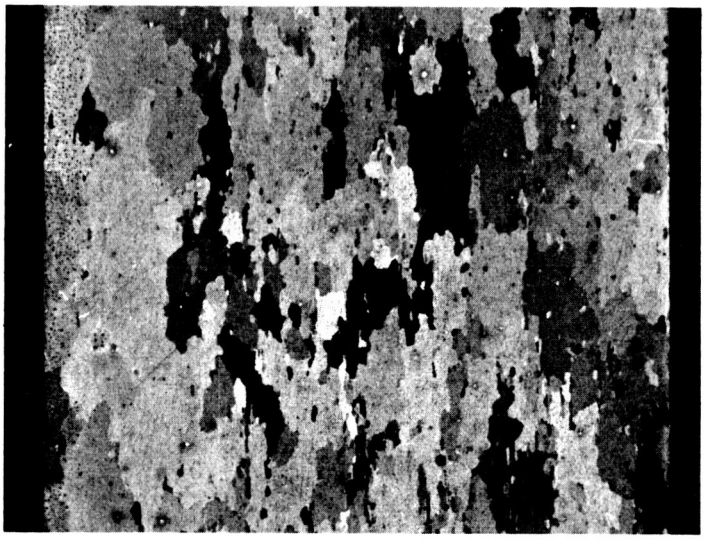

a. Specimen 5-42

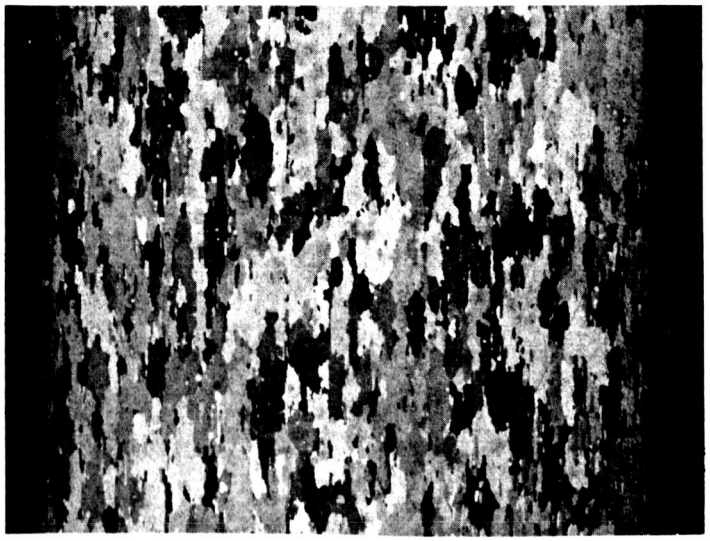

b. Specimen 6-42

Fig. 3 As-Received Longitudinal 2219-T42 (13x macro)

a. Specimen 4-37, Longitudinal 2219-T37

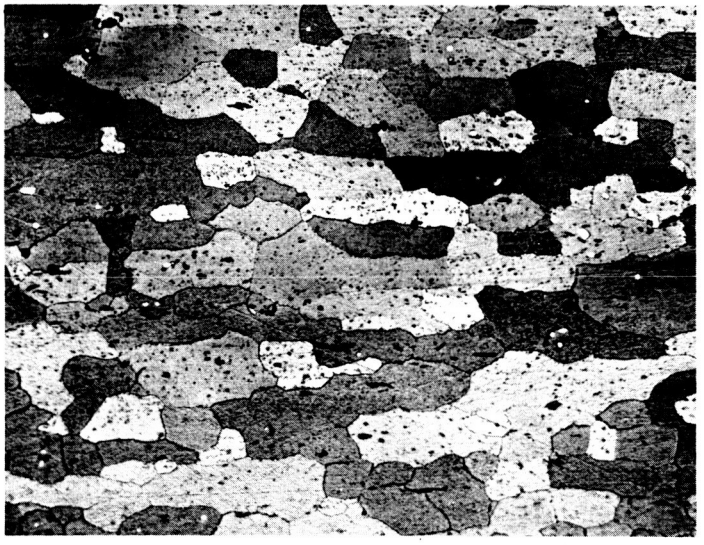

b. Specimen 1-351, Transverse 2219-T351

Fig. 4 As-Received Longitudinal 2219-T37 and Transverse 2219-T351 (200x micro)

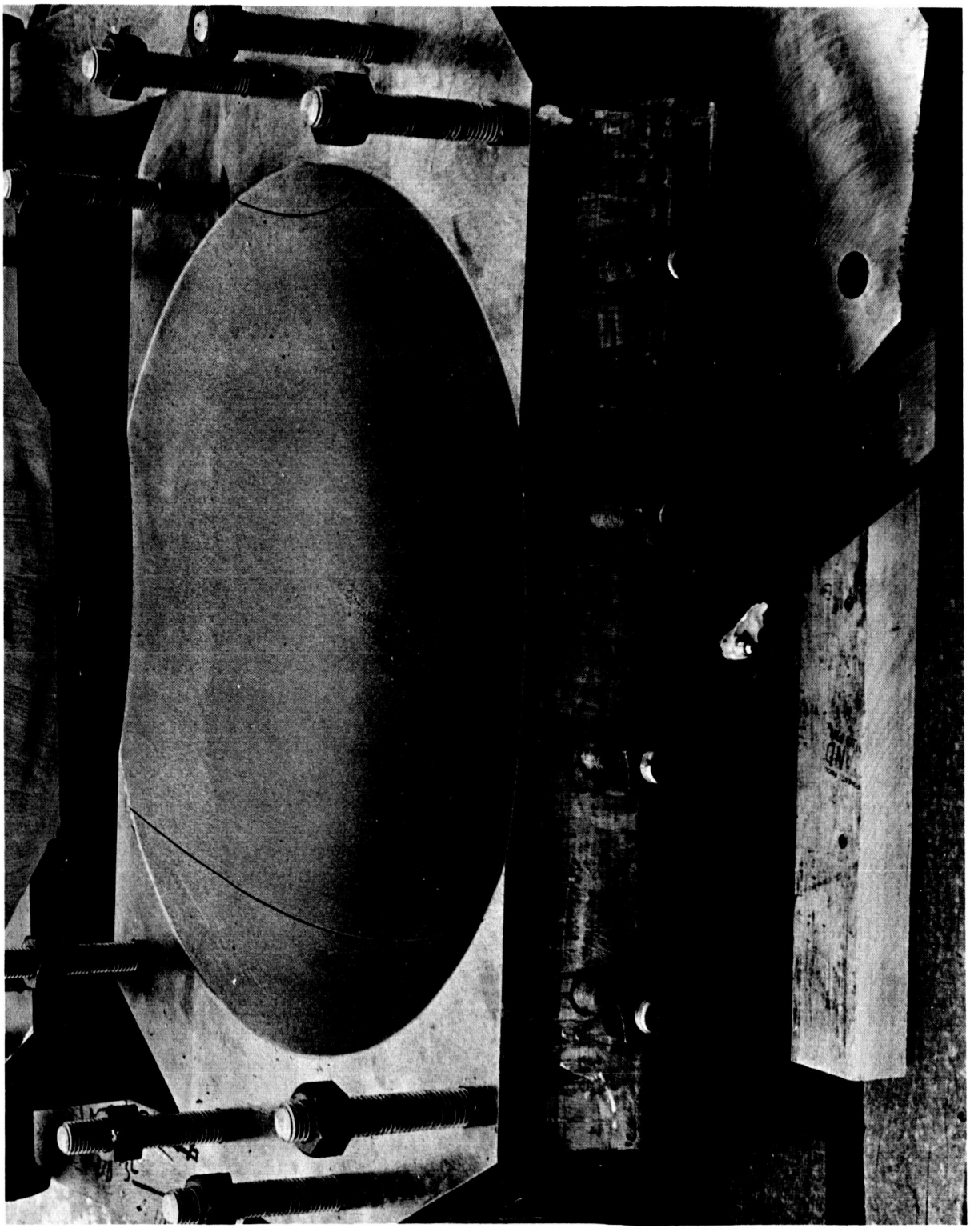

Fig. 5 Upper Gore Die for Forming Experiments

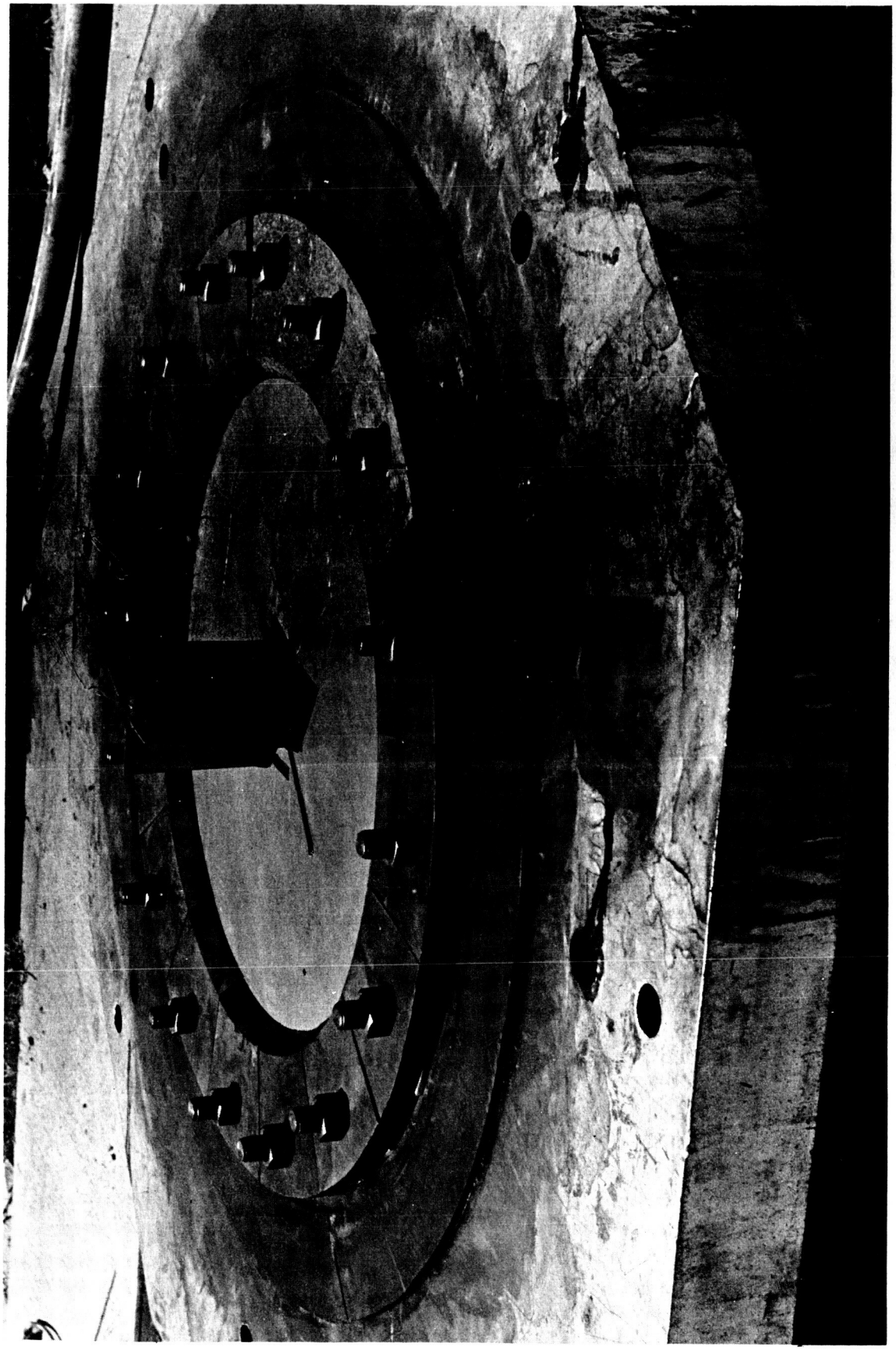

Fig. 6 Central Charge Arrangement for Free-Forming 1/5-Scale Dome Caps

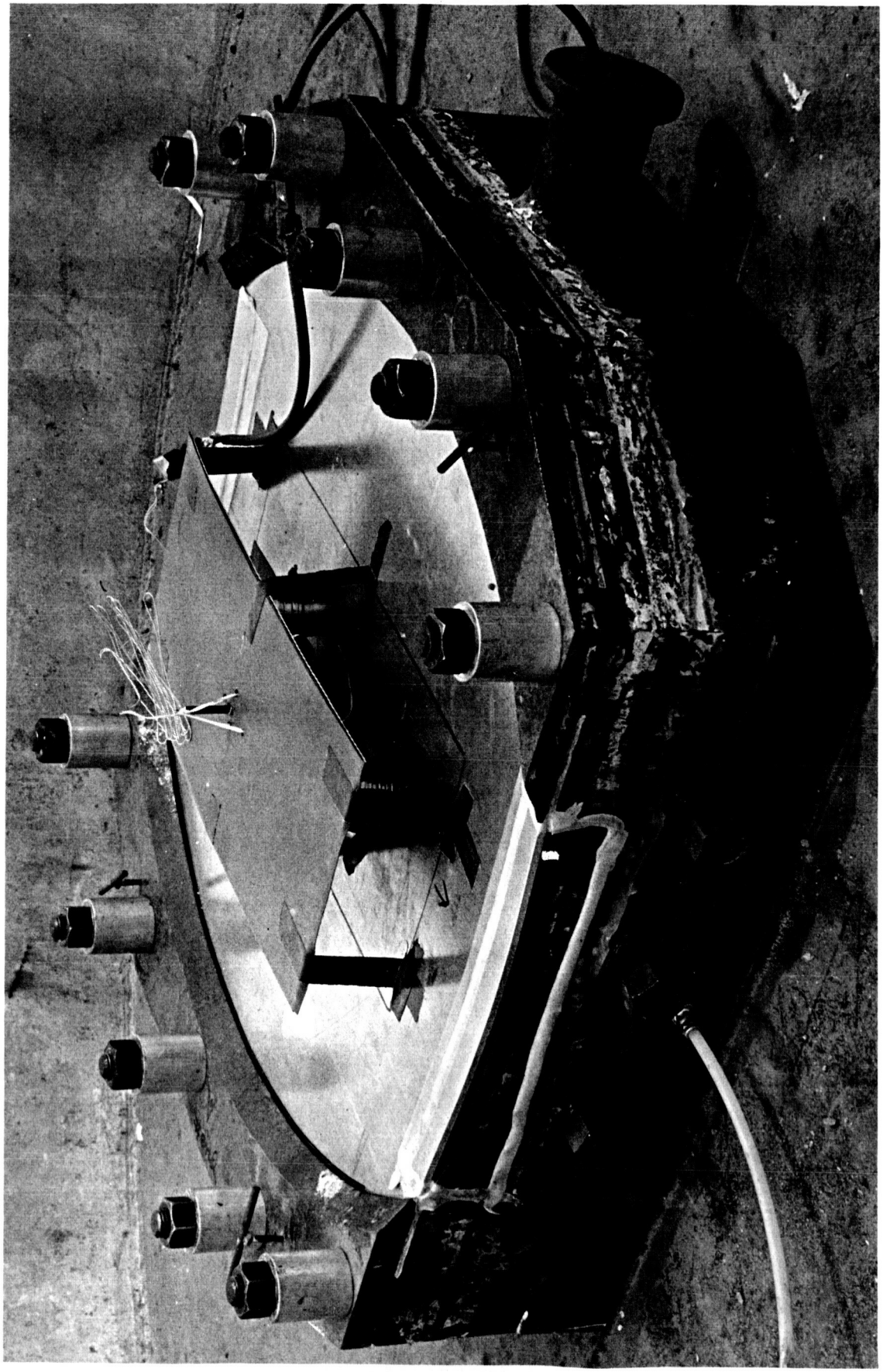

Fig. 7 Sheet Charge Arrangement for Gore Fabrication

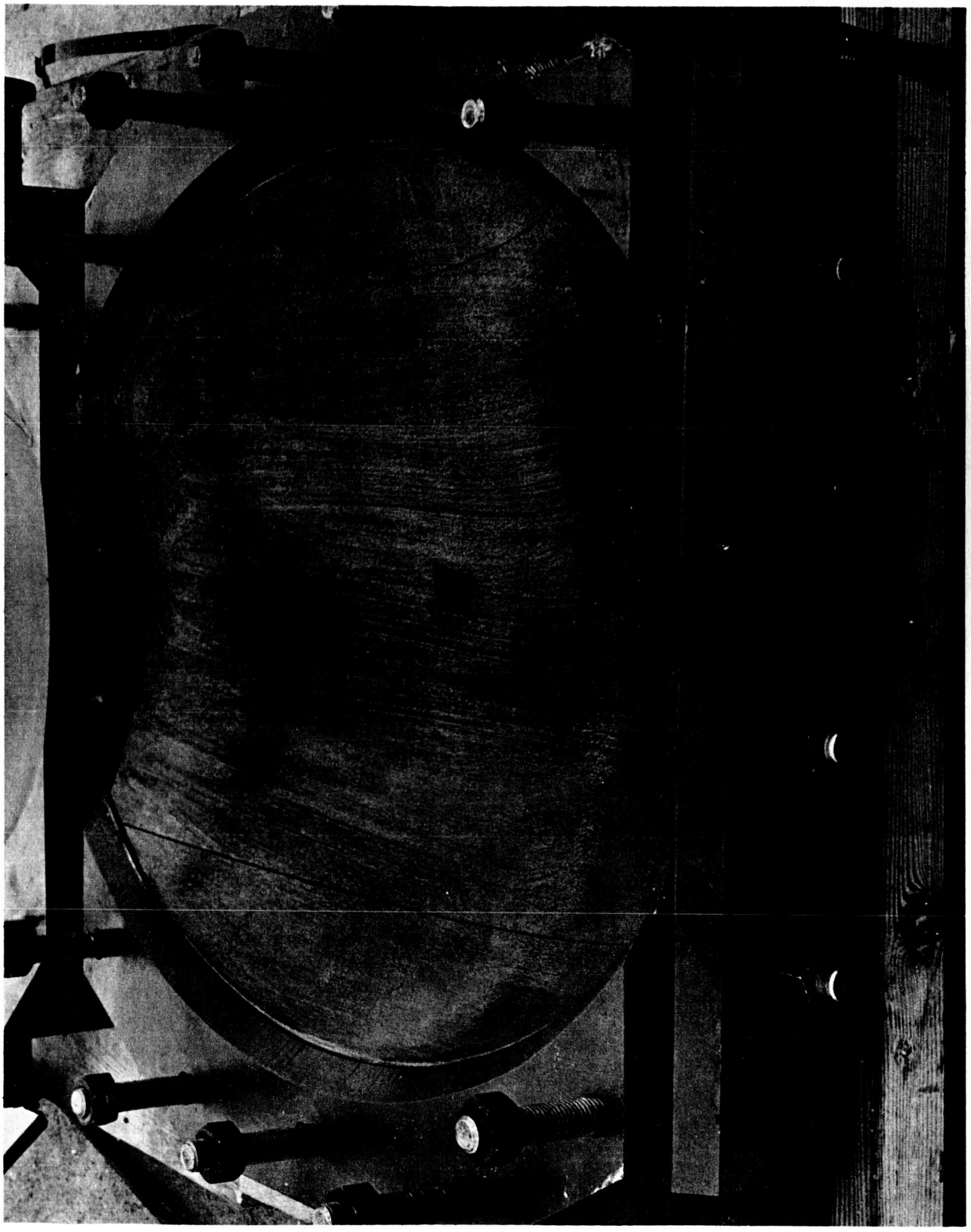

Fig. 8 Lower Gore Die Used to Form 2219 Aluminum

a. One-inch Inserts

A one-inch magnesium insert was placed over the blank clamping areas on both ends of the die. The inserts were machined so that their contours blended smoothly with the die. The die entrance of the inserts was machined to a 0.200 in. radius for one test series and then to a 0.750 in. radius for another series to evaluate the effect of draw radii on forming results with the increased die depth. The inserts were attached to the die with braces constructed of one-inch thick mild steel. The braces were necessary to insure the rigidity of the part of the insert that extends beyond the end of the die. This bracing also provides a solid base for insertion of the clamping studs (Fig. 9).

b. Two-inch Inserts

The draw radii of 0.200 and 0.750 in. were also evaluated with 2-in. inserts. These inserts made use of the bracing arrangement to which the 1-in. inserts were attached. Figure 10 illustrates the method of joining the inserts to the die using the aforementioned bracing. It was necessary to insure a vacuum tight seal between the inserts and the die. This was accomplished by the use of zinc chromate vacuum bagging compound between the two surfaces.

4. Concrete Die

A die was constructed of Embeco, a high strength concrete containing an iron aggregate. The shape of this die is the same as that of the upper gore die with 2-in. inserts in place. It was designed in this manner to furnish the proper comparison with the cast iron die in the evaluation of die material, hardness, and surface finish. The concrete die incorporates iron reinforcing rod in the casting to provide additional strength particularly in the longitudinal direction. The die face and clamping area was coated with a tooling epoxy containing an aluminum powder (Fig. 11). The epoxy die facing was incorporated to provide a nonporous surface for vacuum sealing before forming.

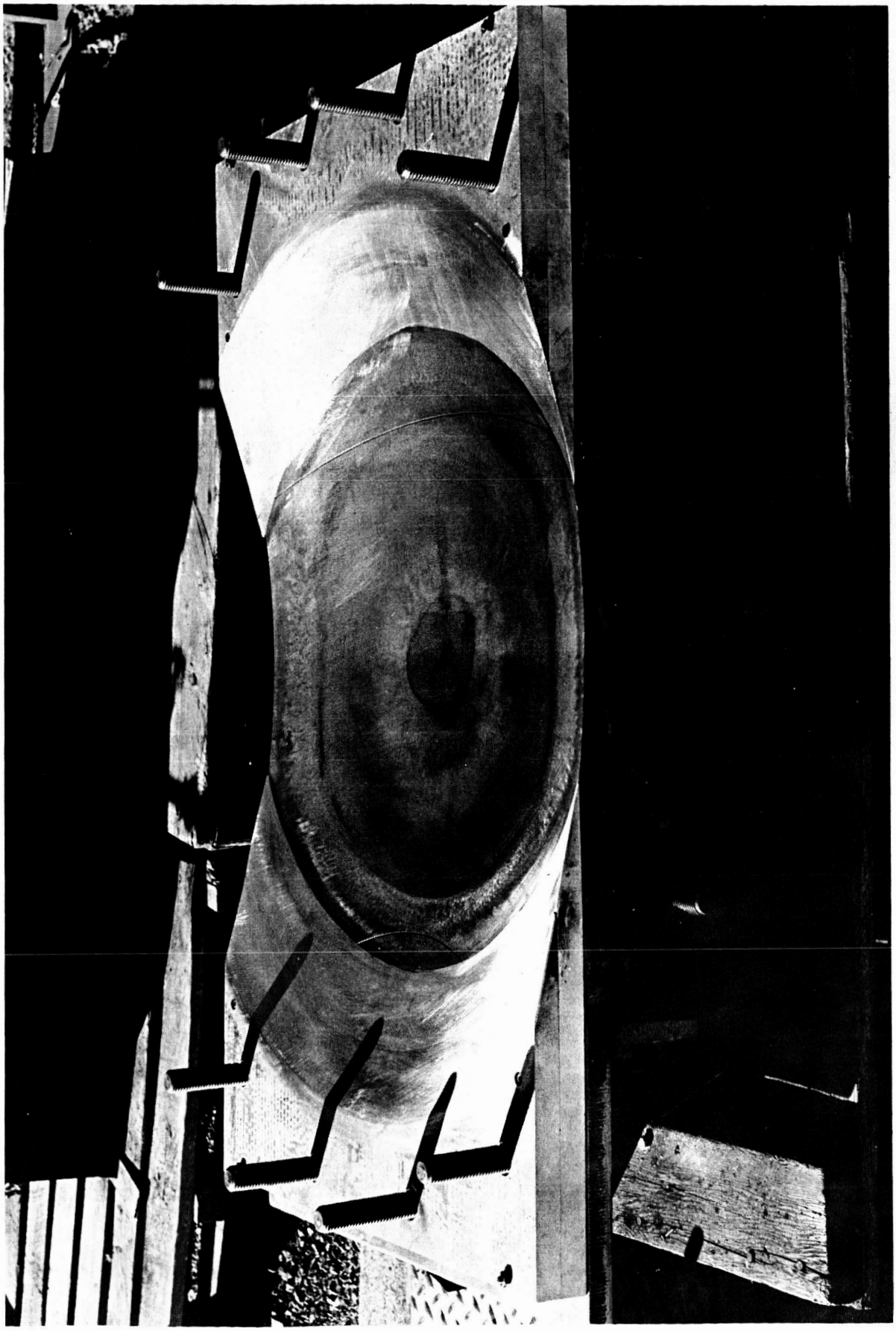

Fig. 10 Upper Gore Die with 2-in. Inserts Installed

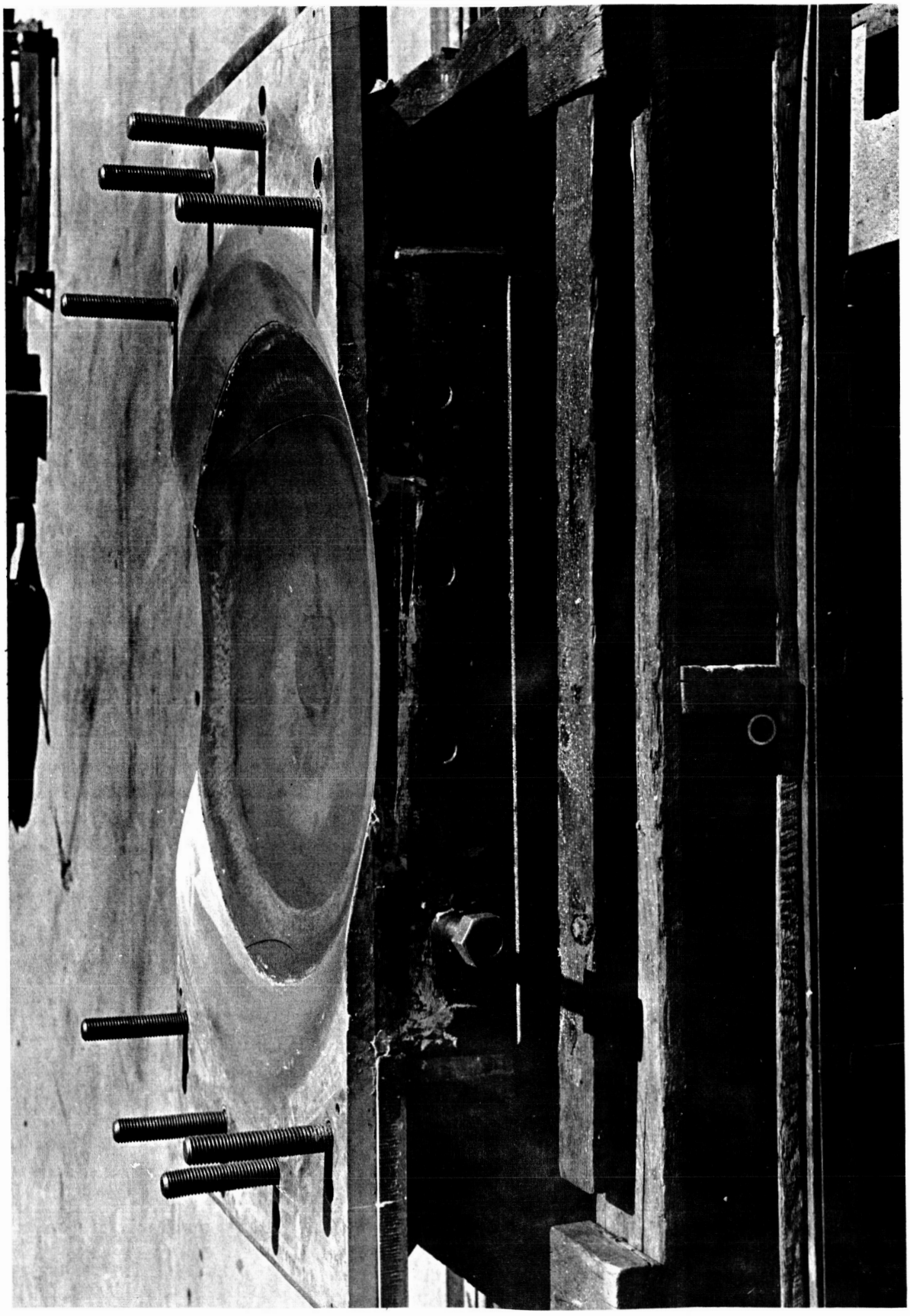

Fig. 9 Upper Gore Die with 1-in. Inserts Attached

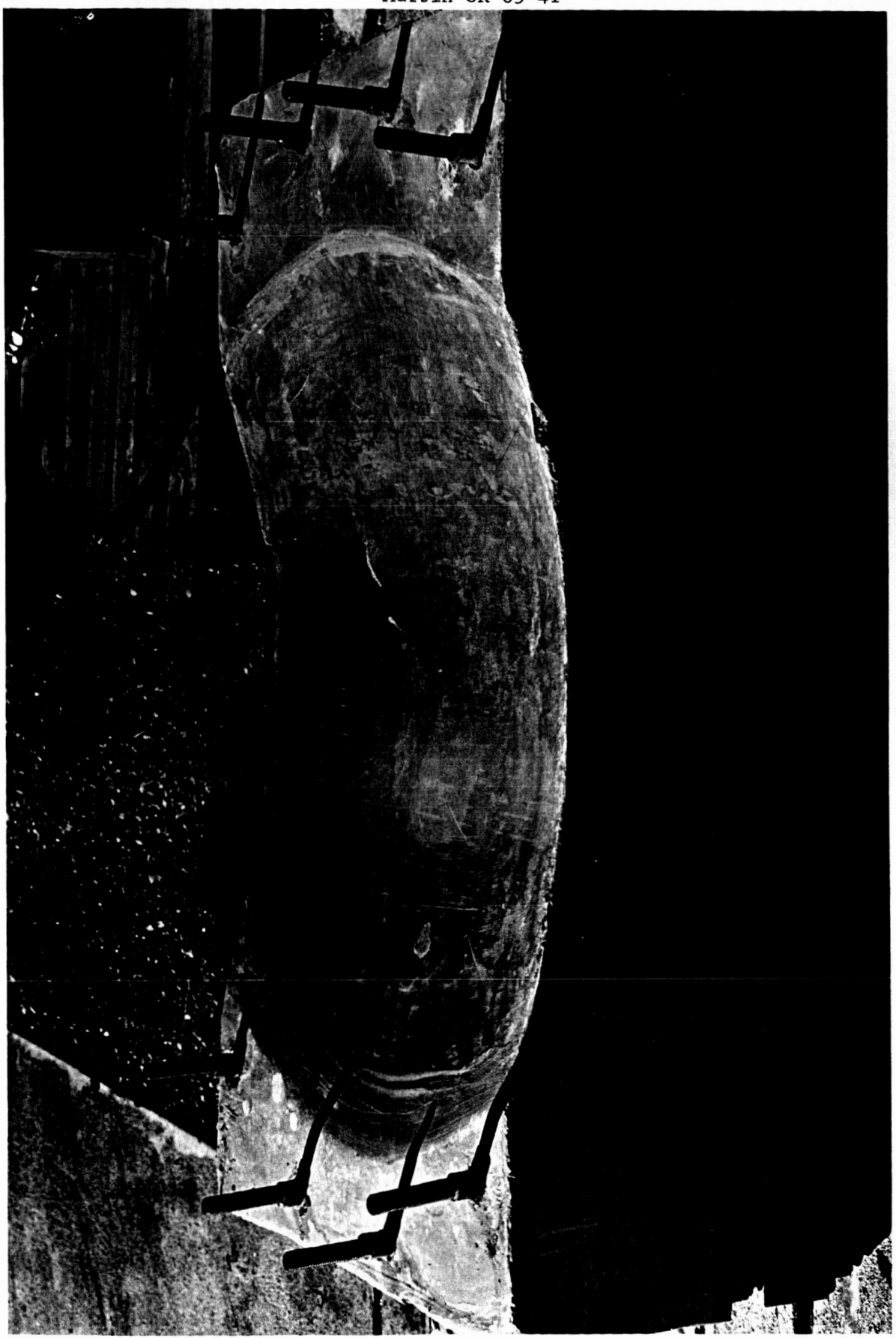

Fig. 11 Cast Embeco Concrete Die for Die Material Studies

5. Integral Blanket

Another method for the investigation of the reduction of springback was an integral blanket concept. This technique involves the use of a blanket material placed over the blank, which causes an elevation in the neutral axis of the blank to a position above the blank surface. This puts both blank surfaces into tension during forming, if the explosive pressures and coefficient of friction between the integral blanket and blank surface can provide sufficient resistance to horizontal shear stress. The resulting increase of plastic deformation would reduce springback significantly. The materials used for integral blanket tests were neoprene rubber of 40 and 80 durometer hardness, polyurethane rubber, and pure lead. All testing was done on a 10.5-in. diameter die with a 30-in. spherical radius. This die has no clamping ring, the vacuum being the only holddown force. This type of die was intended to demonstrate the effect of integral blanket on springback because all forming occurs via the cupping mode. Figure 12 shows a typical setup for the integral blanket studies.

6. Free Forming

A 24-in. diameter die with a 16-piece segmented clamping ring was used to form 1/5-scale model end caps for the ellipsoidal bulkhead domes for Saturn V. Figure 13 shows the die with segmented clamping ring. This die is not an evacuated type of tool, therefore a water barrel is used to contain the water necessary to the forming. The die with water barrel in place is shown depicting a typical forming operation in (Fig. 14). The blanks used in this step were 2219-T351 aluminum, 33.6-in. diameter and 0.250-in. thick. This blank diameter provides a blank diameter to die diameter (B/D) ratio of 1.4, which is optimum for this type of forming.

C. METALLURGICAL ANALYSIS

Evaluation of the microstructure of the explosively-formed 2219 aluminum alloy was divided into two tasks: optical metallography, performed at Martin-Denver; and transmission electron microscopy, performed at Martin-Orlando.

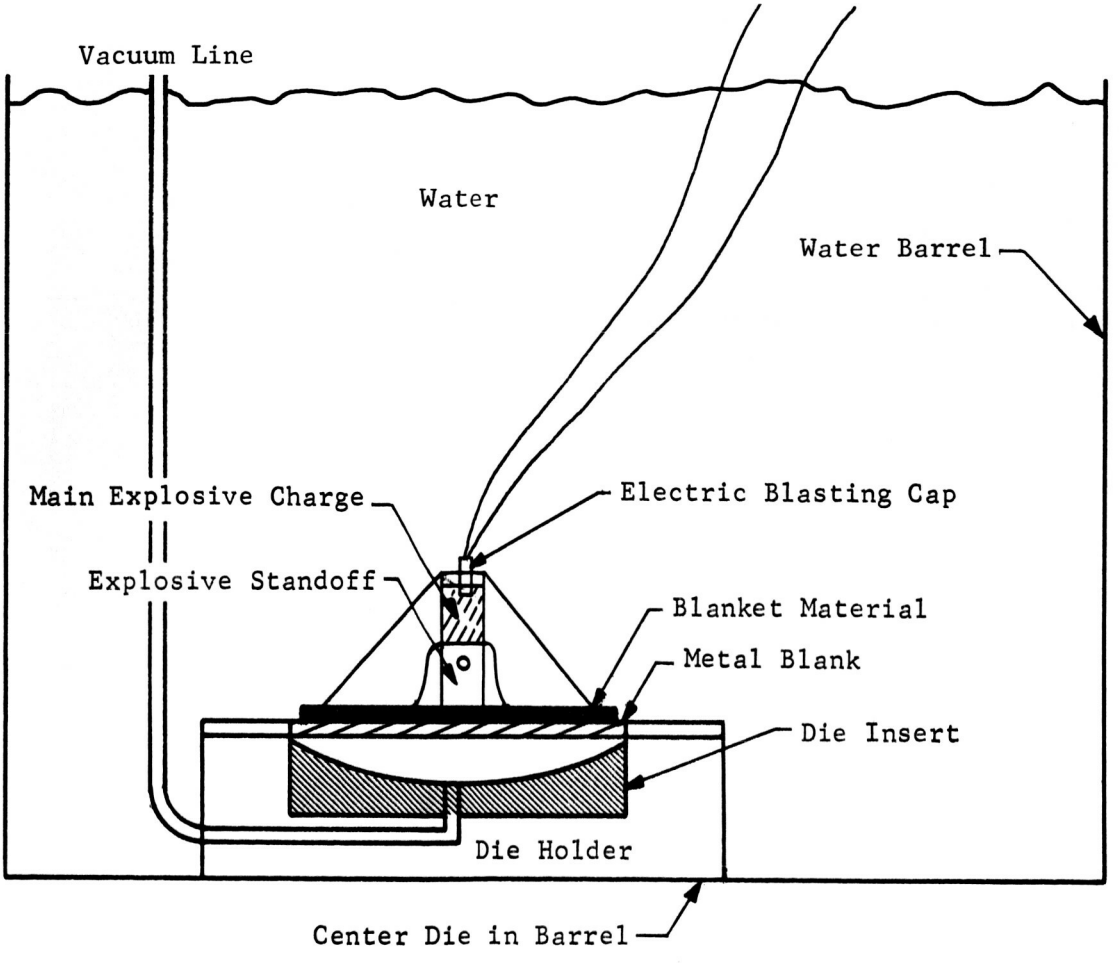

Fig. 12 Forming Arrangement for the Study of Integral Blanket Concepts

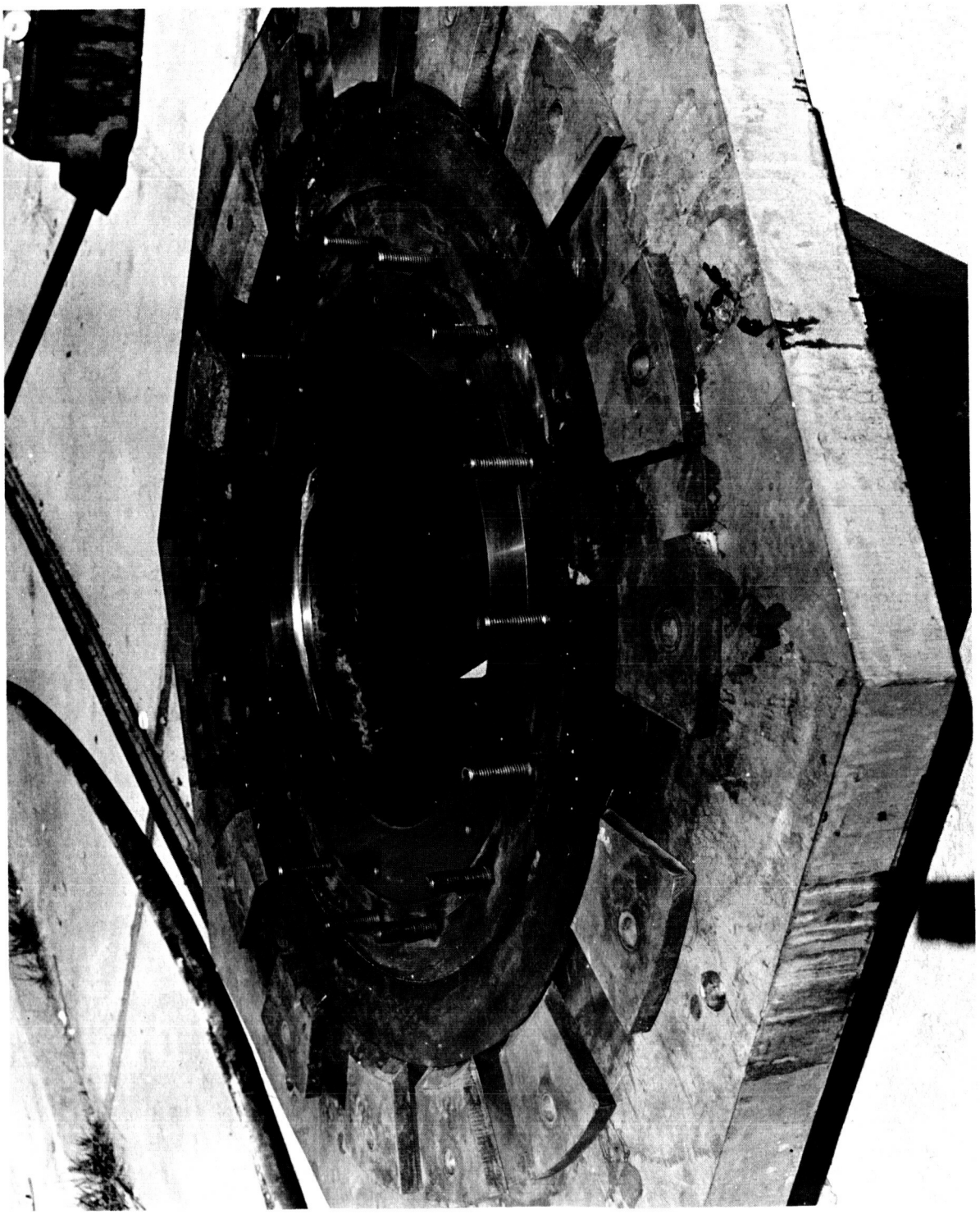

Fig. 13 Free Forming Tool Showing Segmented Draw Ring

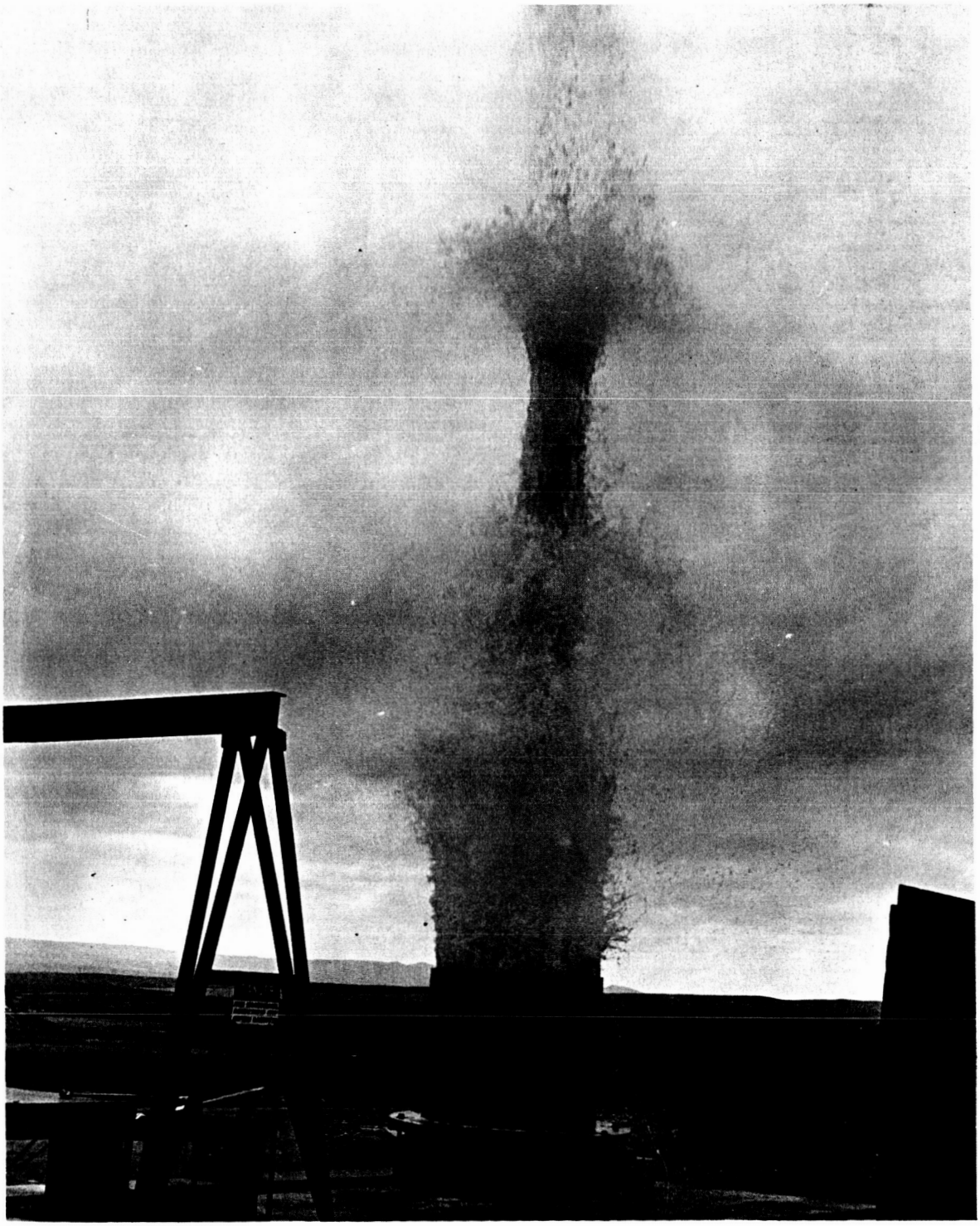

Fig. 14 Typical Free Forming Test in Progress

1. Optical Metallography

Photographs of grain structure of 2219 aluminum in various tempers were taken in the metallography laboratory. Low order magnification photography, up to 20X, was performed on a Bausch and Lomb Model L macro camera with a polaroid attachment. The micro photography work, of higher magnification, was divided between the Balphot and Research metallographs manufactured by Bausch and Lomb.

2. Transmission Electron Microscopy

The materials research department at Martin-Orlando provided all electron microscopy studies required on this contract. The following equipment for specimen preparation and photography was used:

1) Jet electrolytic polisher for preparing thin foils;

2) Siemens Elmskop electron microscope employing these features:

   Accelerating potentials of 60, 80, and 100 kv,

   Five lenses including double condensers, objective, intermediate, and projector,

   Aeon tilting goniometer stage,

   Heating stage,

   Tensile stage,

   Facilities for cinematography

   X-ray micro-probe attachment,

   Facility for reflection electron diffraction.

3) Evaporator of 10^{-6} torr for preparation of replicas of specimen surfaces.

4) Complete photographic darkroom facilities.

Necessary data reduction, where applicable, was furnished by an electronic computer. All specimens used in this study were supplied by the Martin-Denver division. As-received control specimens from every panel received from NASA as well as those specimens from the required explosive forming tests were used in this investigation.

3. X-ray Diffraction

The crystallographic analysis of the 2219 aluminum specimens was performed with the Siemens Crystalloflex IV x-ray diffraction unit. This unit was used to obtain data such as residual elastic strains and variations in lattice parameters. The x-ray unit is a console model with three principal components:

1) X-ray source with appropriate high voltage and current generating circuits (up to 50 kv, 50 ma);

2) A highly accurate mechanical goniometer and step scanning attachment for indicating angles and fluorescent radiation to better than 0.01 deg 2 θ in the Bragg angle goniometer coordinates;

3) An electronic detecting and counting (including pulse height analyzer) component for measuring the resultant radiation with great statistical accuracy.

4. Mechanical Testing

Evaluation of mechanical properties was performed in the Materials Engineering Laboratory at Denver. A 50,000 lb Baldwin-Lima-Hamilton tensile machine was used for evaluating the tensile specimens selected from control panels and explosively formed material. All tensile specimens were machined to dimensions specified in Fig. 15 by the engineering laboratory shop. Strain measurements, during tensile testing, were made with a PR-5 microformer extensometer. These results were recorded on a standard X-Y chart. All specimens were tested at a strain rate of 0.005 in./in./min. The heat treating and aging cycles necessary for the evaluation of the 2219 material were performed in a Lindberg draw furnace, which is accurate to plus or minus 5°F. All heat treating and aging of as-received material was performed in accordance with Martin Material Specification 1117. The formed material required adjustment in aging cycles to avoid loss of properties due to overaging.

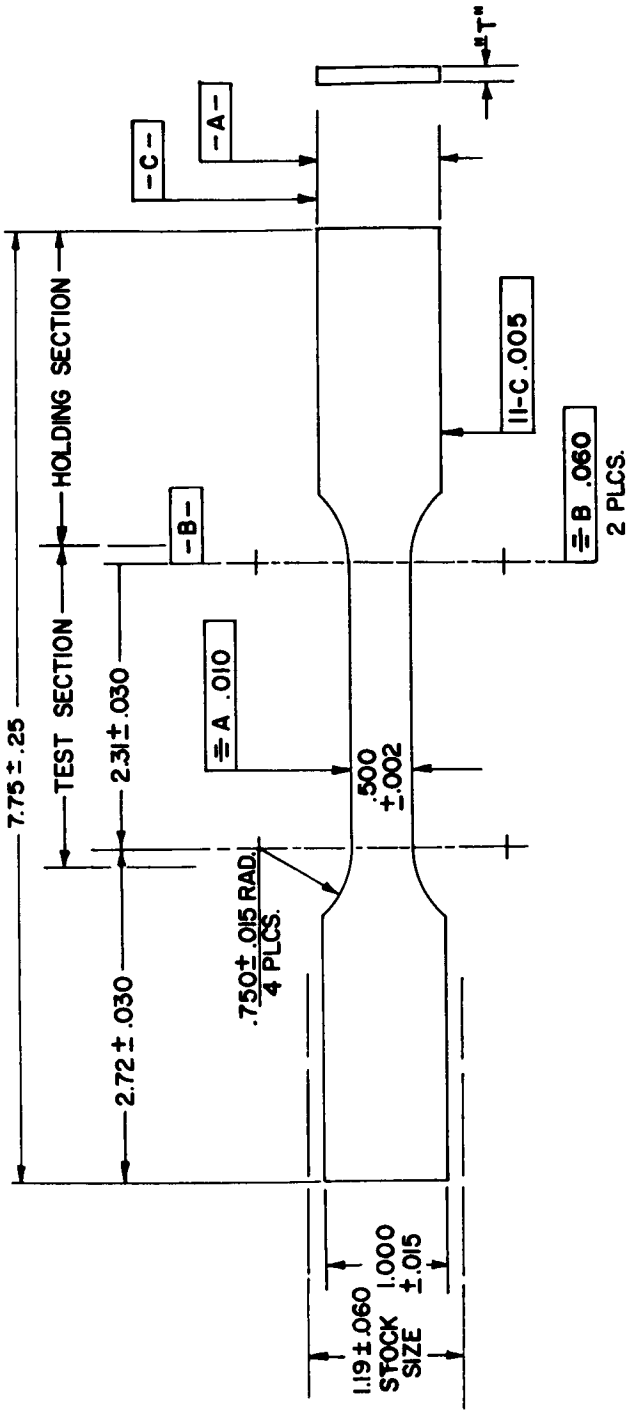

Fig. 15 Typical Dimensions of Tensile Specimens Tested During the Program

5. Springback Measurement

An important part of the program was the use of suitable techniques for the measurement of springback. Initially only measurements of the formed part after removal from the die were taken using a female template. The template is shown in Fig. 16a. However, as experimental work proceeded, it became apparent that measurements of the formed part while still in the die and clamped down would yield meaningful data. Therefore, both types of measurements were made. A male template as shown in Fig. 16b was used for the in-die measurements.

The results of springback data using the templates were not altogether satisfactory since the values recorded were somewhat misleading. For example, using the template technique the maximum contour deviation gave the minimum value of springback, and flange distortion caused some discrepancies in measurement and difficulty in analysis. Therefore, a different technique was developed that provided more accurate data and permitted more meaningful interpretation. It was felt that the die cavity itself would be a more accurate baseline from which to make comparisons than a template machined to the cavity contour. Thus accurate measurements were made of the die cavity contour by dropping perpendiculars from an accurately positioned steel beam across the die surface. For in-die measurements the beam was supported by the holddown ring and adjustments were made for the thickness of the ring. After the clamping force was removed, a steel beam was supported at the draw radius, and vertical distances were then measured using the nonshifting radius points as a reference plane. Figure 17 illustrates the technique used. Although the method of springback measurement is quite simple in concept, it was effective in describing blank deviations from the die cavity contour. No suitable technique was developed to accurately depict the flange distortion present after forming.

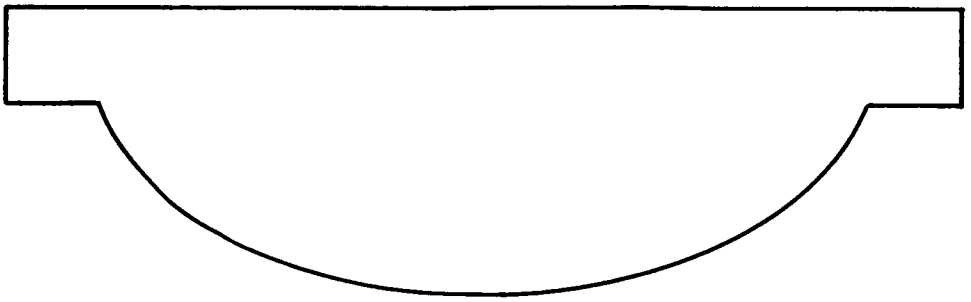

a. Male Template for In-Die Measurements

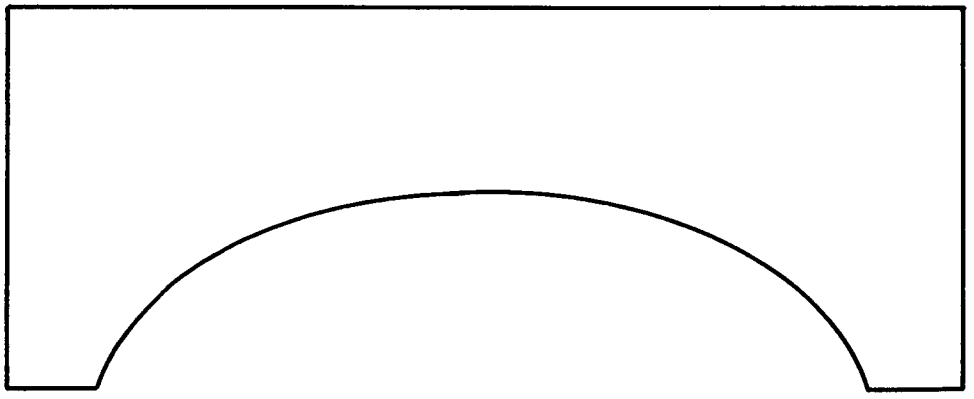

b. Female Template for Out-of-Die Measurements

Fig. 16 Templates Used to Measure Deviations from Forming Die Contour

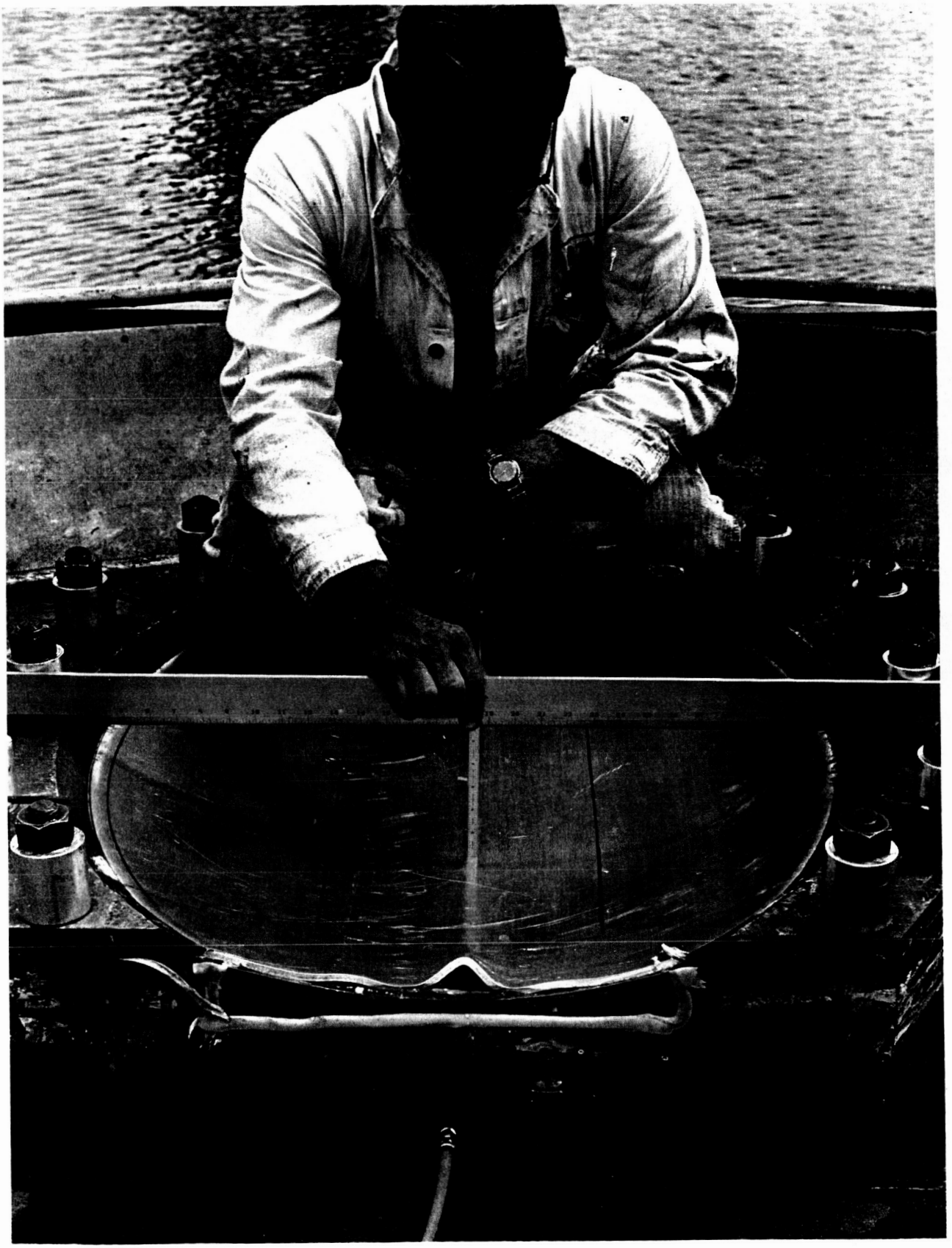

Fig. 17 Springback Measurement of Explosively Deformed 2219-T31 Aluminum

III. TEST RESULTS AND DISCUSSION

A. SPRINGBACK CONTROL

Springback is most severe when forming shallow shapes of high yield strength material. The two factors causing springback are rebound, which results from the impact of the moving part with the die surface and the proportion of elastic strain present in the total deformation. The results discussed in this section pertain to the reduction of these two factors causing springback.

1. Determination of Forming Conditions

Forming parameters were evaluated by a systematic series of tests. Using data that were established in previous work as an initial set of forming conditions, the pertinent parameters were studied; i.e., only one parameter at a time was adjusted. In this manner each condition contributing to springback was evaluated.

a. Standoff

Standoff is the distance between the bottom of the explosive charge and the surface of the blank. This parameter can be expressed as the ratio of charge distance from the blank surface to a characteristic blank dimension (diameter for symmetrical parts, width, or length for rectangular part, etc).

Four different tempers (0, T42, T351, and T37) of the 2219 alloy were used for the evaluation of springback as a function of charge standoff. All blanks in this series of tests were 0.250-in. thick. Charge standoffs of 3.54, 6.36, and 10.60 in. were evaluated for percentage of springback in each temper. A charge standoff of 3.54 in. produced minimum springback in all tempers. However, the 2219-T351 and 2219-T37 blanks exhibited some springback around the edges of the blanks. The results from the tests at a 6.36-in. standoff showed a considerable increase in springback over the entire blank surface in all tempers. Using a standoff of 10.60 in. produced some interesting results. The 2219-0 and 2219-T42 blanks exhibited a high percentage of springback over the entire

blank surfaces particularly in the central portion. The 2219-T351 and 2219-T37 blanks produced the same excessive springback in the central portion of the blank but the springback was markedly decreased near the edges of the blanks. Apparently for low yield materials, where plastic flow occurs easily, edge pinning due to the explosive force is not effective. However, for the high yield strength tempers pinning of the edges was evident. The 3.54-in. standoff was determined as optimum after analysis of all the data. Standoffs of less than 3.54 in. produced erratic results and excessive blank damage under the charge. Figure 18 illustrates the effects of charge standoff on metal springback.

b. Explosive Charge

The results from this series of tests were used to establish charge type and shape.

Three types of explosives were evaluated to determine the one that produced the minimum springback and to establish a charge equivalency ratio for explosives of different burning speeds. Cyadyn 3 (a 48% nitroglycerine dynamite manufactured by American Cyanamid) was used in the initial testing because it was economical and readily available. It has a burning speed of 7000 fps. It was also evaluated for comparison purposes with explosives of higher burning speeds. Penta erythritol tetranitrate (PETN) powder, with its burning speed of about 26,000 fps, was used to evaluate the merits of a high explosive. The PETN used in this series of tests was in two different forms:

1) PETN powder that is the type contained in PETN primacord;

2) DuPont Deta-sheet containing 68% by weight of PETN.

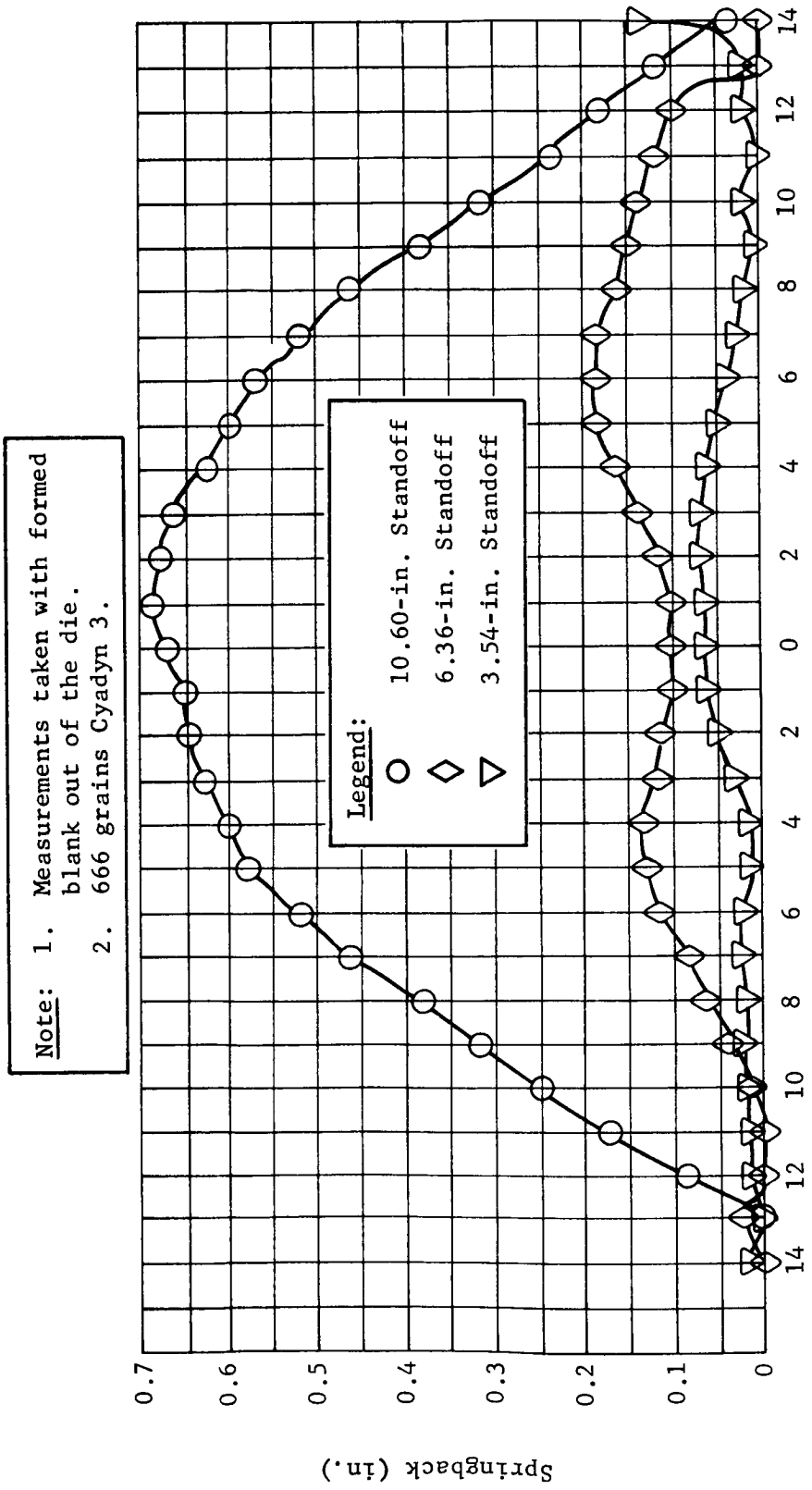

Fig. 18 Effect of Charge Standoff on the Springback of 2219-T31 Aluminum

Two shapes of charges were evaluated, the cylindrical charge was used because a direct comparison between PETN powder and Cyadyn 3 could be made (with the proper adjustment for differences in energy release). The charge equivalency, by weight, of Cyadyn 3 to PETN was established to be 2.02 to 1. The PETN was determined to be more satisfactory. A typical comparison shown in Fig. 19 shows a more desirable springback curve when PETN was used. The edge pinning coupled with the more uniform general springback was the first sign of suitable forming conditions. The uniform springback was also indicative of more uniform blank properties. The sheet explosive was then evaluated to provide a comparison between a centrally located point source of energy (cylindrical shape) and a sheet charge of the same contained energy that covers a much larger area of the blank surface. The sheet explosive was determined to be the most desirable type of charge because it consistently produced uniform and evenly distributed strain throughout the blank surface. Initially the cylindrical-shaped charge produced the lowest percentage of springback but the strain was very unevenly distributed. When the other conditions affecting springback had been optimized, the sheet explosive then produced a low springback with its accompanying uniform strain distribution. Blanks formed with sheet explosive showed a greater percentage of contact with the die surface in every case than those formed with an equivalent cylindrical charge. Figure 20 compares springback using central PETN charges and sheet explosive. Use of sheet explosive is particularly advantageous because the area of blank coverage by the charge may be kept constant as charge requirements are varied due to blank temper and thickness. This is accomplished of course, merely by selecting a thickness of sheet that will contain the proper weight of explosive. This type of sheet is available in a variety of useful thicknesses.

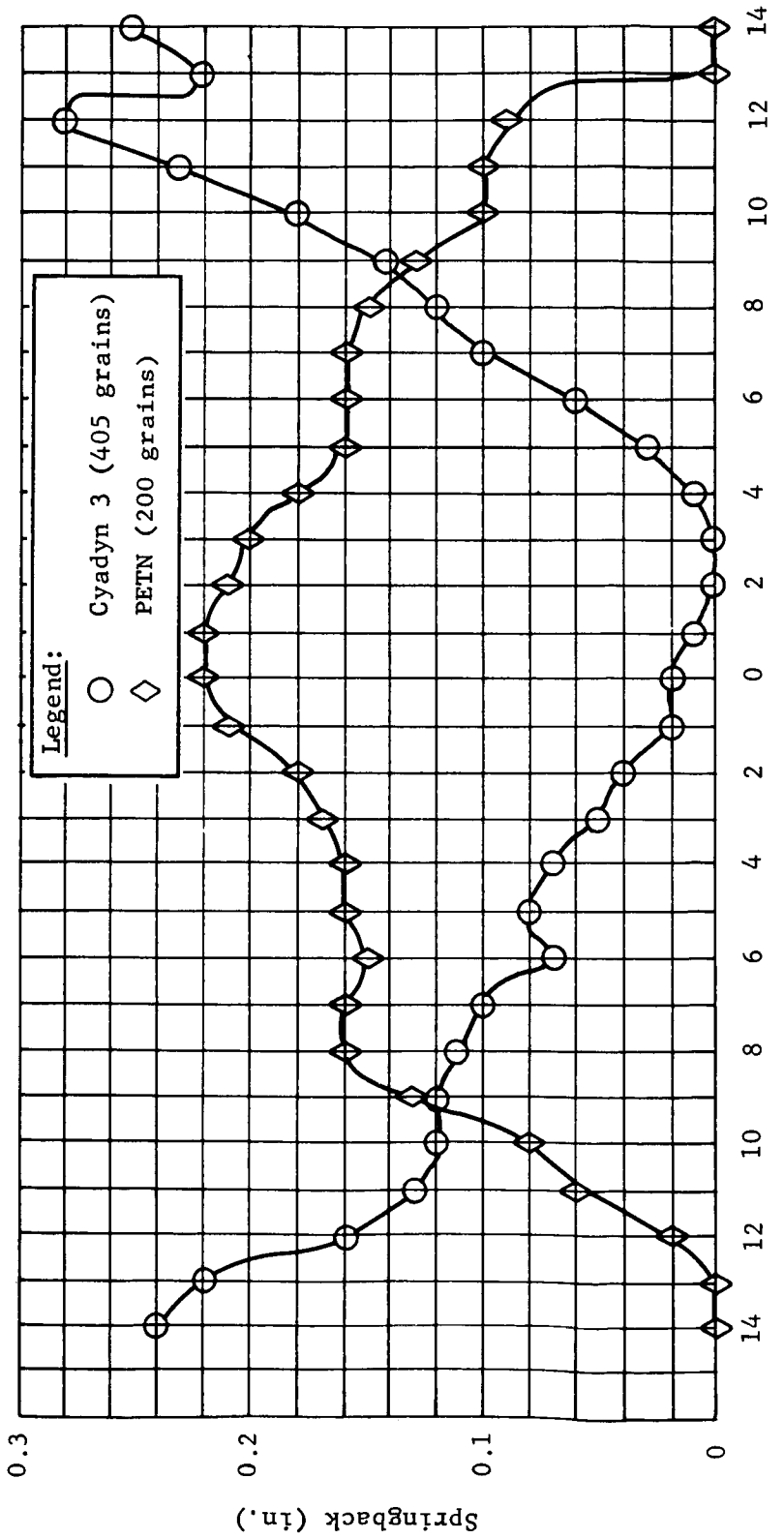

Fig. 19 Effect of Central Charges on Metal Springback Using Different Detonation Velocities

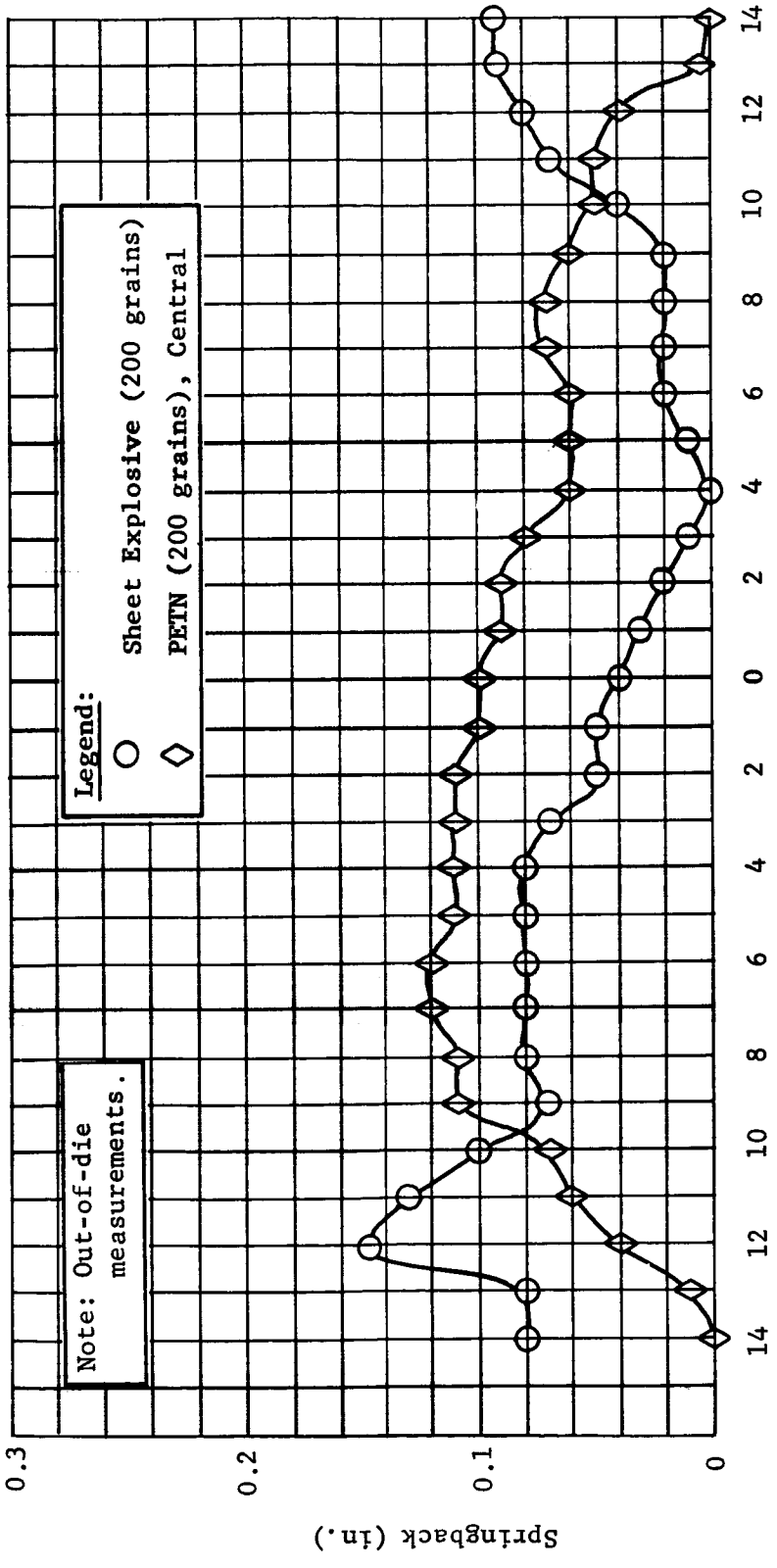

Fig. 20 Effect of Charge Shape on the Springback of 2219-T31 Aluminum Plate

c. Clamping Effects

The upper gore die has four 1 in. 8 NC studs on each end. The clamping plates are placed over the blank and tightened by a predetermined torque applied to the nuts. A curve relating torque and holddown pressure for 1 in 8 NC bolts with lubricated nuts and studs is presented in Fig. 21. The tension on the studs was adjusted to produce 100 psi of clamping pressure on the blank ends. This pressure was selected because it represented a reasonable torque level that could be applied to the studs without thread damage and clamping plate bending. During the initial testing, it was noted that the 100 psi pressure was still not sufficient to prevent the blank ends from slipping under the clamping plates when the die was evacuated. The slippage that occurred reduced the amount of plastic strain. Because springback is a function of the amount of plastic deformation of the blank, it was decided to increase the coefficient of friction by knurling the clamping plate faces rather than increasing the torque level on the studs.

The increased friction on the blank ends produced a marked decrease in springback. It was decided to check the effects of knurling during the testing that was performed on the lower gore die. Two blanks were formed before knurling and three after knurling. The three blanks formed after the clamping plate faces were knurled showed a higher percentage of induced strain with accompanying reduced springback. Figure 22 compares blanks formed with and without the knurling. The effect is typical for both upper and lower gore tests.

The clamping pressure on the lower gore die was raised to 150 psi to provide increased blank restraint. This was possible because the lower gore has five 1-in. 8 NC studs on each end.

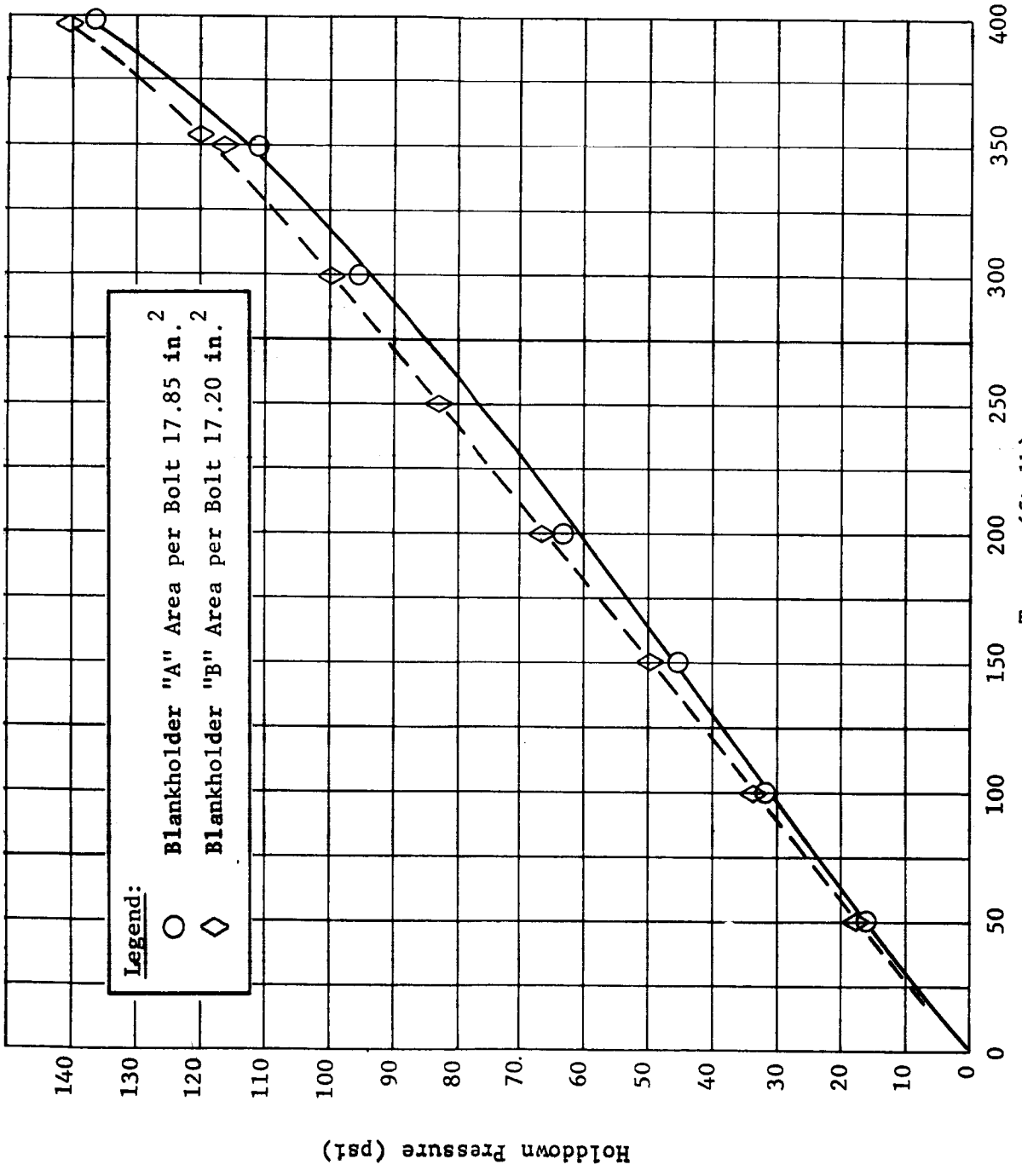

Fig. 21 Holddown Force as a Function of Holddown Pressure (Upper Gore Segment Die)

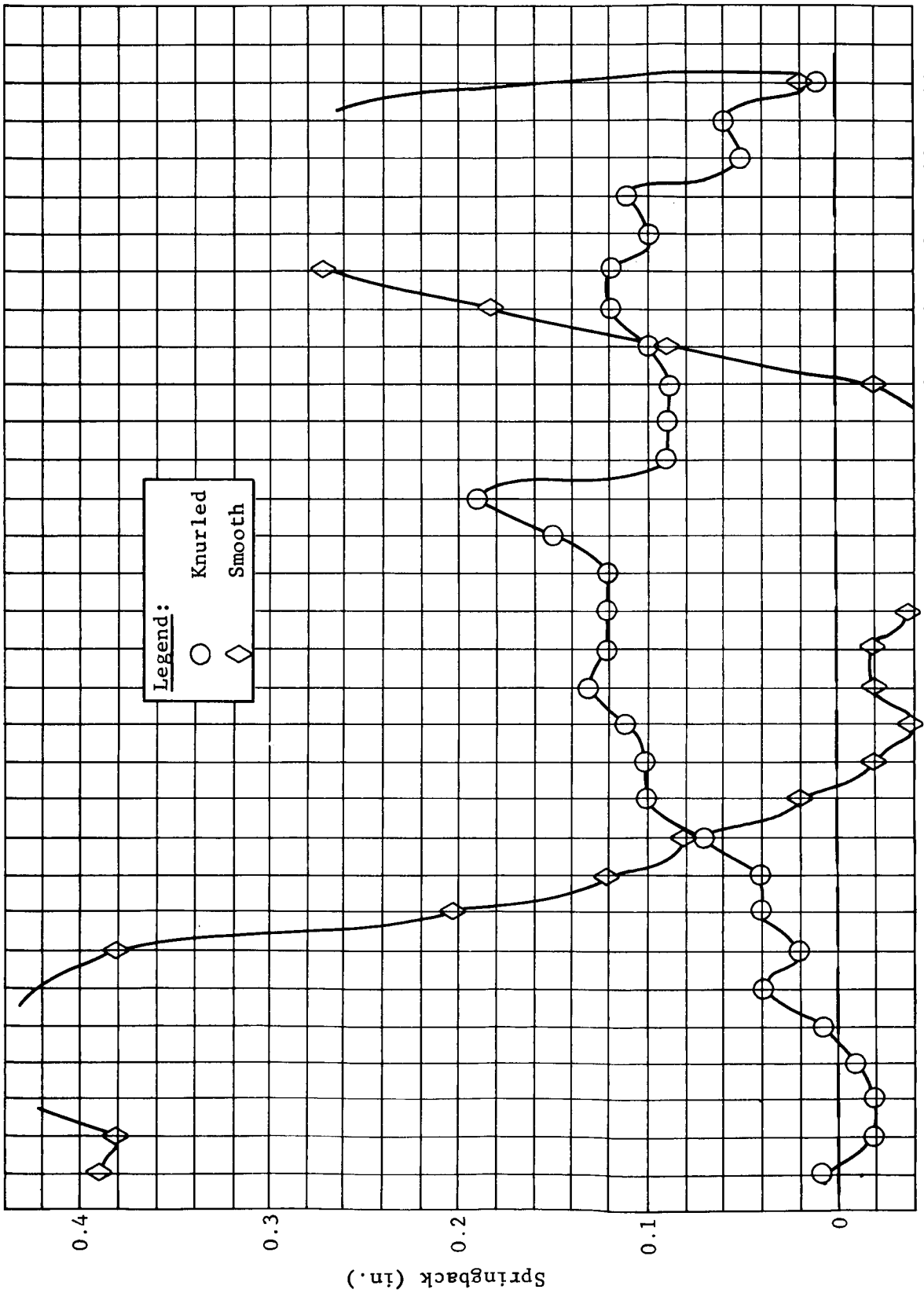

Fig. 22 Influence of Knurled Blank Holders on Springback of 2219-T31 Aluminum Plate

2. Effect of Blank Thickness

A study was made to determine the influence of blank thickness on the springback characteristics of 2219-T31. Thus, a minimum thickness could be established below which one might encounter problems with elastic strain resulting in increased springback. Charges were placed centrally over the blank to effect necessary forming. Both PETN and 0.025-in. sheet explosive were used. Material thicknesses formed were 0.032, 0.090, 0.132, and 0.250 inch. Thus different radius of curvature to thickness ratios could be studied (i.e., r/t = 470, 167, 114, and 60 respectively). It has been found from conventional forming experiments that springback varies as an inverse function of thickness; i.e., as the thickness decreases the amount of springback increases. This was also found to be the case for explosive forming. Either the bulk PETN charges or the central sheet charges gave similar results. Figures 23 and 24 show typical curves for 2219-T31. Because of the particular die design used, the unrestrained edges of the blank were allowed to pull-in freely as the blank was plastically deformed. For the 0.032- and 0.090-in. thick material this resulted in rather severe springback. In fact for the 0.032-in. thick blanks the springback was so severe after the holddown ring was removed that measurements were not attempted. Both the 0.090- and 0.132-in. thick blanks warped quite badly in every test. The warpage occurred in a diagonal direction along the restrained axis and was more readily apparent when the formed parts were removed from the die. Based on the test results using a die not permitting complete edge restraint the minimum thickness of 2219-T31 that can be formed without warpage or excessive springback is 0.250-in. for a 1/5-scale model. This corresponds to a thickness of 1.25-in. for the full-scale part.

3. Effect of Lubrication

Generally lubricants are used during sheet metal forming to encourage metal flow into the die without attendant high plastic strains. This permits the attainment of greater draw depths without excessive thin-out. In the forming of shallow contoured parts, however, the plastic strain has to be maximized in order to minimize the springback. Thus it is generally necessary to avoid lubricants when explosively forming shallow parts. There are other reasons why lubricants are detrimental to successful forming of close tolerance parts: (1) lubricant drawn into the die cavity before forming due to the reduced pressure under the blank can detonate causing dents in the part; (2) the compressed lubricant can detrimentally affect the part surface finish.

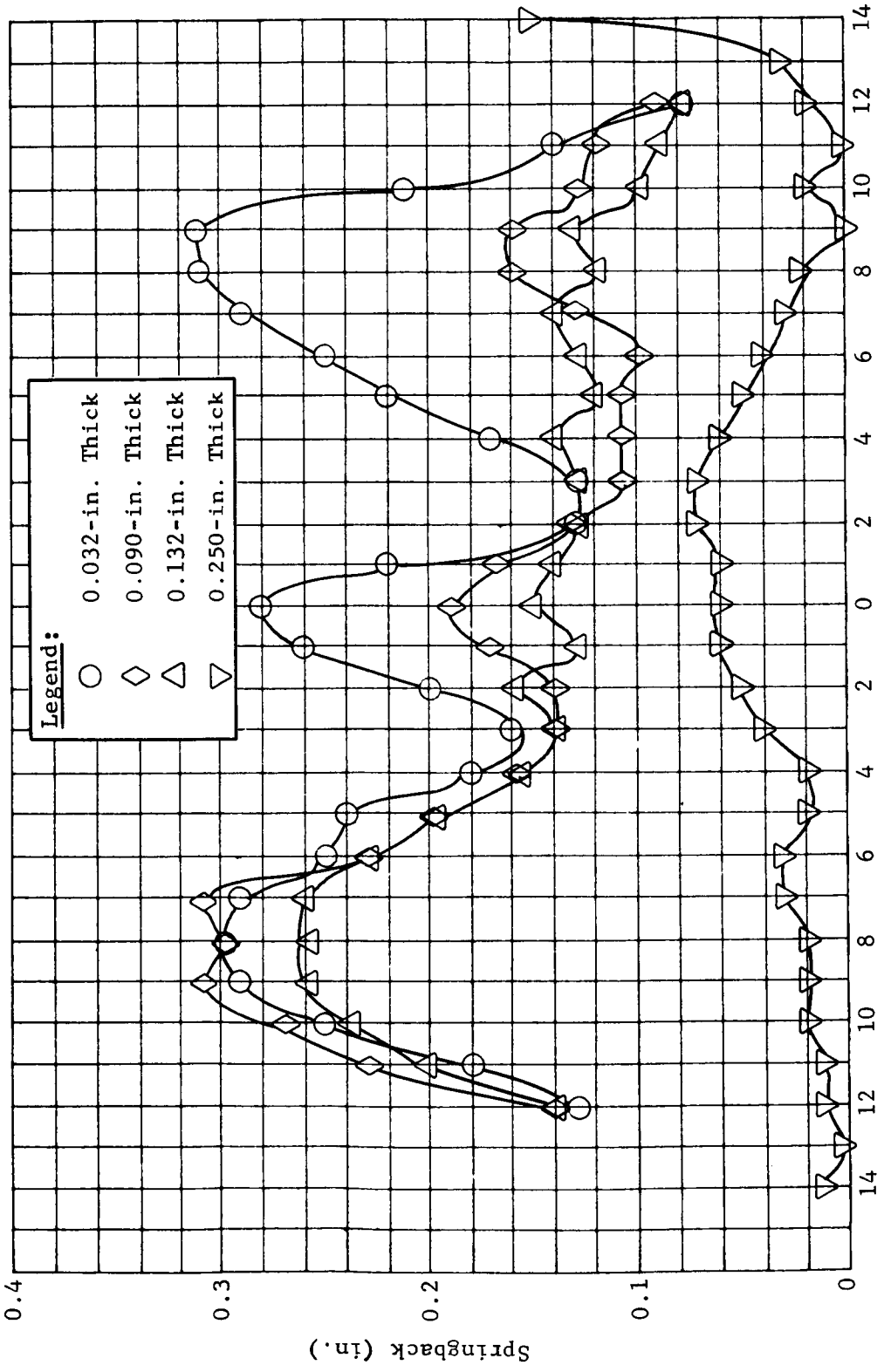

Fig. 23 Effect of Metal Thickness on the Springback of 2219-T31 Aluminum (Measurements Taken with Blank in Die)

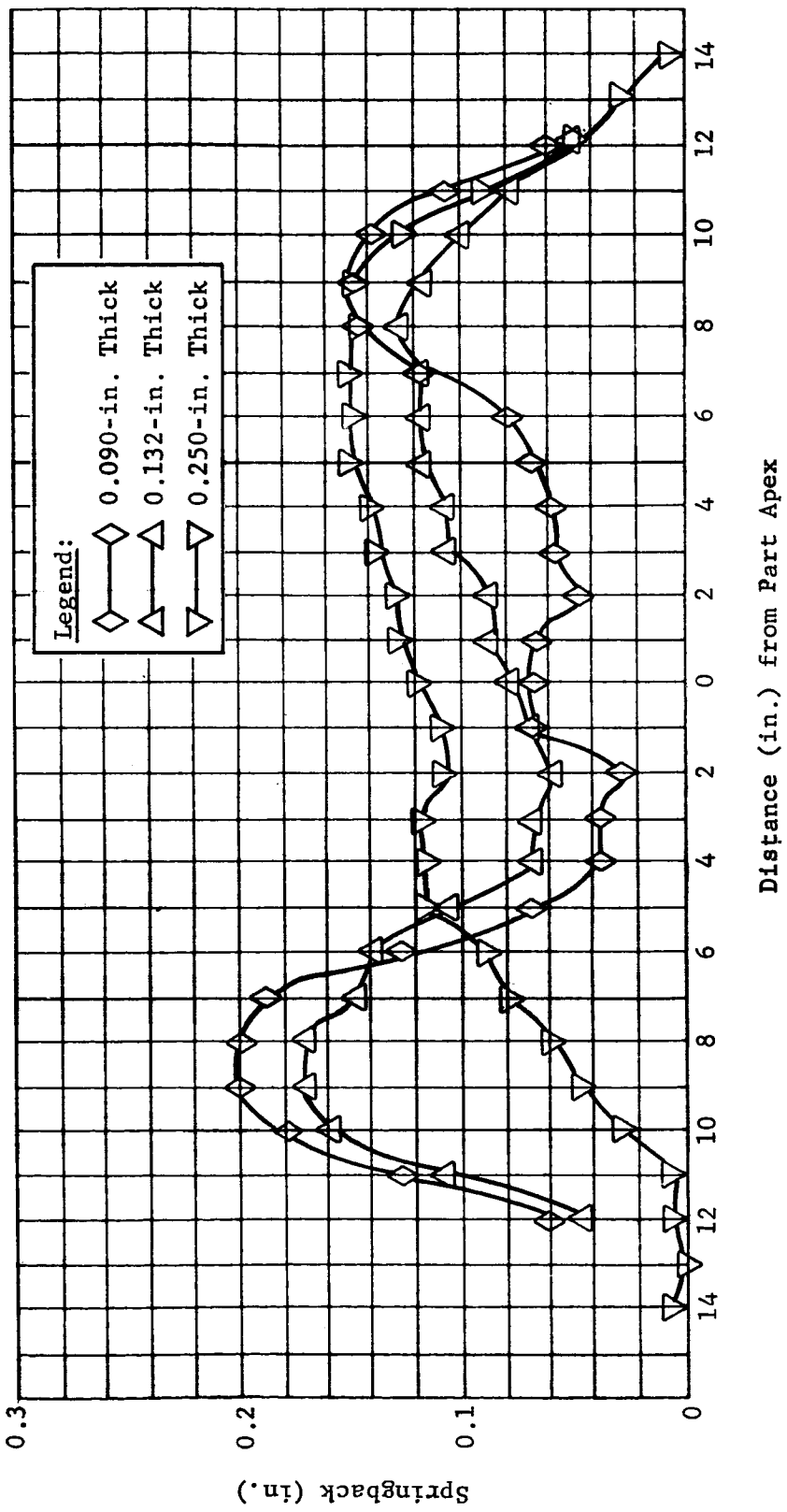

Fig. 24 Effect of Metal Thickness on the Springback of 2219-T31 Aluminum (Measurements Taken with Blank Out of Die)

In spite of the known influences of lubricant on metal behavior during fabrication, it was considered desirable to establish a more quantitative effect of lubrication on the behavior of explosively formed blanks by conducting a limited number of experiments. Aluminum alloy 2219-T31 blanks in thicknesses of 0.032, 0.132, and 0.250 in. were formed with and without the use of celvacine high vacuum grease as the lubricant. In all cases the amount of springback increased when lubricant was used on the die draw radius. Typical results are shown in Fig. 25.

For the explosive forming of shallow gore shaped parts, lubricant is not recommended, and is, in fact, definitely detrimental to the forming operation.

4. Effect of Draw Depth and Draw Radius

In conventional forming it has been determined by experience that the amount of metal springback is reduced by using sharper die entrant radii and deeper draws. Thus, it was of interest to determine whether similar behavior occurred during explosive forming. A series of experiments were conducted using 0.250-in. thick 2219-T31 aluminum. Draw radii of 0.2 and 0.75 in. and draw depths of 3 and 4 in. were evaluated.

In general, less springback resulted when sheet explosive was used rather than an equivalent charge of PETN bulk explosive. Since the sheet explosive gave the most uniform springback, the comparisons of draw depth and draw radius shown in this section are between experiments conducted with central charges of sheet explosive.

Figure 26 shows the influence of draw depth on the springback of 0.250-in. thick 2219-T31 using a 0.2-in. draw radius. The same comparison for a 0.75-in. draw radius can be seen in Fig. 27. Similar springback curves result in both cases, illustrating that at a given draw radius draw-depth does not affect springback to any appreciable degree. These are not expected results since for completely restrained blanks one achieves lower springback with an increase in draw-depth using a given draw-radius. However, the lack of restraint on the gore die used allowed excessive metal flow into the die cavity causing a modified stress pattern in the panel that influenced springback. This was confirmed by taking strain measurements to permit an evaluation of lateral blank stretching. It was found that a region exists along the centerline of the blank perpendicular to the long axis where foreshortening occurs. This shortening of the blank in the long transverse direction allows metal to gather with the result that edge buckles are produced causing a modification in the springback behavior of the metal.

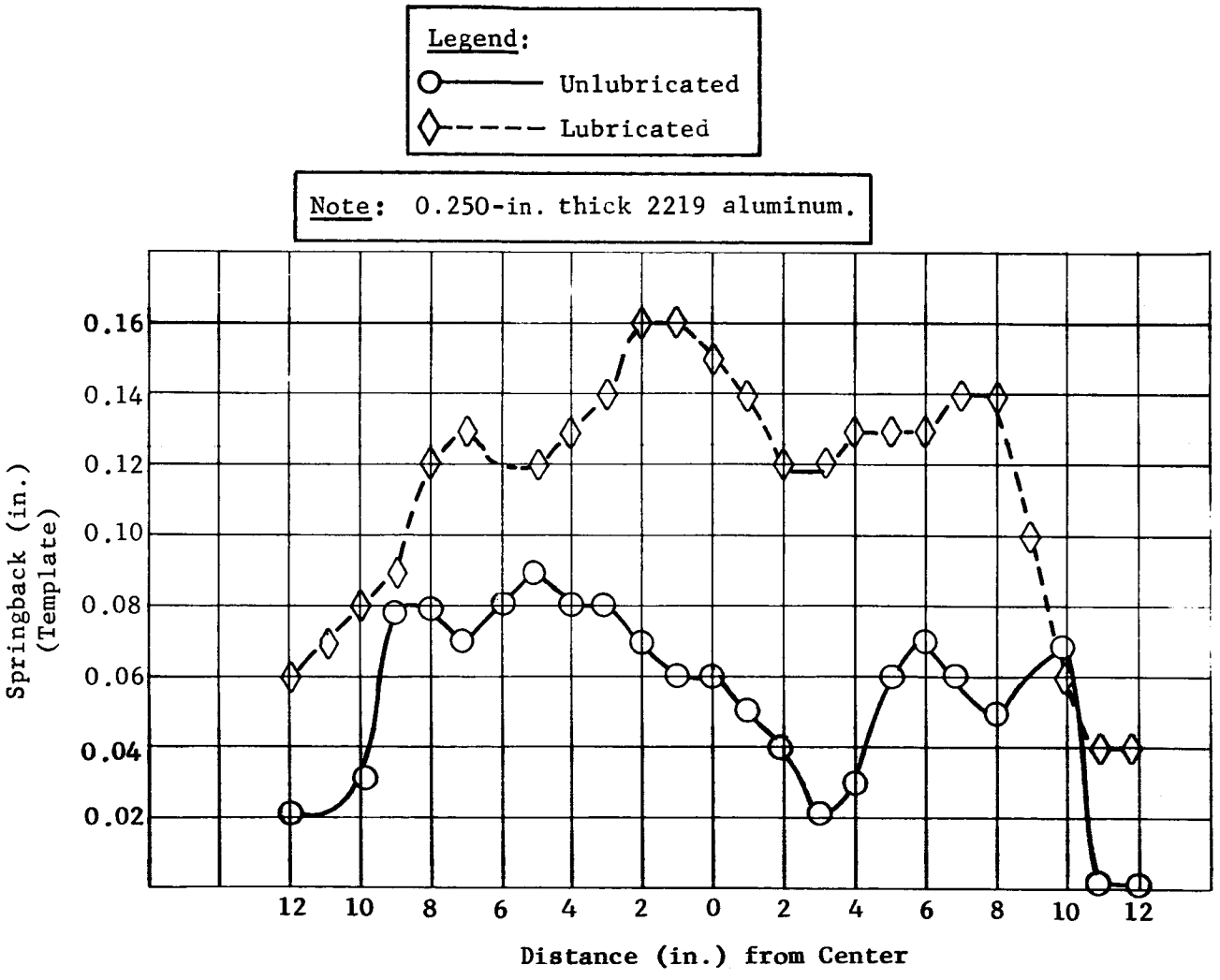

Fig. 25 Effect of Die Lubrication on Metal Springback

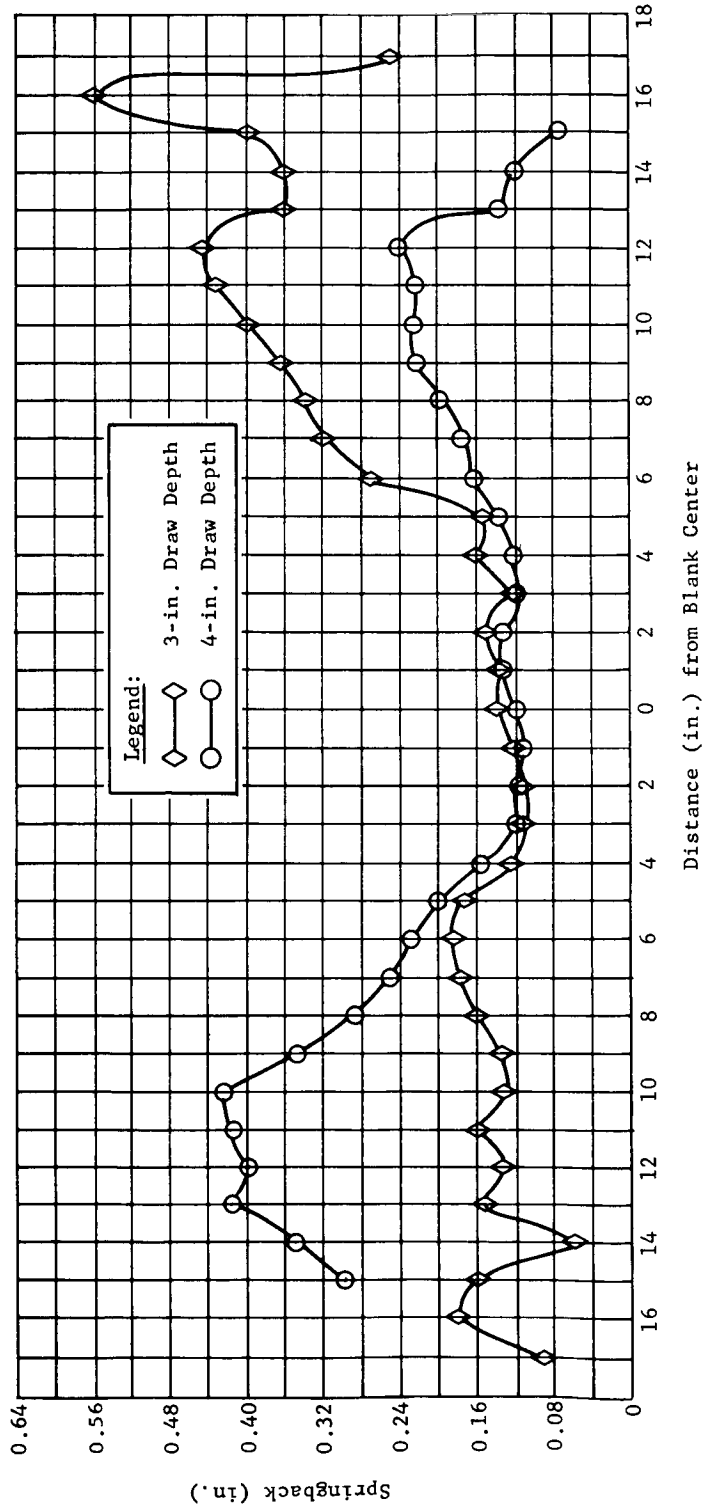

Fig. 26 Effect of Draw Depth on Metal Springback of 0.250-in. Thick 2219-T31 Aluminum (0.2-in. Draw Radius)

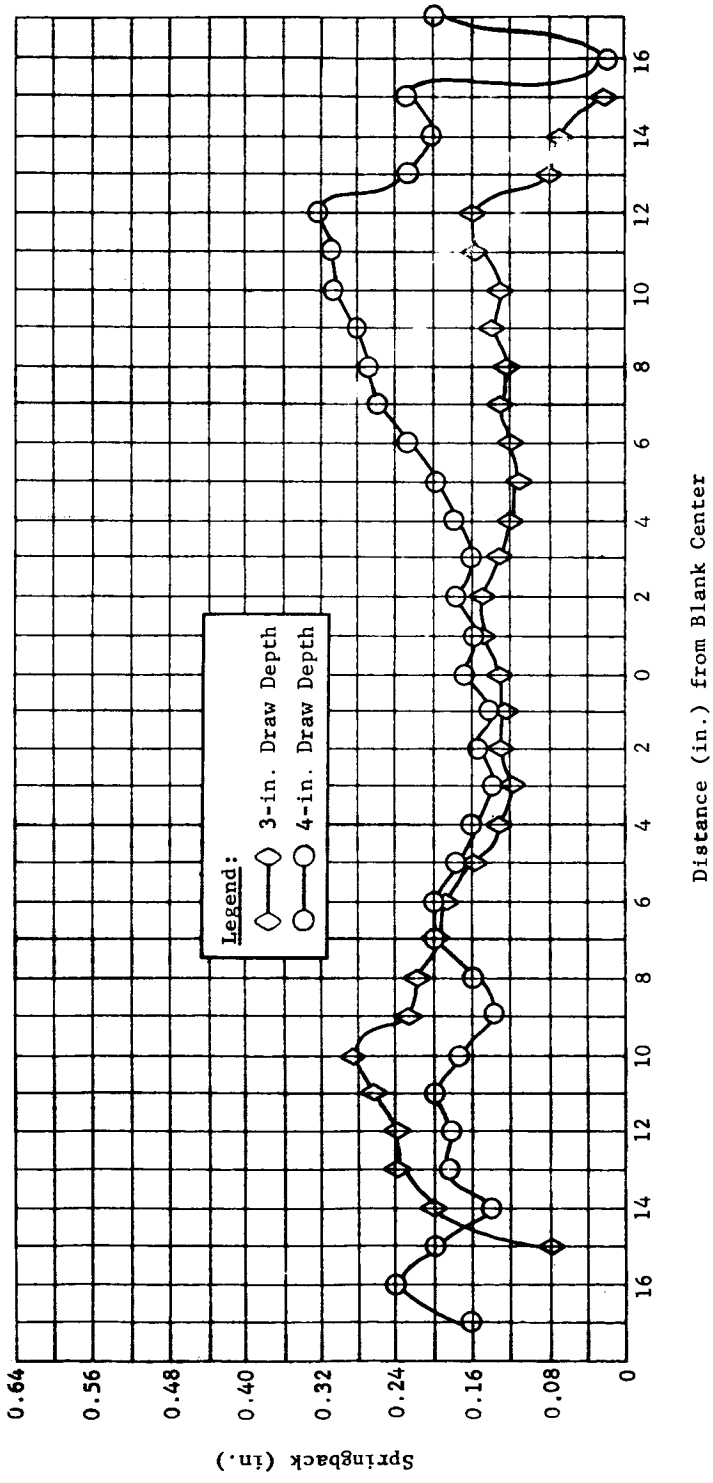

Fig. 27 Effect of Draw Depth on Metal Springback of 0.250-in. Thick 2219-T31 Aluminum (0.75-in. Draw Radius)

Figures 28 and 29 show the influence of draw radius on the springback at a constant draw depth. Based on results reported in the literature one expects a reduction in springback with the use of smaller radii. However, little influence was observed of draw radius on resulting springback after explosive deformation.

One aspect of the explosive forming of blanks in the modified upper gore die was the severe springback experienced at the flange area when the holddown bolts were released. The amount of movement was on the order of 3/4 to 1 1/2 in. using the one-inch inserts and 2 to 4 in. using the 2-inch inserts. Because of the severe flange distortion no contour measurements were taken with the blank out of the die since the draw radius reference plane used to measure contour deviations had changed. Thus the conclusions drawn from the forming experiments were based on "in-die" measurements. The effect can be seen in Fig. 30 where an unoptimized charge was used that did not force the blank into intimate contact with the die. Notice that after the holddown clamping force is removed the blank is deflected downward as a result of the upward movement of the flanges. The effect is much more pronounced when optimum charges are used.

In summary, there is little effect of draw-depth or draw-radius on springback. These unexpected results appear to be caused by unrestricted metal flow from the transverse edges of the die.

5. Effect of Die Material and Surface Finish

One primary aspect of metal springback that one must consider in sheet metal forming is rebound from the die. This rebound can contribute significantly to total measured springback and therefore must be evaluated. To permit an evaluation of the influence of die material on springback, a high-strength concrete die was constructed as described in Chap. II.B.4. to the same configuration as the meehanite upper gore die. Unfortunately the design was unsatisfactory and a break occurred through the die across the narrower dimension. The crack appeared to start from the vacuum connection at the side of the die. One repair was made on the die to permit the forming of two blanks. Some difficulty was experienced in evacuation of the die cavity due to porosity from casting. However, the problem was solved by applying a layer of tooling epoxy over the die forming surface thus effecting a suitable seal to air leakage.

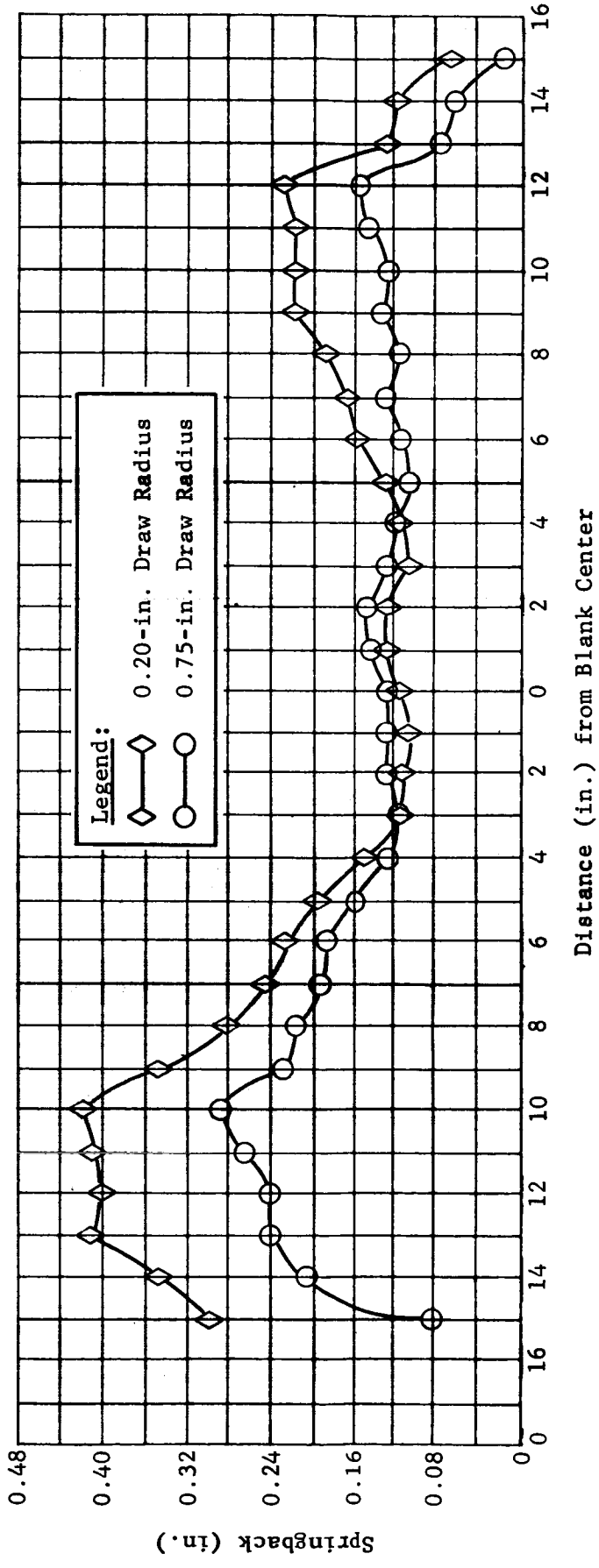

Fig. 28 Effect of Draw Radius on the Springback of 0.250-in. Thick 2219-T31 Aluminum (3-in. Draw Depth)

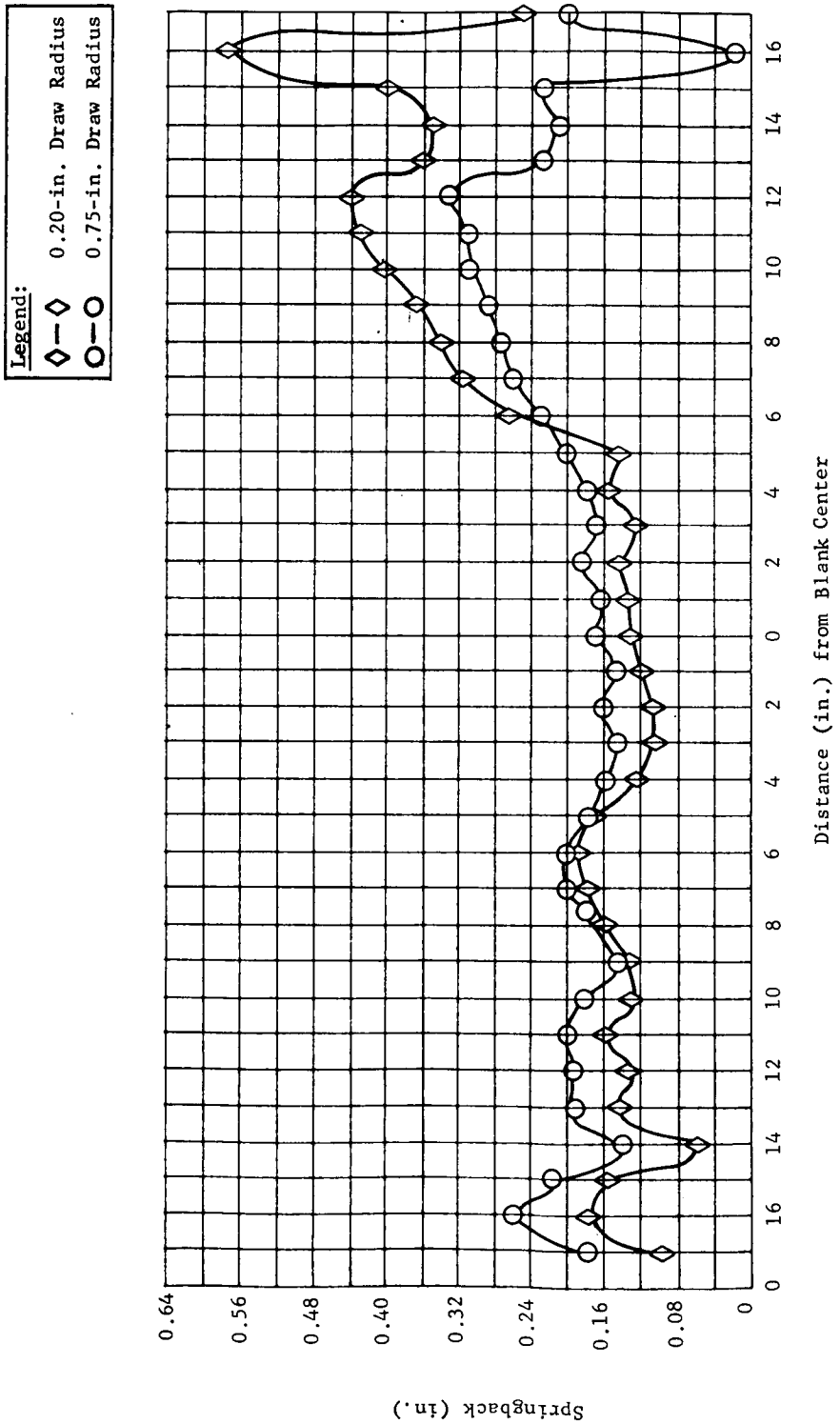

Fig. 29 Effect of Draw Radius on the Springback of 0.250-in. Thick 2219-T31 Aluminum (4-in. Draw Radius)

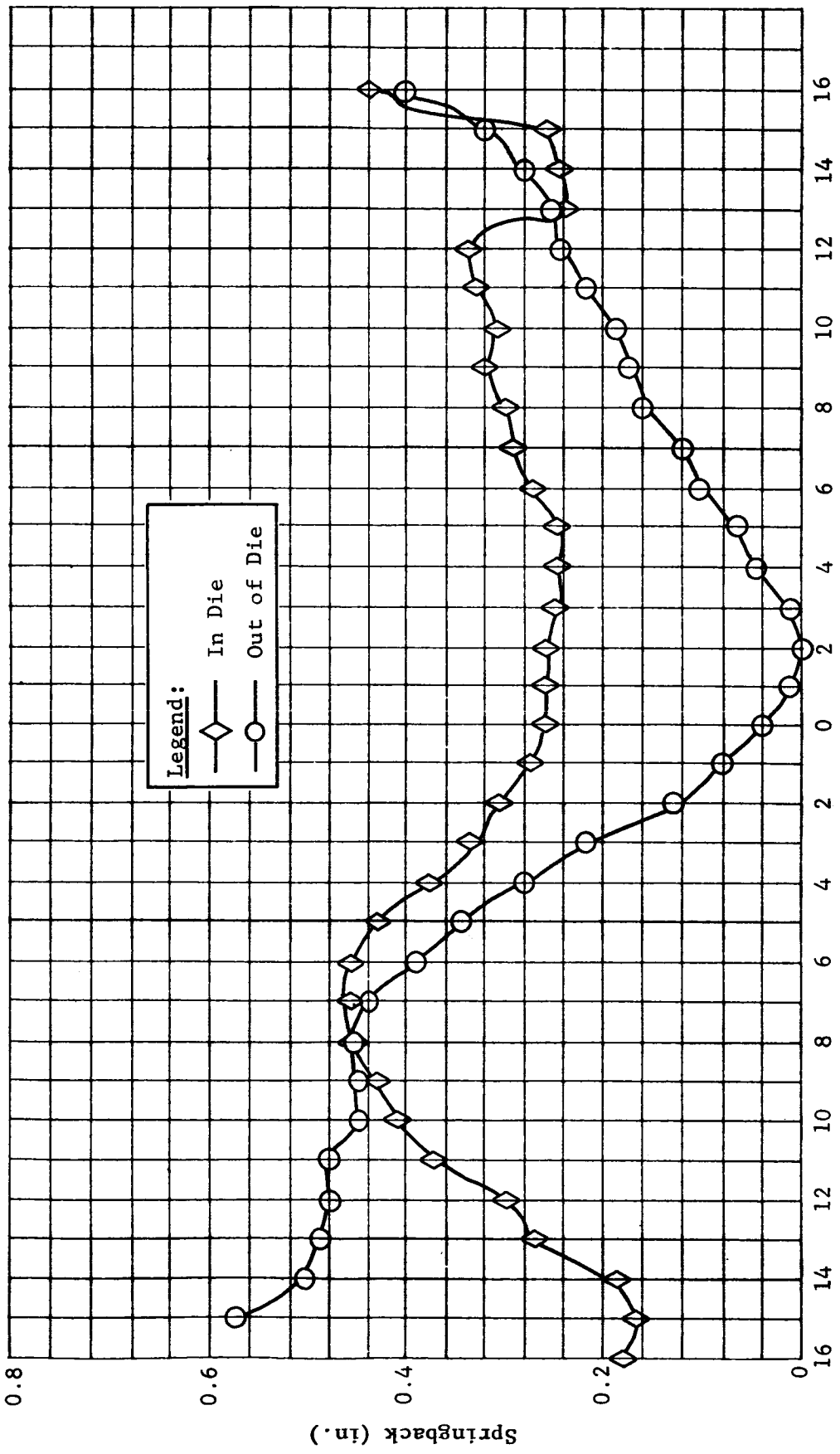

Fig. 30 Influence of Flange Distortion on Metal Springback

One blank each of 2219-T31 in thicknesses of 0.090 and 0.250 in. were formed in the concrete die. The data did not permit a valid comparison between meehanite and concrete die materials due to the failure of the die during experimentation. Figure 31 shows the measured springback resulting from the two sets of forming experiments. Note that the measurements taken on the concrete die involved several negative values. This could have been due to die movement caused by the formation of a crack.

Although springback may be reduced by the use of concrete dies, there are several inherent disadvantages in the use of concrete:

1) Evacuation of the die cavity is more difficult than for metal dies:

2) Design is more critical since shock loading produces high loads that are difficult to accommodate;

3) For forming more than 25 parts, concrete cannot withstand the additional repeated loading necessary.

It is well known that concrete withstands rather high loads in compression but cannot tolerate tensile stresses of very high magnitude. Therefore, it is essential in the design of a concrete die to construct the tool so the primary forces acting on the concrete are compressive in nature. This can be accomplished by encasing the concrete in a steel shell. The acoustic impedence of the concrete relative to the steel shell is such that the shock waves are reflected from the die surfaces as compression waves.* Thus, with proper design, concrete can be used effectively in explosive forming operations for limited production runs. More experiments are necessary to establish the necessary criteria for optimum die design. For the purpose of this contract the concrete die used was not satisfactory since conclusive data on reduction in metal springback could not be obtained.

*Acoustic impedance is the product of the density of the material and the velocity of sound in the material. Compressive stresses can be produced by putting a material of low acoustic impedance within a material of higher acoustic impedance; i.e., concrete in steel.

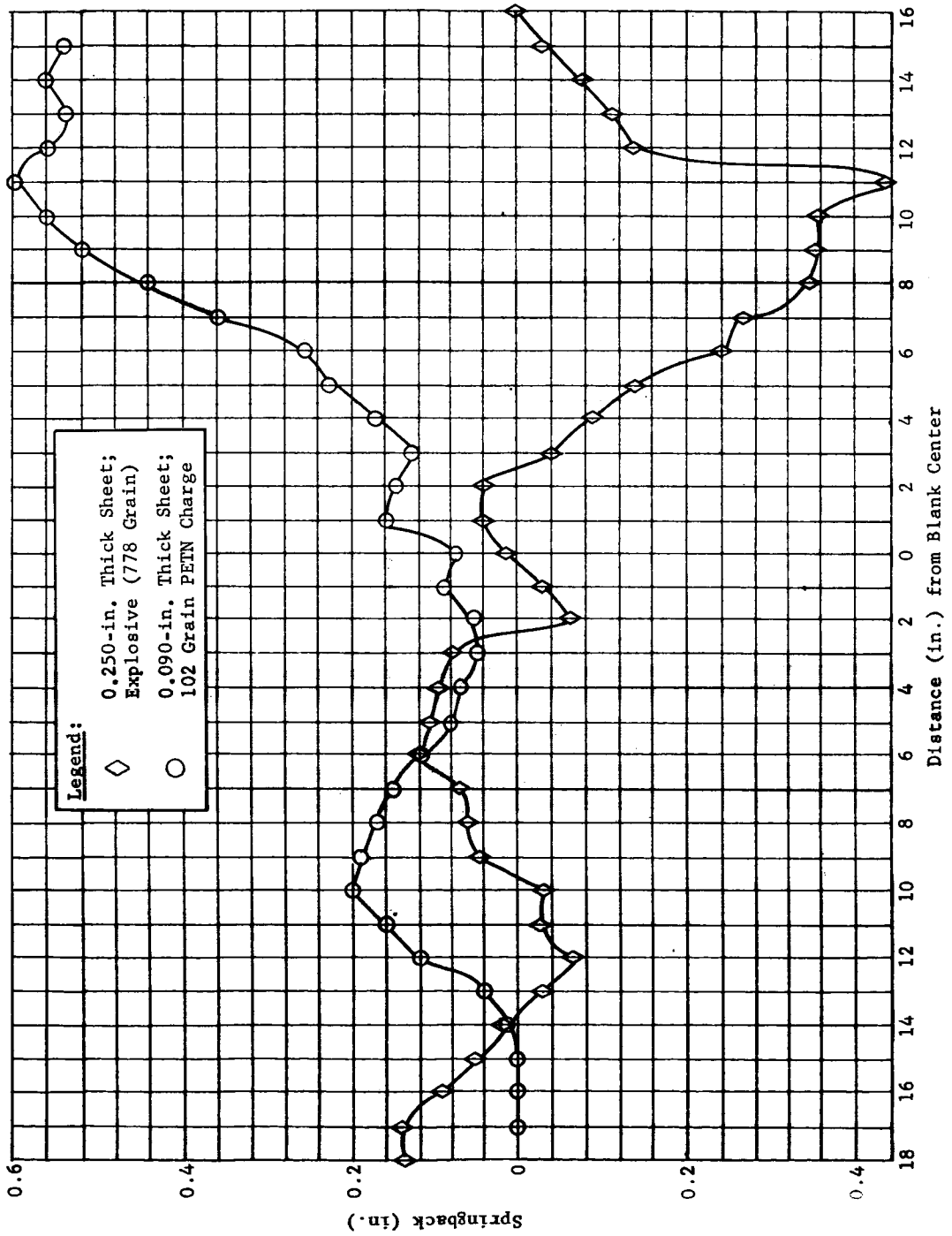

Fig. 31 Effect of Die Material on Springback for 2219-T31 Aluminum Sheet and Plate (Concrete Die)

6. Effect of an Integral Blanket

A concept for the possible reduction of metal springback was studied during the experimental program. Basically, the idea involves the application of a layer of material over the metal blank to be formed in such a way as to raise the neutral axis of the composite section above the metal interface. By shifting the neutral axis to a position above the metal blank, one can effect complete plastic deformation with the subsequent reduction in springback. This concept has been called an integral blanket.

There are several aspects of the blanket material that must be considered to effect the necessary shift in the blank neutral axis. In general, the thickness of the blanket material is an inverse function of its modulus of elasticity; i.e., a lower modulus material requires a greater thickness, while raising the modulus permits the use of a thinner layer of material. The thickness relationships are influenced by the yield strength of the blank material as well as its physical characteristics. A factor which strongly influences the integral blanket thickness is the ratio of blank radius of curvature to blank thickness. The relationship for aluminum of two different strength levels is shown in Fig. 32 and 33.

In order to establish the merit of the integral blanket concept in the explosive forming of 2219-T31 aluminum, experiments were conducted using 10.5-in. diameter blanks on a die having a 30-in. spherical radius. Blanket materials of neoprene rubber (both 40 and 80 Durometer hardness), lead, and polyurethane rubber were used to evaluate the influence of modulus of elasticity on the efficiency of the blanket. No holddown was used on the die since maximum springback was desired to permit a determination of any springback reduction resulting from the use of the integral blanket. The thicknesses of integral blankets required for different materials are given in Fig. 32 and 33. The results are summarized in Table 4 and are shown in Fig. 34. No valid conclusion can be drawn from such limited data. Limitations of time and money did not permit the additional experimental work needed to clarify the results.

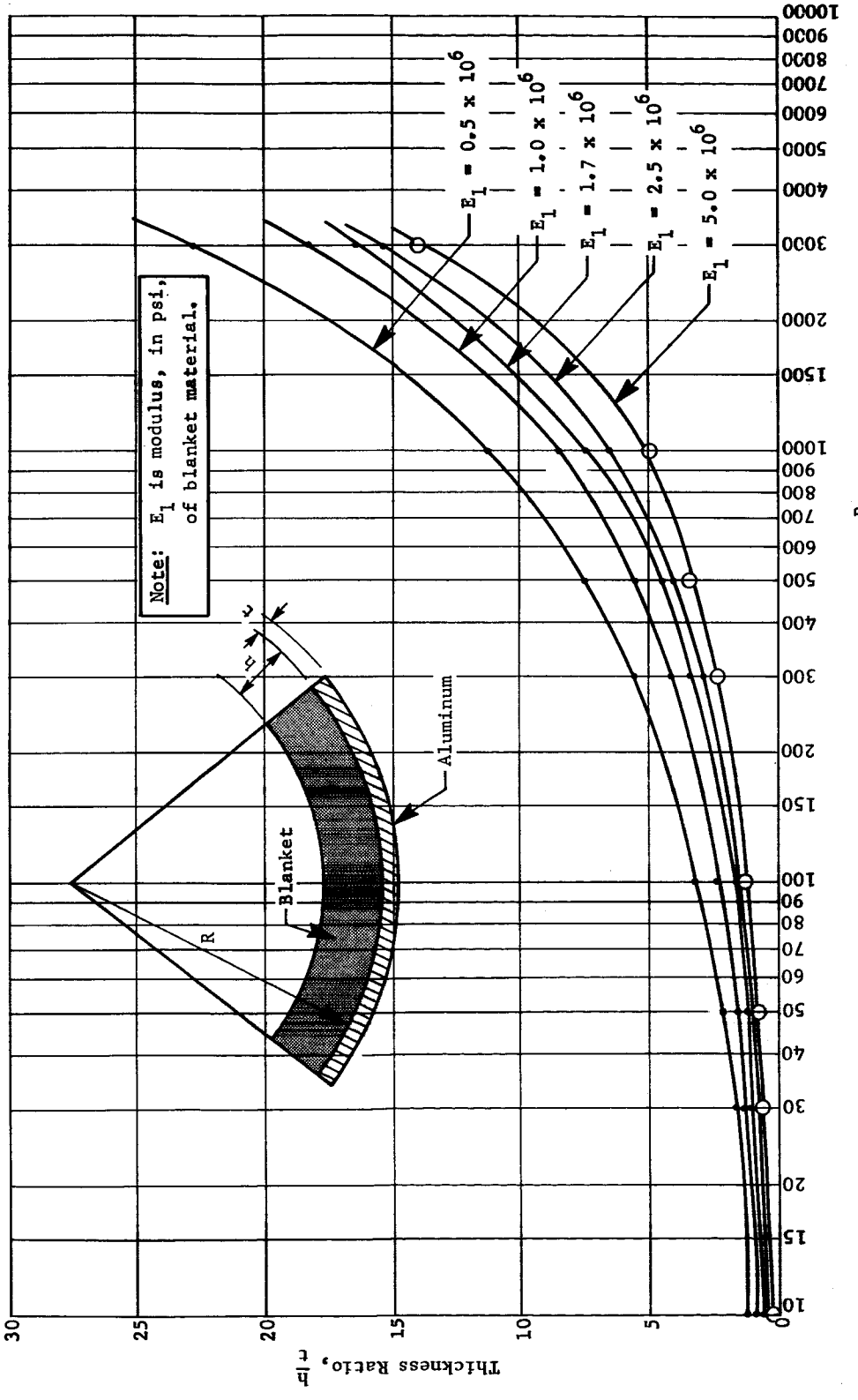

Fig. 32 Relation of Blanket Thickness to Blank Thickness for Various Blanket Materials (20,000-psi Yield Strength Aluminum)

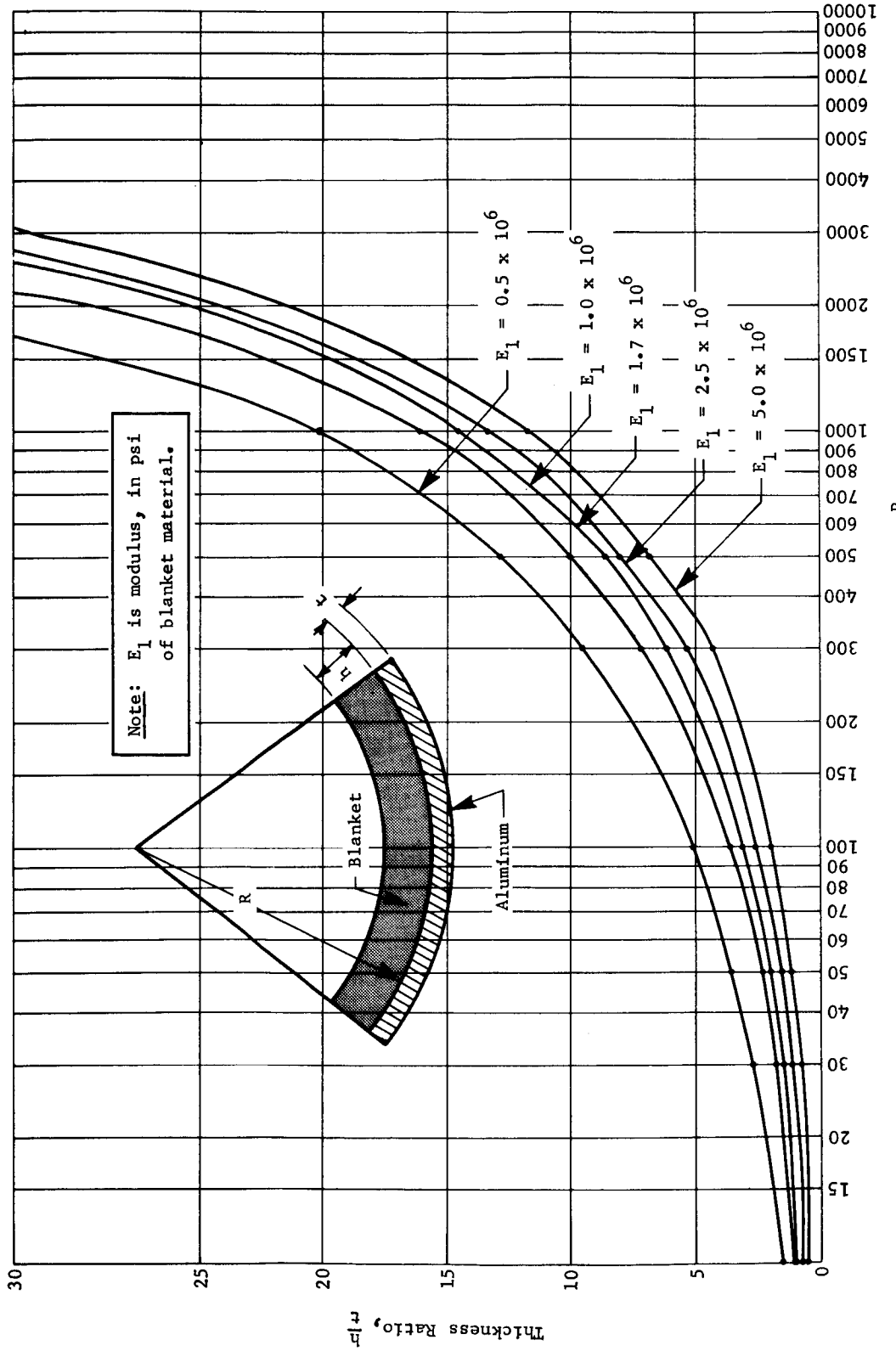

Fig. 33 Relation of Blanket Thickness to Blank Thickness for Various Blanket Materials (50,000-psi Yield Strength Aluminum)

Table 4 Springback as a Function of Blanket Material for 2219-T31 Aluminum, 0.132-in. Thick

Specimen	Deviation from Die Contour Measured at the following Distances from the Center,				Modulus of Blanket Material x 10^6 psi	Charge (grains)
	1 in.	2 in.	3 in.	4 in.		
No Blanket	0.004	0.004	0.012	0.043	---	50
No Blanket	0.003	0.005	0.004	0.001	---	150
No Blanket	0.015	0.031	0.020	0.022	---	100
Lead	0.017	0.046	0.084	0.123	2.5	100
Lead	0.019	0.023	0.059	0.100	2.5	50
40 D Rubber	0.009	0.012	0.019	0.034	0.5	50
40 D Rubber	0.018	0.019	0.014	0.019	0.5	100
40 D Rubber	0.020	0.019	0.020	0.020	0.5	50
40 D Rubber	0.019	0.018	0.022	0.020	0.5	150
40 D Rubber	0.022	0.025	0.018	0.020	0.5	50
80 D Rubber	0.021	0.016	0.016	0.028	0.5	50
80 D Rubber	0.021	0.018	0.020	0.020	0.5	100
Polyurethane	0.019	0.014	0.019	0.037	0.5	100
Polyurethane	0.013	0.016	0.014	0.019	0.5	150
Polyurethane	0.013	0.017	0.020	0.019	0.5	50

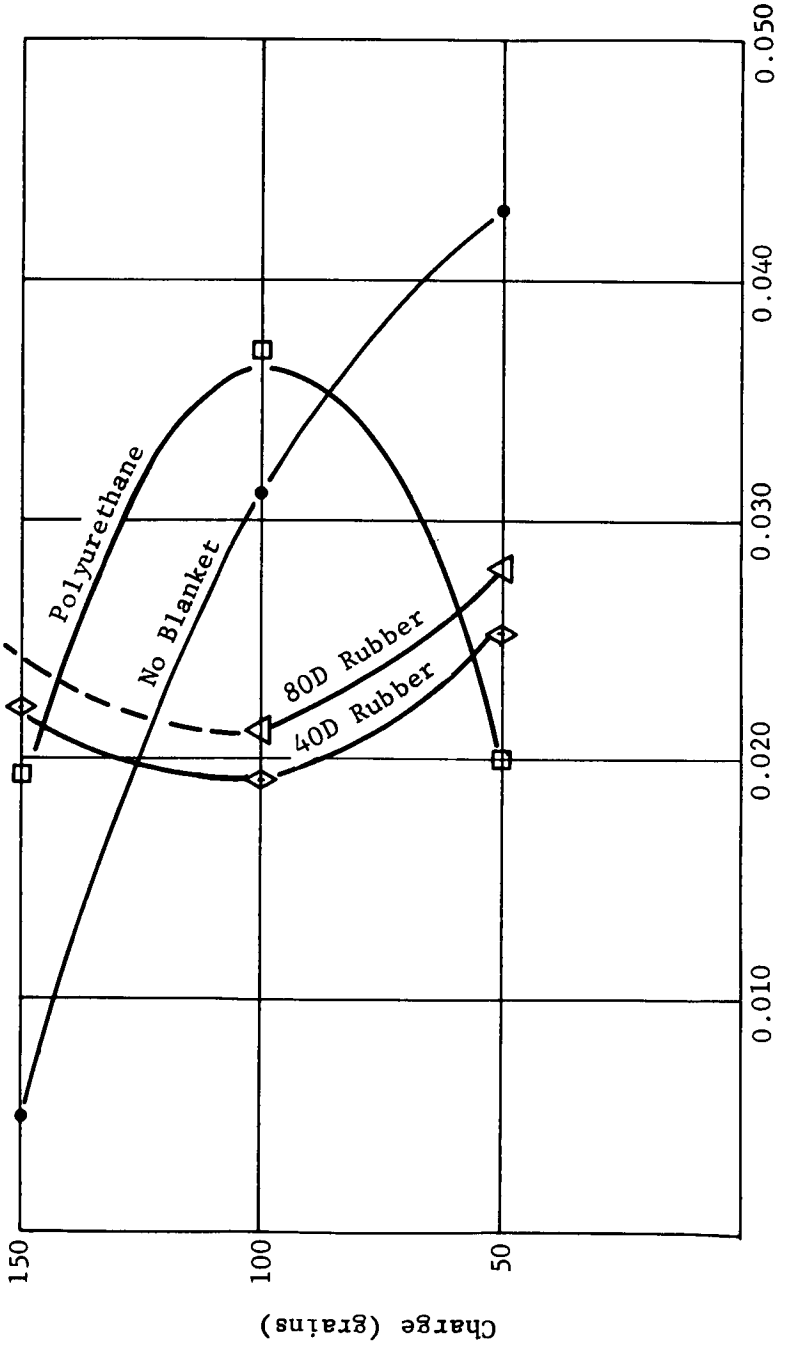

Fig. 34 Results of Integral Blanket Tests

It is possible that the frictional forces at the interface between the integral blanket and the metal blank were not high enough to resist the horizontal shear that would result from composite action of blanket and blank. This would reduce the effectiveness of the blanket in raising the neutral axis above the metal interface and increasing the plastic deformation in the metal. A possible technique for providing resistance to horizontal shear at the blanket-metal interface is shown in Fig. 35. It may be worth investigating this concept in a future program

7. Alloy Temper

Four 2219 tempers (2219-0; 2219-T42, 2219-T351, and 2219-T37) were investigated for effects of springback.

It was anticipated that the annealed 2219 would be relatively simple to form and would therefore exhibit the least springback of any of the tempers. This was not true however since most of the series of tests produced parts from harder tempers that had more desirable contours and less springback. The annealed 2219 was evaluated primarily for comparison purposes because it was apparent that the strain induced by forming would be lost during the solution heat treating process. Initially, the contour measurements from the 2219-T42 material indicated that it would be the optimum temper to complete the remaining steps in the contract. It was determined, however, after tensile specimens had been taken from panels with low percentages of springback, that the minimum 2219-T87 properties could not be achieved after aging. Apparently the strain plus hardening induced by explosive forming was insufficient to provide the necessary 7 to 10% cold work. A charge of 4320 grains of Cyadyn 3 was used for a test in the attempt to increase the cold work produced by explosive forming. The properties were increased in the 2219-T42 panel, however the yield strength remained 3000 psi below minimum. An additional disadvantage of using such an excessively large charge was the accompanying surface damage to the blank. The springback, presumably from rebound, was also greater than that produced with charges a fraction of the size of the 4320 grains charge.

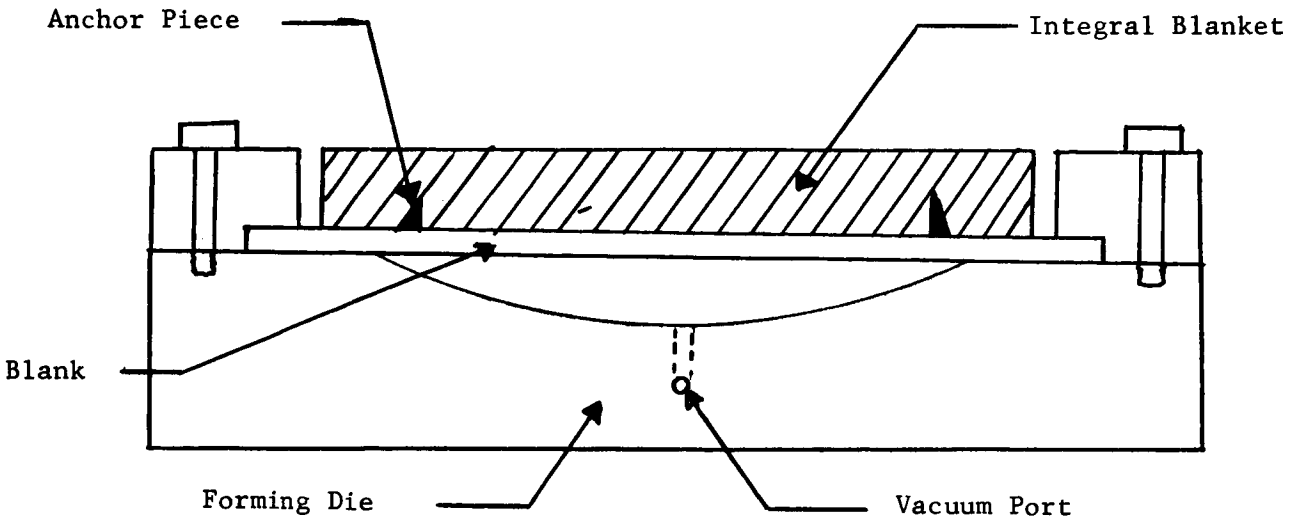

Fig. 35 Technique for Release of the Integral Blanket after Blank Deformation

It then became necessary to select a temper containing cold work before forming for optimization of springback. The 2219-T351 blanks formed after charge and standoff parameters had been established showed smaller percentages of springback than any other temper. The 2219-T351 produced the best part contours and least springback of the four tempers when the best series utilizing sheet explosive was developed. The sheet explosive also induced the necessary cold work into the 2219-T351 blanks for response to full 2219-T87 properties subsequent to aging. Figure 36 shows a comparison of springback for the various tempers. The 2219-T37 material was the most difficult to form as was anticipated. The high yield strength possessed before forming made this material extremely resistant to plastic deformation, which subsequent strain measurements confirmed. This material consistently produced the highest springback percentages in the majority of tests. Adjustments were made in the related parameters in an attempt to reduce the percentage of springback of this temper, however the resulting springback realized remained excessive.

In conclusion, the 2219-T351 was selected as the temper to complete the remaining steps in the contract not only because of its low springback characteristics but also because it responded well to aging after forming.

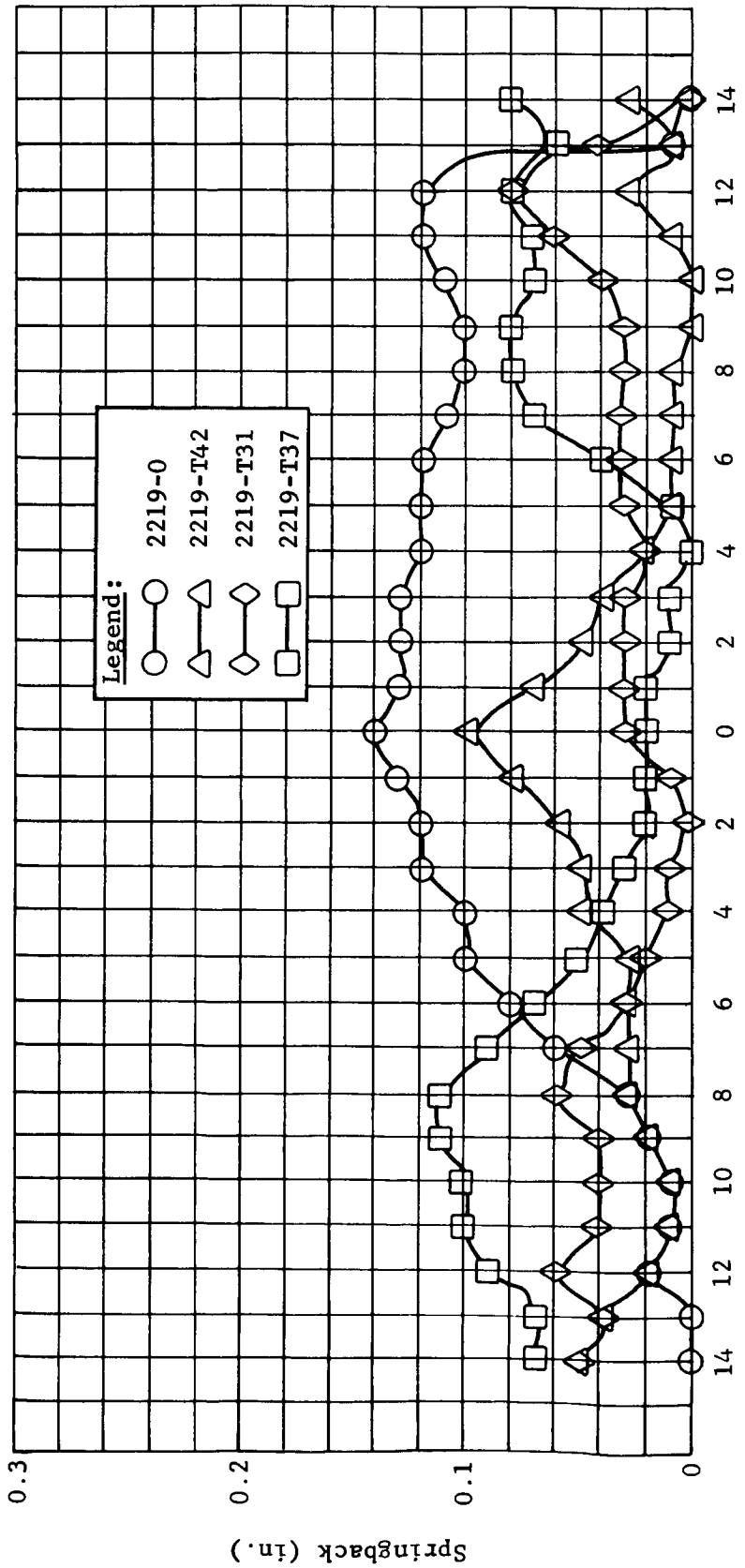

Fig. 36 Comparison of the Various Tempers of 2219 Aluminum Showing the Best Springback Achieved

B. METALLURGICAL EFFECTS

1. Metallographic Studies

a. Optical Microscope

Standard metallographic techniques using the optical microscope permitted the observation of microstructural changes resulting from explosive deformation. As outlined in Chap. II, some of the material obtained from NASA was quite variable with respect to grain size and these variations were reflected in the attendant mechanical properties. Thus a variable was introduced into the program over which very little control could be exercised. Subsequent heat treatment of the as-received material did not result in the full response of all alloy tempers indicating the significant influence of variation in properties and microstructure on alloy behavior.

Using the light microscope it was difficult to observe any significant changes in microstructure resulting from explosive forming. Some grain elongation caused by cold reduction was about the only observable change found. Figure 37 thru 39 illustrate the grain changes caused by plastic deformation of the 2219 alloy plate. Note that for both the 2219-T42 and 2219-T37 materials the effects of forming are quite apparent. Little change can be seen between the as-received and the explosively-formed 2219-T351 samples. Since the use of the light microscope appeared to be of little value in evaluating microstructural changes occurring from high velocity metal deformation, structural changes were subsequently studied using transmission electron microscopy and x-ray diffraction techniques, which are described in the following paragraphs.

a. As Received

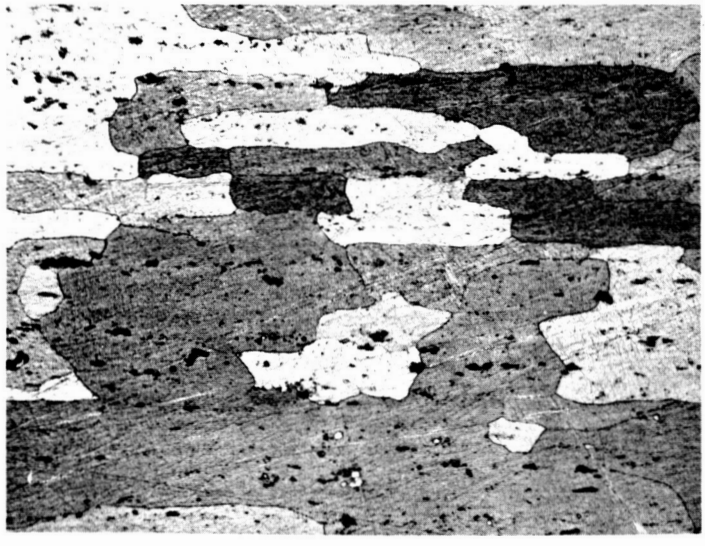

b. Explosively Formed

Fig. 37 Microstructure of 2219-T42 Aluminum Plate, Longitudinal Grain Direction, 200x

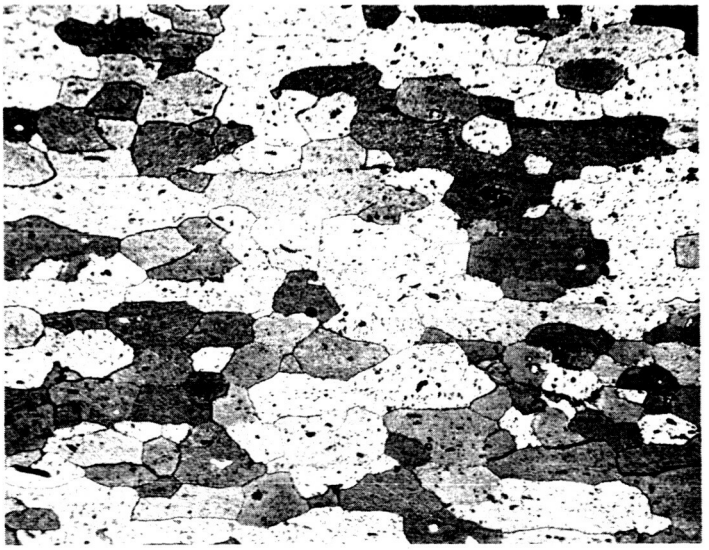

a. As Received

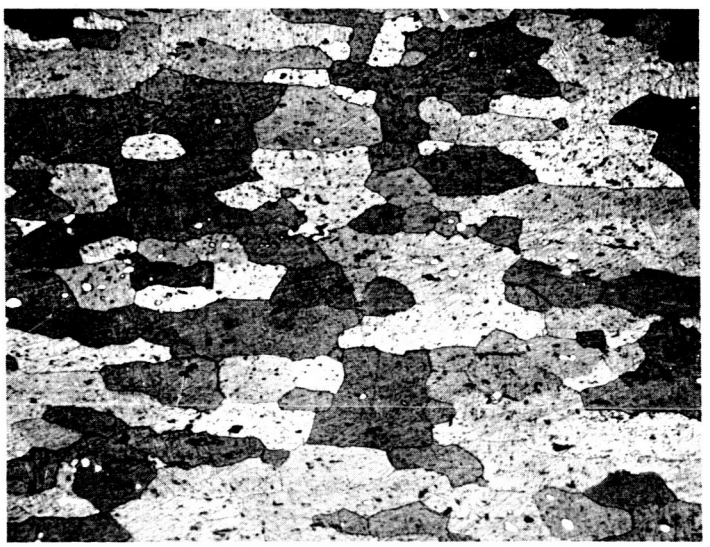

b. Explosively Formed

Fig. 38 Microstructure of 2219-T351 Aluminum Plate, Transverse Grain Direction, 200x

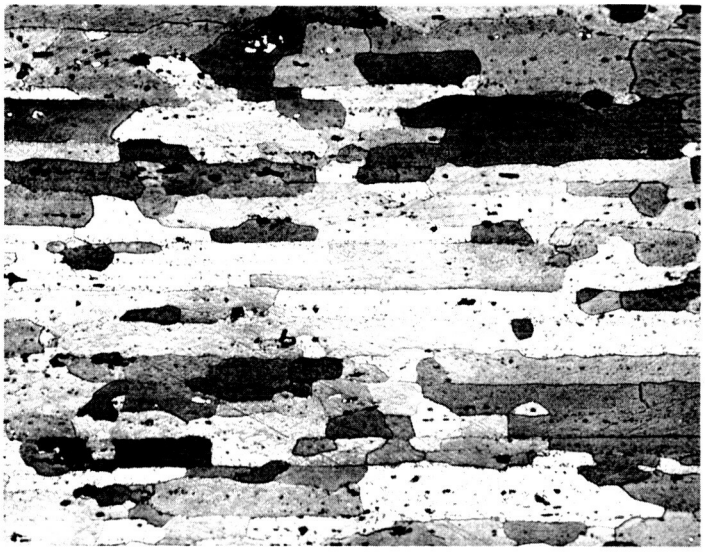

a. As Received

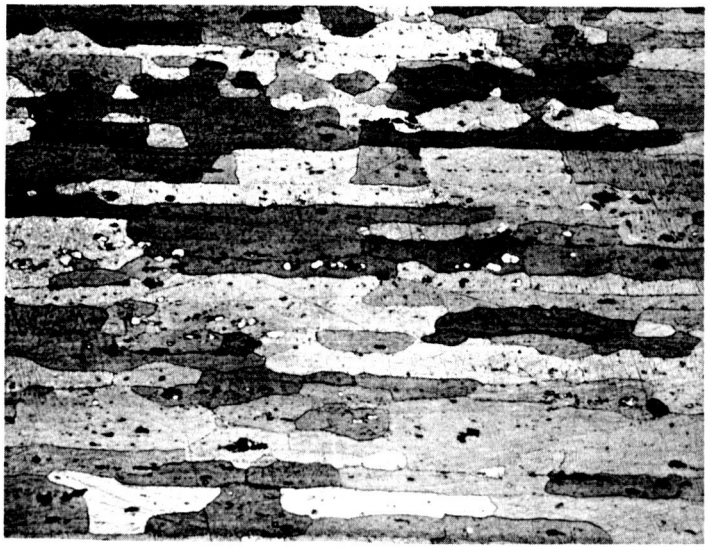

b. Explosively Formed

Fig. 39 Microstructure of 2219-T37 Aluminum Plate, Longitudinal Grain Direction, 200x

b. Crystallographic Imperfections in 2219 Aluminum Produced by Explosive Forming

The anticipated types of crystallographic imperfections induced by explosive forming 2219 Aℓ are specifically:

1) Dislocations;

2) Stacking faults (planar atomic stacking mistakes);

3) Twins, both microscopic and macroscopic;

4) Microcracks;

5) Point defects, such as, vacant atomic sites or simply vacancies.

The types of imperfections induced in 2219 Aℓ by explosive forming are illustrated in Fig. 40. The metallurgical treatment of the specimen shown in Fig. 40 is annealed, slow-cooled, and explosively-formed, in that order. The fine black lines; e.g., at "A" are dislocations generated by the forming operation. The stable precipitate θ results from the approach of the alloy to equilibrium by slow cooling. The metastable θ' phase is only in evidence at isolated regions. The presence of an excess concentration of vacancies is inferred by dislocation loops that can be formed by vacancy segregation followed by a dislocation reaction involving partial dislocations. Dislocation loops that are thought to have formed by vacancy migration are seen at "B" in Fig. 40. The probable source of excess vacancy concentration is the mechanism of stress-induced climb of jogs on screw dislocations. Such a mechanism is favored by the application of impulsive loading inherent in explosive forming. Although jogs on dislocations cannot be resolved, due to their small size (<10 angstroms), their presence is strongly implied by the cusps seen at "C" on most of the dislocations. The influence of excess concentrations of vacancies in explosively formed 2219 Aℓ on the desired mechanical properties achieved through aging is discussed later.

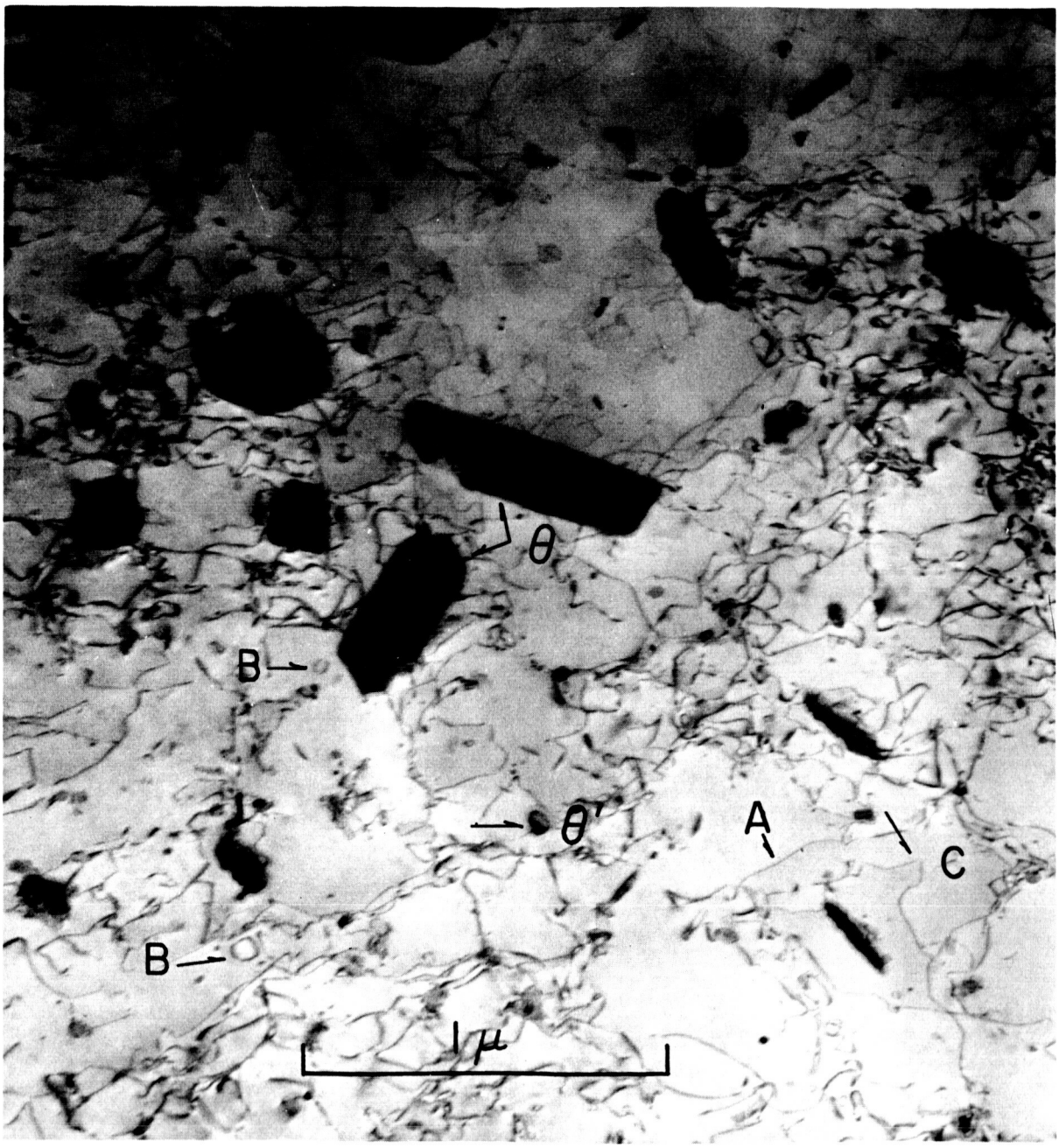

Fig. 40 Transmission Electron Micrograph of 2219 Aluminum, Annealed, Slow Cooled, and Explosively Formed Showing Metastable θ', Stable θ, and Dislocations Induced by Explosive Forming

The effectiveness of θ' as a barrier to dislocation movement is illustrated in Fig. 41 at "A." The orientation of the crystal in Fig. 41 affords a view of θ' platelets edge on. Since θ' precipitates on the $\{100\}$ planes of the aluminum matrix, one θ' set is seen edge-on and the other two make angles of less than 90 deg to the foil surface. The banded appearance of the θ' is due to the presence of dislocations at the interface. The origin of these dislocations is uncertain, since they could result from incoherency strains between θ' and the matrix or could result from intersections of moving dislocations with θ'.

The anticipated types of crystallographic imperfections listed previously were never observed in any of the more than 300 transmission micrographs taken of explosively-formed 2219 Aℓ. The most obvious imperfections introduced by explosive forming 2219 Aℓ are dislocations. In some regions of the deformed specimens dislocation densities in the range of 10^{11} to 10^{12} lines/cm^2 have been observed. The presence of excess vacancies produced by explosive forming is apparent by their influence on dislocations (loop formation) and on the acceleration of diffusion in the aging process. The detailed description of observations made during electron microscopy studies are presented in the following paragraphs.

Transmission electron microscopy specimens prepared from thin-foil sections were studied to determine the nature and distribution of precipitate, dislocation densities, and orientation effects caused by explosive deformation. Alloy tempers studied were 2219-0, 2219-T42, 2219-T351, 2219-T37, and 2219-T81. Direct observations of the precipitation process during aging were made by using the heating stage of the electron microscope.

2219-0 Aluminum - Figure 42 shows a typical transmission micrograph of undeformed 2219-0 aluminum. The large precipitate visible is the θ phase of this alloy system. At areas typical of "A" in the micrograph, one can see a much smaller precipitate (500 to 50 Å in size). These particles of θ' phase are the most effective in pinning dislocations and increasing the alloys resistance to plastic deformation. The effectiveness of the θ' particles in pinning dislocations is illustrated in Fig. 43 where several examples of precipitate-dislocation interaction can be seen in the upper left and right center of the micrograph. An energetically-stable distribution of dislocations in the form of quasi-hexagonal networks is shown in Fig. 44. These networks are indicative of an annealed material.

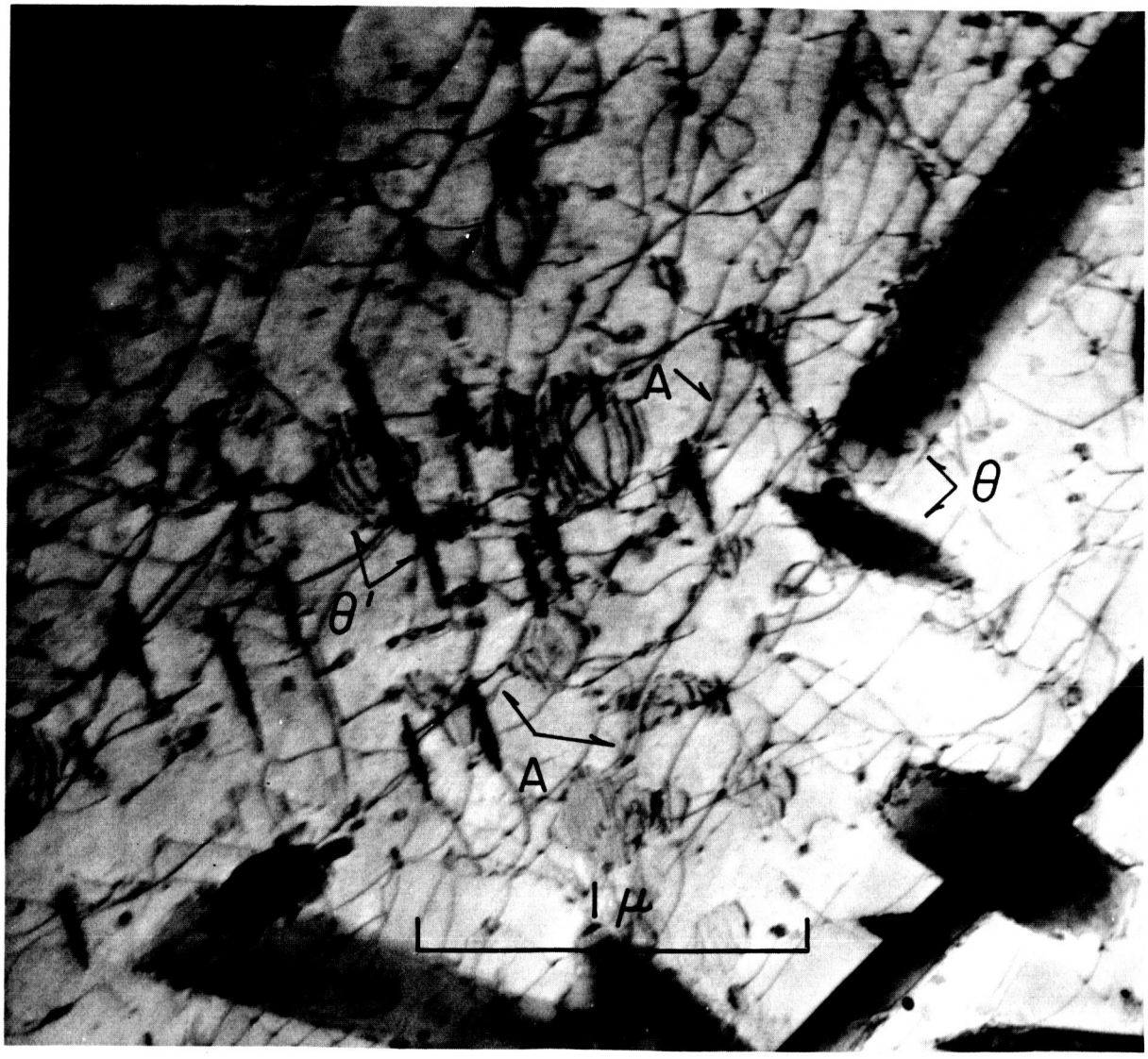

Fig. 41 Transmission Electron Micrograph of 2219 Aluminum, Annealed, Slow Cooled, and Explosively Formed, Showing the Effectiveness of θ' Precipitates as Barriers to Dislocation Motion

Note: 1. Diffraction index shown at the right.
2. Foil normal is given by the Miller indices in brackets.

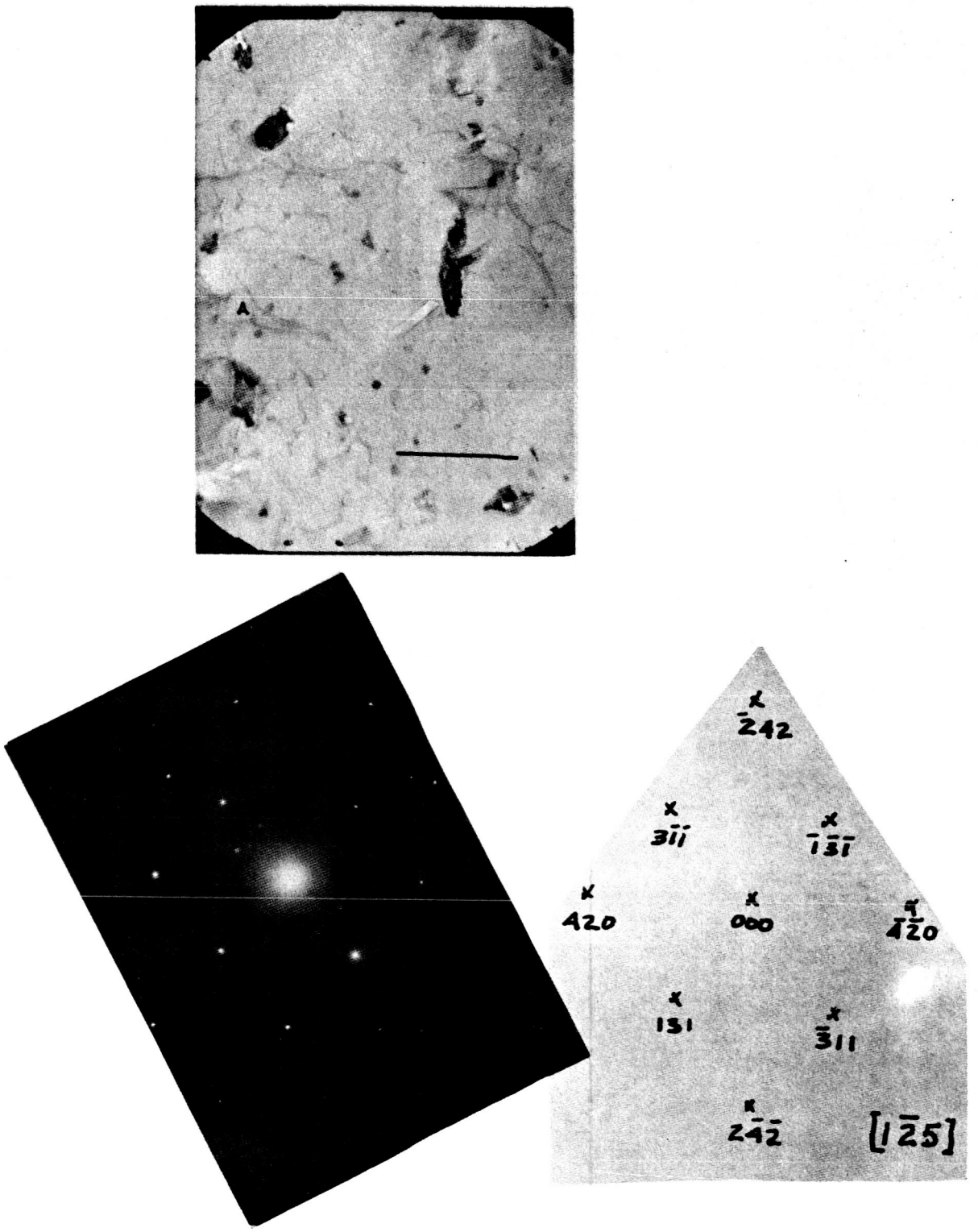

Fig. 42 Transmission Photomicrograph of Undeformed 2219-0 Aluminum Showing θ and θ' Phases

Note: 1. Diffraction index shown at the right.
2. Foil normal is given by the Miller indices in brackets.

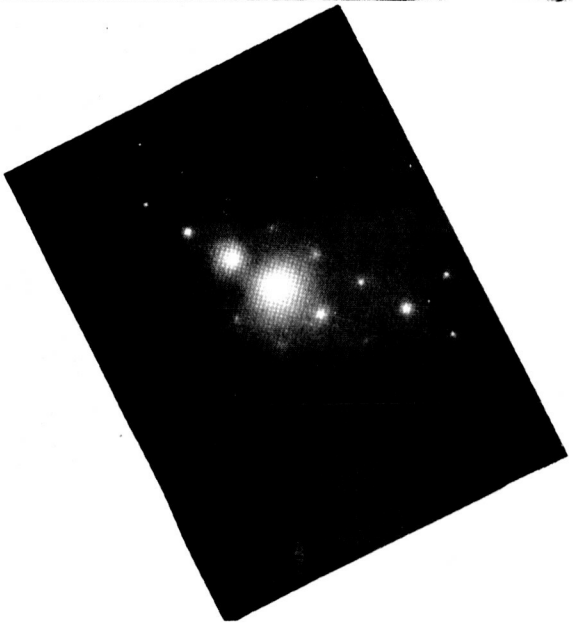

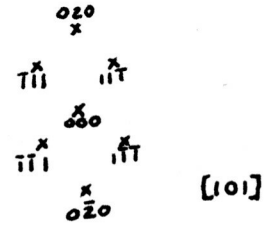

Fig. 43 Examples of Dislocation Pinning by θ' Precipitate

Note: 1. Diffraction index shown at the right.
2. Foil normal is given by the Miller indices in brackets.

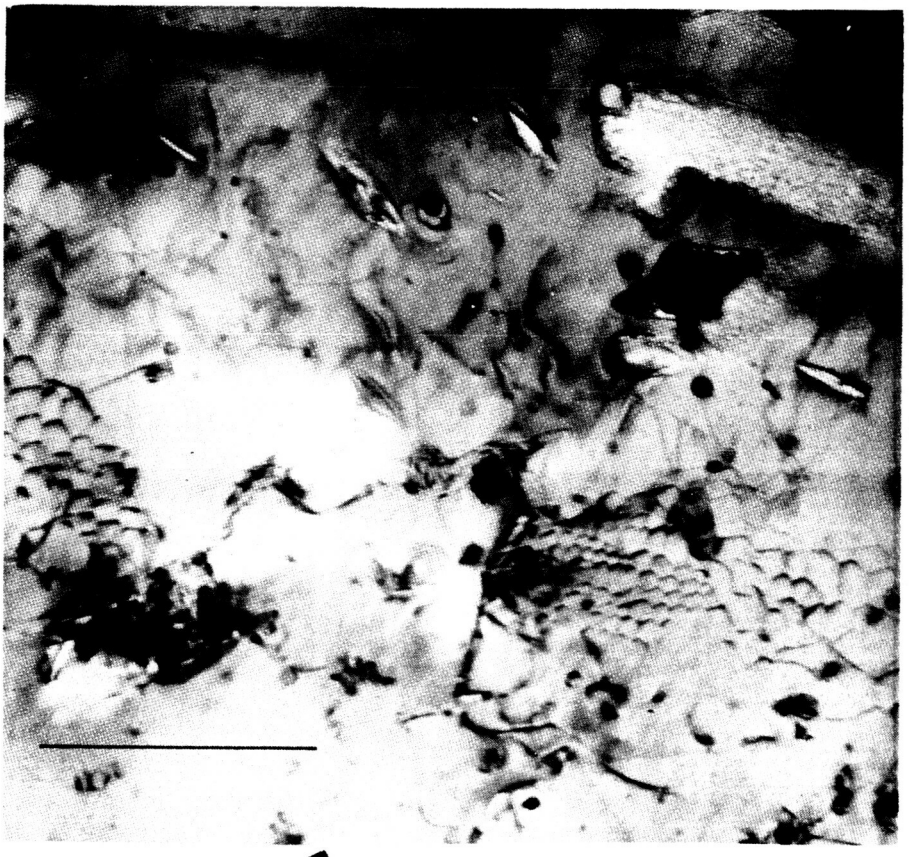

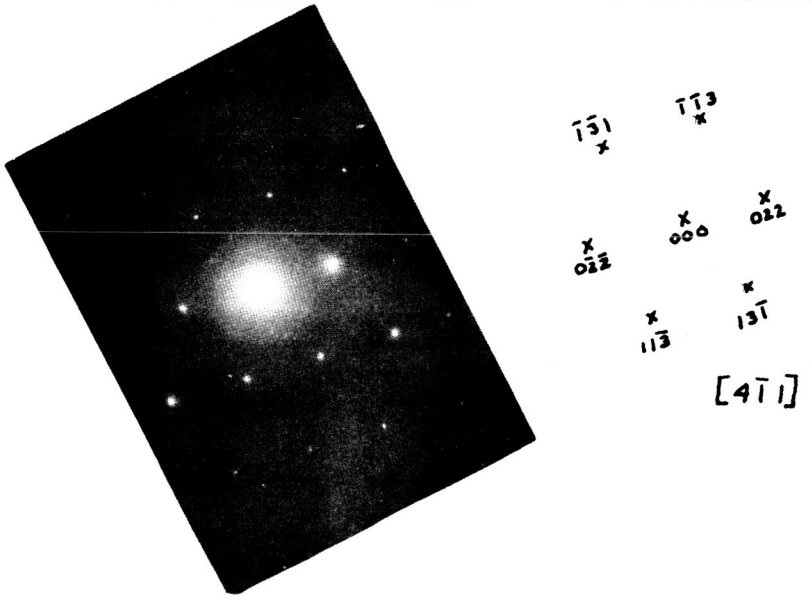

Fig. 44 Dislocations in the Form of Quasi-Hexagonal Networks Illustrating an Energetically Stable Distribution

In the preparation of thin foils, one sometimes encounters problems with foil deformation caused by local bending effects. Figure 45 illustrates bend contours shown by the dark bands (extinction contours). The influence of the local bending of dislocation formation is clearly evident by the dislocation array along the bend contours. It is important to prevent local bending of the thin foil samples during preparation since influences of high energy deformation cannot be accurately established if the starting material structure is disturbed.

Specimens were taken from explosively-formed 2219-0 aluminum blanks at positions near the blank apex. Areas were selected based on the amount of plastic deformation imposed on the blank to permit the evaluation of maximum effects resulting from explosive forming. Figure 46 is a typical transmission photomicrograph of a sample taken from such an area. If one compares this micrograph with Fig. 42, it is quite evident that a significant increase in the number and complexity of dislocations occurs from explosive deformation. The θ' precipitates encourage dislocation tangling that impedes the plastic deformation of the alloy. Dislocation loops are also formed during high energy deformation. A correlation of the transmission microscopy results with tensile results confirms the expected greater resistance of the 2219-0 aluminum to plastic deformation. In the undeformed condition, the alloy exhibits properties as follows:

Ultimate tensile strength (KSI)	28.6 to 29.4
Tensile yield strength, 0.2% offset (KSI)	12.8 to 14.4
Percent elongation in 2 inches	23.5 to 24.0.

After explosive forming, there is only a small increase in ultimate tensile strength but the yield strength has increased about 6000 psi with a corresponding reduction in ductility. Results of specimens taken from explosively formed 2219-0 aluminum blanks were found to be:

Ultimate tensile strength (KSI)	29.1 to 29.6
Tensile yield strength, 0.2% offset (KSI)	18.3 to 20.9
Percent elongation in 2 inches	19.0 to 23.5.

Note: 1. Diffraction index shown at the right.
2. Foil normal is given by the Miller indices in brackets.

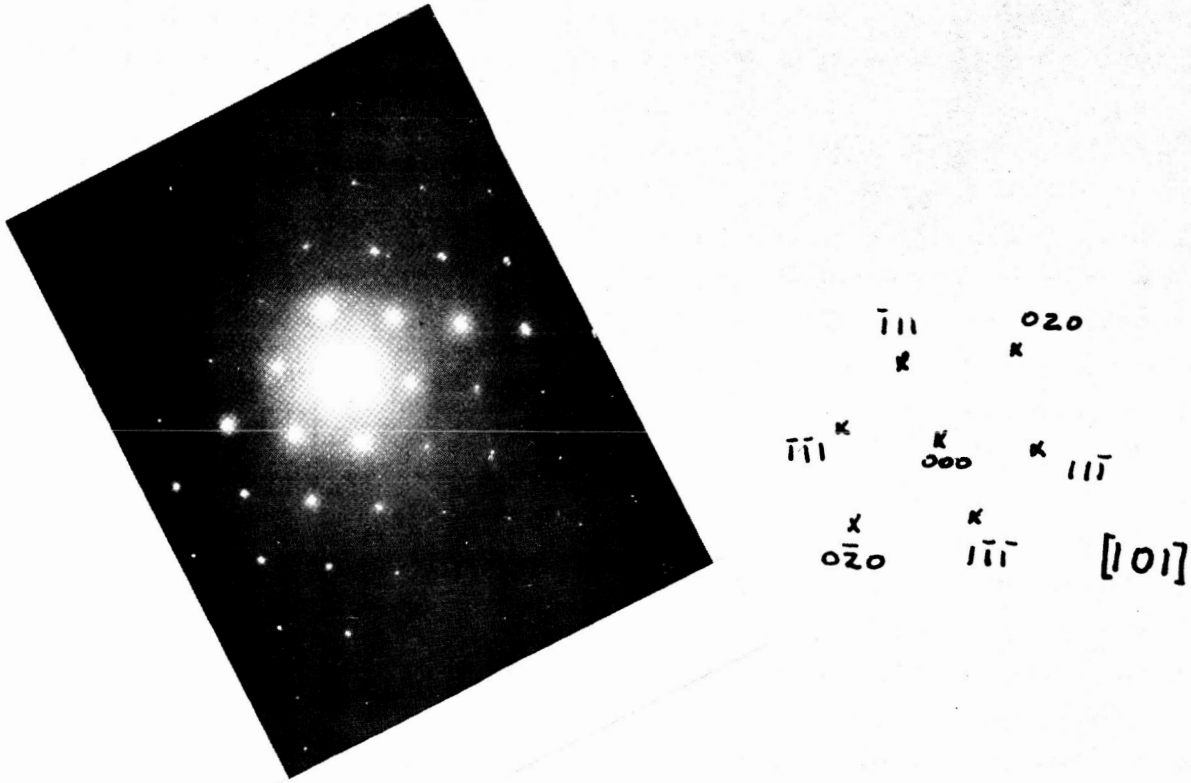

Fig. 45 Bend Contours (Extinction Contours) Resulting from Slight Local Bending of the Foil (Note Dislocations Along Extinction Contours)

Note: 1. Diffraction index shown at the right.
2. Foil normal is given by the Miller indices in brackets.

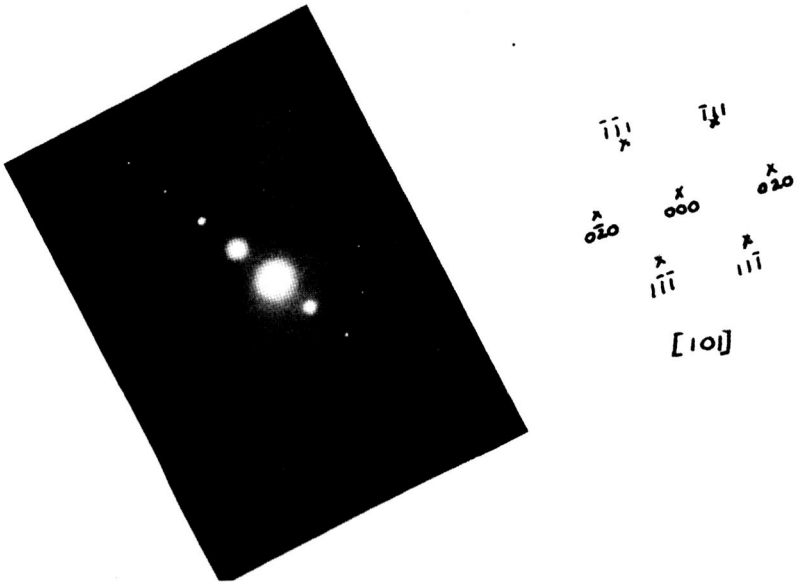

Fig. 46 Explosively Formed 2219-0 Aluminum Showing Complex Dislocation Networks and Dislocation Tangling Around θ' Precipitate

Thus, increases in tensile strength with attendant ductility reduction can be suitably explained by the presence of dislocation tangles and loops which, upon interaction, discourage plastic deformation.

c. Influence of Explosive Forming on Aging Behavior

Aging experiments were performed on 2219 Aℓ thin foil specimens of tempers T37, T42, and T351 in the undeformed and explosively-formed condition. These experiments were undertaken to determine possible changes in the aging behavior resulting from explosive forming. The specimens were aged in the heating stage of the microscope to allow direct observation of the precipitation process as it occurs.

The specimens were prepared from undeformed and explosively-formed panels by spark machining, spark planing, and electropolishing. The explosively-formed specimens were taken from the region of the formed dome apex.

Undeformed 2219 Aℓ of temper T37, T42, and T351 exhibit the following macroscopic mechanical properties:

	T37	T42	T351
Yield strength (0.2% offset)	38,000 psi	17,000 psi	28,000 psi
Ultimate tensile strength	49,000 psi	45,000 psi	46,000 psi
Elongation in 2 inches	20%	6%	6%

When fully aged, 2219 Aℓ of tempers T37, T42, and T351 in the nonexplosively-formed condition will exhibit the mechanical properties given below:

	T87 (Aged T37)	T62 (Aged T42)	T851 (Aged T351)
Yield strength (0.2% offset)	50,000 psi	36,000 psi	44,000 psi
Ultimate tensile strength	63,000 psi	54,000 psi	61,000 psi
Elongation in 2 inches	5%	6%	6%

The reason the mechanical properties increase upon aging is that the metastable θ' and the stable θ phases precipitate in the quenched Aℓ-Cu alloy to give a dispersed distribution of barriers to dislocation motion. Overaging occurs when the fraction of θ precipitates increases, since θ grows at the expense of θ' and the θ' is more finely distributed in addition to being a more effective barrier to dislocations than θ.

This precipitation process is a diffusion-controlled mechanism. Because diffusion rates are markedly increased by the presence of excess vacancies in the alloy, the aging time required in the explosively-formed alloy, to obtain a distribution of θ' corresponding to the aged mechanical properties, should be less than that for 2219 Aℓ in the undeformed condition.

As was mentioned previously, the source of the excess vacancies is the explosive forming, since explosive forming requires high dislocation velocities in the alloy, a high concentration of vacancies is expected in the alloy as a result of the stress-induced climb of jogs on screw dislocations. Thus, the aging process should be accelerated in the explosively-formed alloys. The determination of the magnitude of the acceleration forms the purpose of this series of aging experiments.

A point of criticism exists concerning conclusions based on precipitation observations in thin foils. The point is that precipitation processes occur more rapidly in thin foil specimens than in bulk form. The reasons for such behavior are:

1) The precipitation is occurring close to the surface that is a source of vacancies;

2) A thin foil is essentially a two-dimensional body; i.e., there is a lack of restraint in one dimension that aids precipitation of phases that introduce strains in the matrix crystal.

However, a comparison between the kinetics of precipitation processes between two thin foils of different metallurgical condition can be made. Hence, the results from a comparison measurement can be projected to give a reasonable prediction of the precipitation behavior in the bulk form of the alloy.

2219-T42 - Specimens were prepared from undeformed and explosively-deformed panels by spark machining, spark planning, and electropolishing. The explosively-formed samples were taken from the region of the formed gore apex.

The aging behavior of 2219-T42 in the undeformed condition at 325°F is shown as a function of time in Fig. 47a thru 47f. The plane of the foil, Fig. 47a thru 47c, is (001). Figures 47d thru 47f are from an adjacent crystallite in (110) orientation. Thus, the projected image of precipitates in this sequence appear different because of the difference in crystal orientation. The small angle boundaries at "A" in Fig. 47a and the isolated dislocations at "B" are typical features of this alloy in the solution heat-treated and quenched condition. The existence of some residual precipitates at "C" is an indication of incomplete solution heat treatment. However, since the volume fraction of residual precipitates is small, deleterious effects due to these, in subsequent metallurgical treatments, are unlikely. The rate at which residual dislocations are annealed out in these thin foils is shown in Fig. 47b where only a few dislocations remain after 4 minutes at 325°F. The precipitation and growth of θ' is seen to have occurred in 10 minutes in Fig. 47c. The traces of the θ' precipitates in Fig. 47c are consistent with the known habit planes of θ'; i.e., the (001) of the aluminum matrix. Figure 47d shows the extent of precipitation in 11 minutes in a crystallite in (110) orientation adjacent to the crystallite of precipitation in Fig. 47a thru 47c. There are two reasons why the extent of precipitation in Fig. 47d is greater than in Fig. 47c although the difference in elapsed time is only one minute. These are the foil thickness is greater in Fig. 47c and the orientation at Fig. 47d is such as to produce better precipitate contrast than in Fig. 47c. The thickness and length of θ' that lies normal to the foil; i.e., θ' precipitating on (001), has increased by a factor of about three in four minutes as seen by comparison of Fig. 47e with Fig. 47d. In the (110) orientation, θ' precipitating is projected in true thickness of θ' in Fig. 47e to give values ranging from 16Å up to 200Å. The distribution of θ' shown in Fig. 47f is representative of the fully-aged alloy that corresponds to the mechanical properties for 2219-T62.

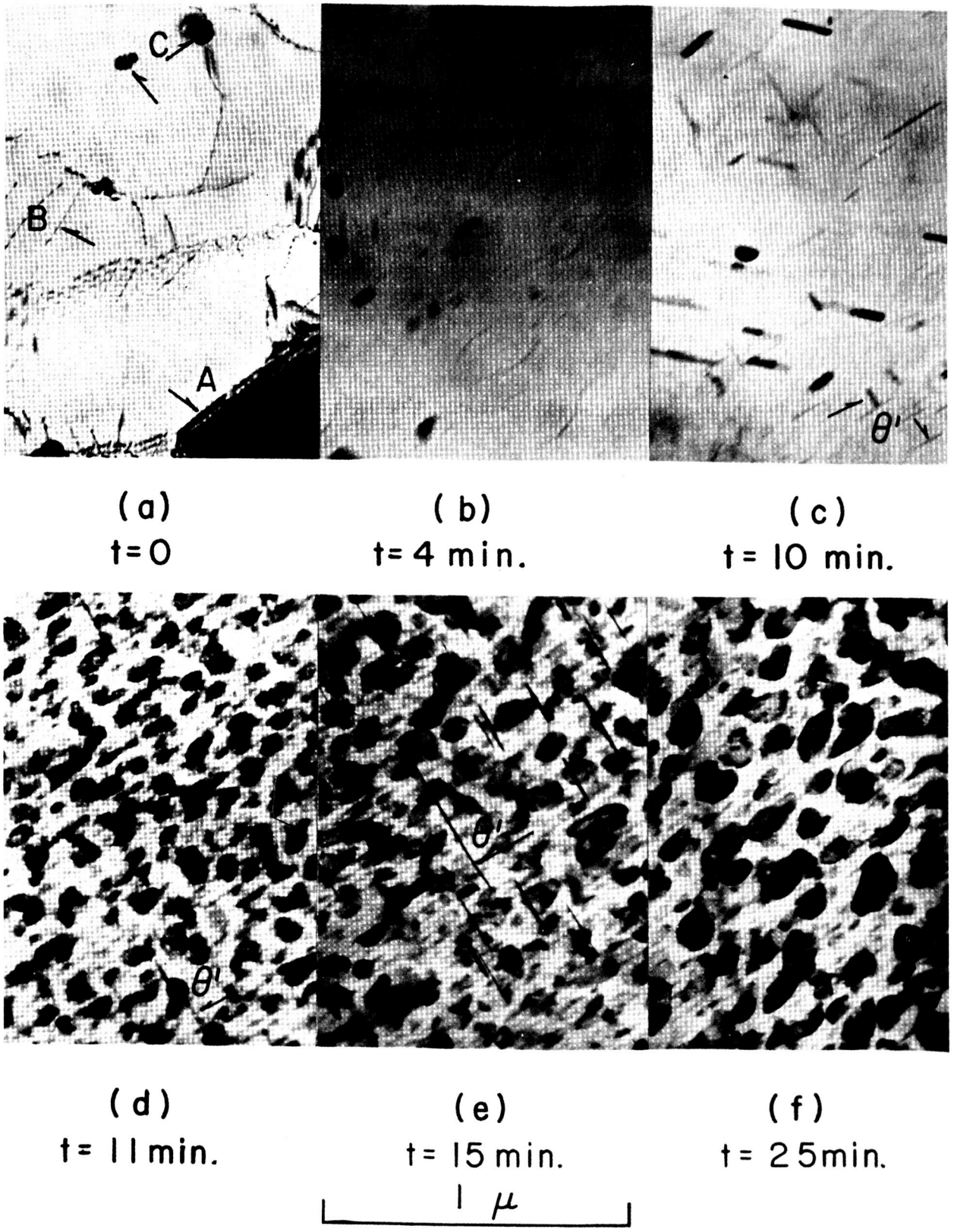

Fig. 47 Transmission Electron Micrographs of the Aging Behavior at 325°F of Undeformed 2219-T42 as a Function of Time

The aging behavior of 2219-T42 in the explosively-formed condition at 325°F is shown as a function of time in Fig. 48a thru 48f. After explosive forming, small angle crystallite boundaries (boundaries composed of simple geometric gridworks of dislocations) are unobserved because the dislocations in these boundaries have been dispersed by the forming operation. Figure 48a shows the dislocation distribution before aging. The plane of the foil in this sequence is (013). In this orientation, one of the three habit planes of θ' is normal to the foil surface. Therefore, one set of θ' platelets appear as dark streaks, as at "A" in Fig. 48d. The distribution of θ' as shown in Fig. 48c is representative of the fully-aged condition that exhibits the mechanical properties given for 2219-T62. The over-aged condition is suggested by the appearance of θ precipitates as seen in Fig. 48f. A comparison of Fig. 47 and 48 indicates that the aging process occurs by a factor of about 0.1 faster in the explosively-formed specimen. This difference in aging behavior is unlikely to produce any marked changed in the macroscopic mechanical properties when the aging treatment specified for 2219-T42 in the undeformed condition is applied to 2219-T42 in the explosively-formed condition.

2219-T351 - Some interesting observations were made during transmission electron microscopy studies of 2219-T351, which further justify the selection of the alloy temper for use in Saturn gore segment fabrication. These observations are summarized in the following paragraphs.

The aging behavior of 2219-T351 in the undeformed condition at 325°F is shown as a function of time in Fig. 49a thru 49f. The high density and rather even distribution of dislocations introduced in the solution heat-treated material by tensile stretching is shown in Fig. 49a before aging. Most of these dislocations have been annealed out at 325°F after 3 minutes, and the θ' is seen to start precipitating at "A" in Fig. 49b. The third set of θ' platelets are parallel to the foil surface and are responsible for the mottled appearance of the micrograph. The distribution of θ' as shown in Fig. 49f corresponds to the fully-aged condition that produces the mechanical properties of 2219-T851.

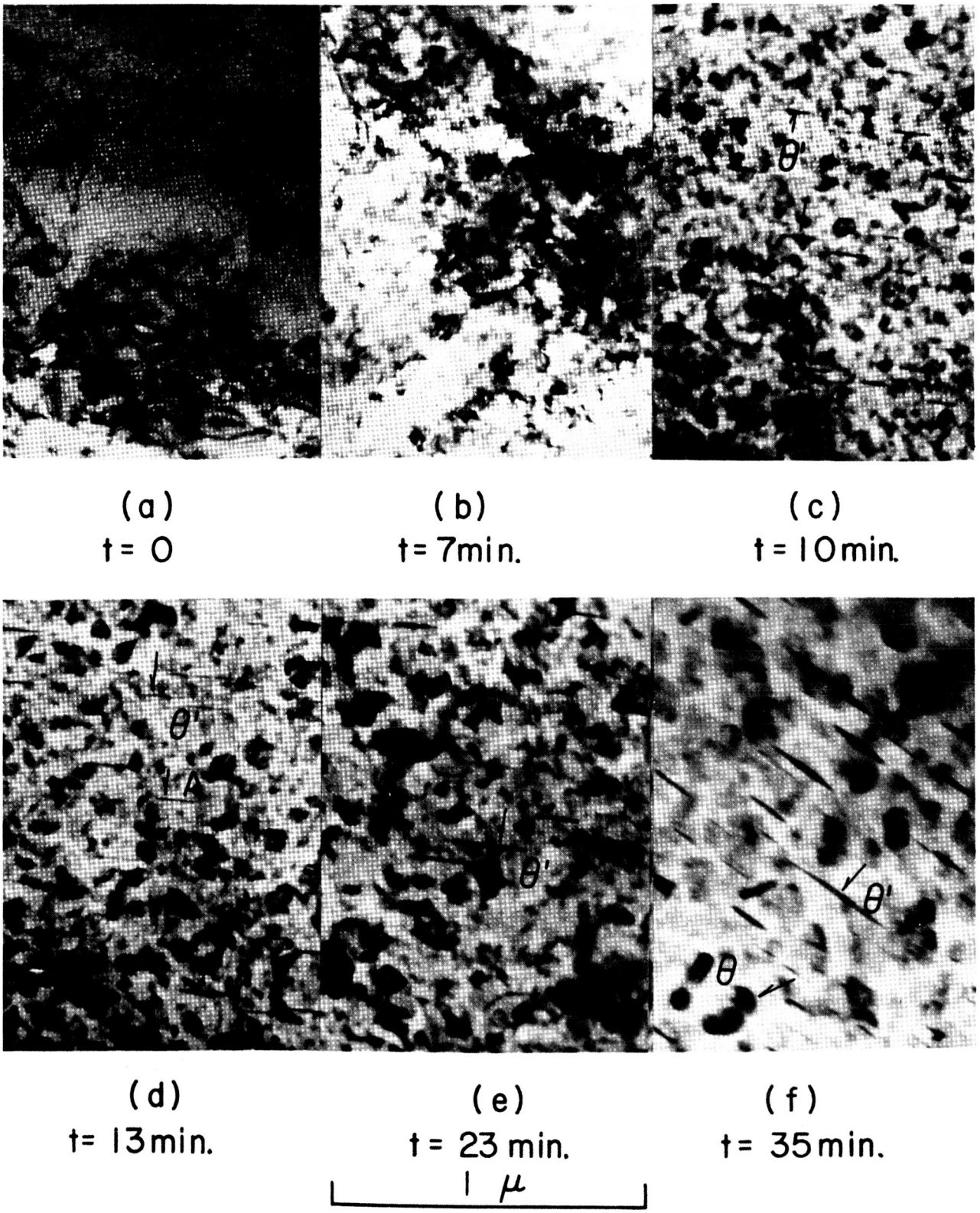

Fig. 48 Transmission Electron Micrographs of the Aging Behavior at 325°F of Explosively Deformed 2219-T42 as a Function of Time

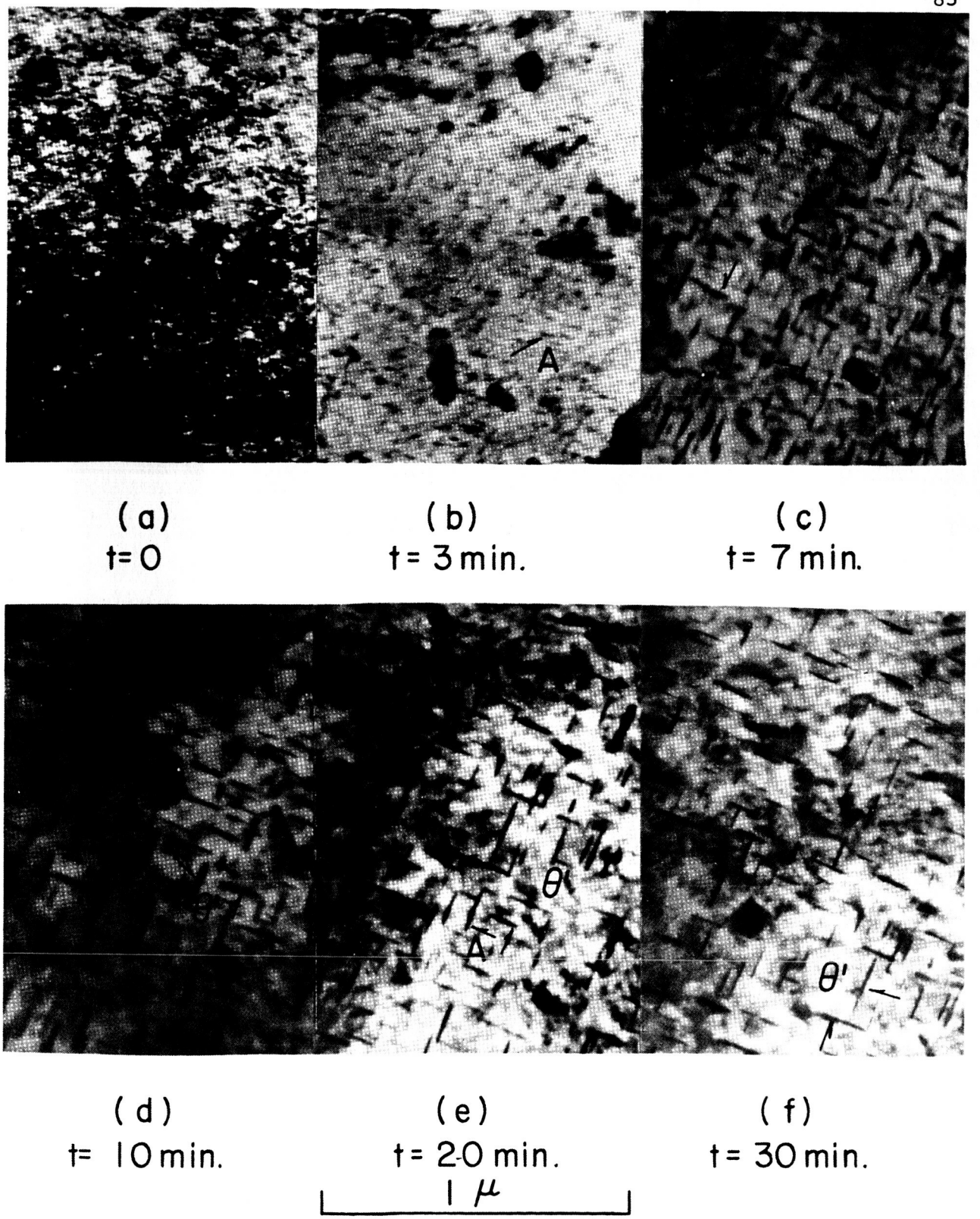

Fig. 49 Transmission Electron Micrographs of the Aging Behavior at 325°F of Undeformed 2219-T351 as a Function of Time

The aging behavior of 2219-T351 in the explosively-formed condition at 325°F is shown in Fig. 50a thru 50f. The foil surface of this sequence is parallel to the (110) plane. The banded appearance at "A" (Fig. 50a), in the immediate region of the dislocations, results from extensive strain fields around the dislocations. This is suggestive of segregation of copper solute atoms to the dislocations. Such segregation of copper atoms could be considered the initial step in the precipitation of θ' and, therefore, it is indicative of the occurance of aging before heat treating. The internal strain energy introduced into the alloy by explosive forming is the likely "driving force" for this phenomenon. After 6 minutes at 325°F, the growth of θ' precipitates is well developed as seen in Fig. 40b. However, the θ' habit plane that is normal to the foil surface is as yet unobserved. In the (110) foil orientation, two sets of θ' platelets make an angle of 45 deg to the foil surface and the third set lies normal to it as shown at "A" in Fig. 50c.

The distribution of θ' shown in Fig. 50d corresponds to the fully-aged condition having the mechanical properties of 2219-T851. The over-aged condition is indicated in Fig. 50e and 50f by the disappearance of θ' normal to the foil surface and the appearance of θ. A comparison of Fig. 49 and 50 indicates that the fully-aged condition is achieved by a factor of about 0.3 faster in the explosively-formed condition. In addition, the appearance of the images of the θ' in the explosively-formed and aged alloy suggests that higher coherency strains are associated with the precipitates than those in the undeformed-aged specimens. Extensive coherency strains near the precipitate interface increases the impedance, offered by the precipitate, to the movement of dislocations. This phenomenon would indicate that a higher yield and ultimate tensile strength is possible in explosively-formed and fully-aged specimens than in undeformed and aged material. Hence, it is recommended that the aging time for explosively-formed 2219-T351 be reduced to 70% of the aging time presently used. The latter aging time should produce higher yield and ultimate tensile strengths than those corresponding to 2219-T851.

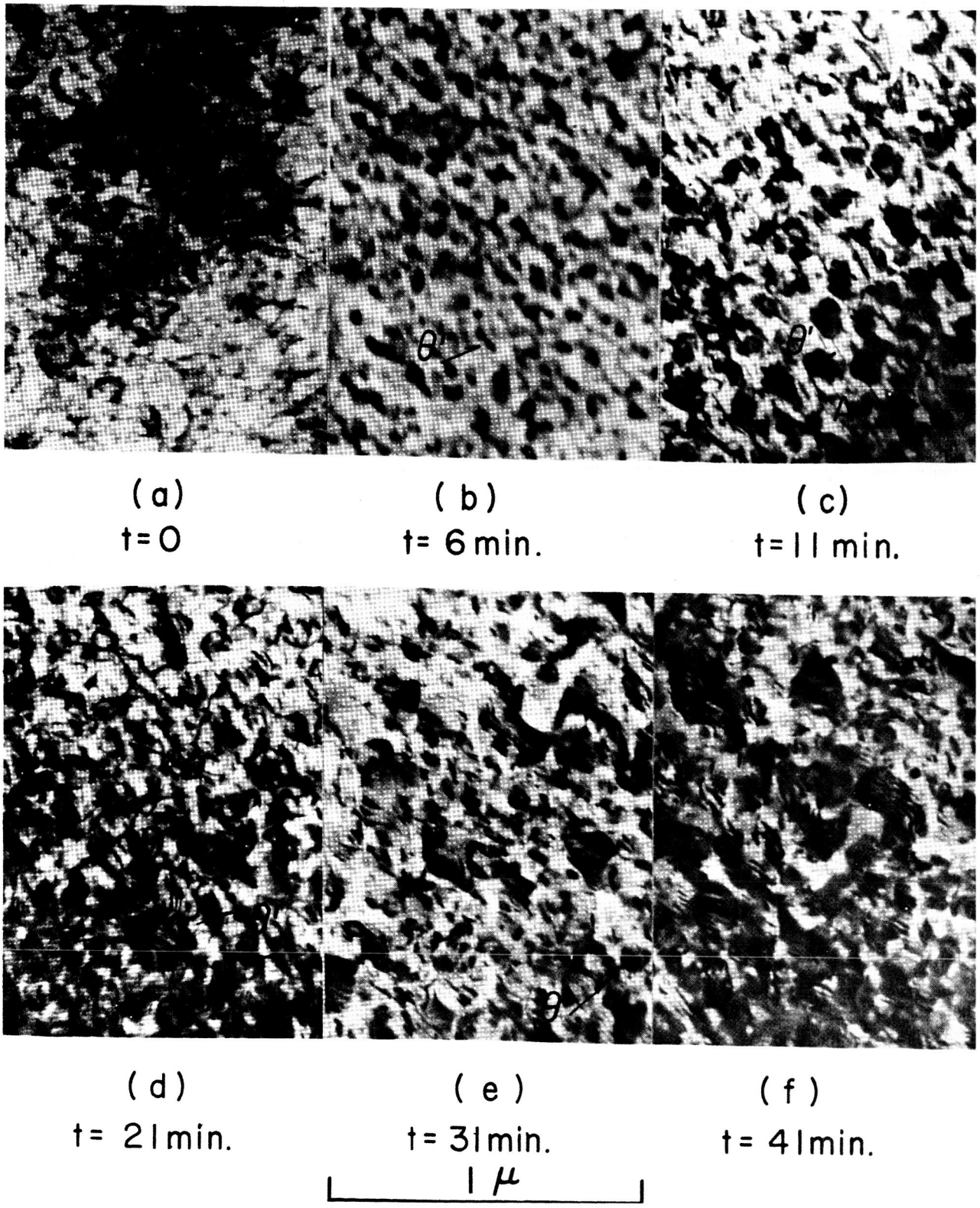

Fig. 50 Transmission Electron Micrographs of the Aging Behavior at 325°F of Explosively Formed 2219-T351, as a Function of Time

2219-T37 - Since the properties obtained from the conventional heat treatment of 2219-T37 after explosive forming were below the minimum values stipulated by applicable company and military specifications, it was suspected that over-aging was occurring as a result of the high-induced energy present from forming. Thus, a study was made to establish the extent of over-aging and to determine a heat treatment schedule that would produce optimum alloy properties. Since explosive forming requires high dislocation velocities in the alloy, a high concentration of vacancies is expected in the alloy as a result of the motion of jogs on screw dislocations. Upon aging (24 hr at 325°F) the precipitation of the second phases θ' in 2219-T37 (not shock loaded) produces optimum mechanical properties.

The precipitation process is a diffusion controlled mechanism. Because diffusion rates are markedly increased by the presence of excess vacancies in the alloy, the aging time required at 325°F in the explosively-formed alloy (to obtain a distribution of θ' corresponding to the 2219-T87 mechanical properties) should be less than that for 2219-T37 in the undeformed condition. This means that aging 2219-T37 after explosive forming at 325°F for 24 hours as specified in Martin Material Specification 1117, is likely to produce an over-aged condition with a corresponding decrease in the ultimate tensile and yield strengths.

Thin foil specimens of 2219-T37 in the deformed and undeformed conditions were aged in the heating stage of the electron microscope at 325 $\pm$ 10°F and continuously observed for periods up to 3 hours. The specimens representing the explosively-formed condition were taken from the region of the dome apex. Precipitation processes occur more rapidly in thin foil specimens than in the bulk form. Reasons for this behavior are speculative and should be dealt with at a later time. However, a comparison between the kinetics of precipitation processes between two thin foils of different metallurgical condition can be made. Hence, the results from a comparison measurement can be projected to give a reasonable prediction of the precipitation behavior in the bulk form of the alloy.

The 2219 alloy after solution heat treatment and cold work reduction of about 8%; i.e., temper T37, exhibits a dislocation distribution as shown in Fig. 51. The cold working after solution heat treatment introduces a copious amount of uniformly distributed dislocations. The diffuseness near the dislocation images is believed to be the result of segregation of solute copper atoms to the strain fields of the dislocations. Changes in the number and distribution of dislocations after explosive forming the alloy were unobserved; i.e., Fig. 51 is representative of 2219-T37 in the as-received and explosive-formed condition. Furthermore, a high degree of springback occurs when using 2219-T37 as a starting temper because of the high density ($\sim 10^{11}/cm^2$) and uniform distribution of dislocations that is characteristic of this temper.

The sequence of electron transmission micrographs shown in Fig. 52 and 53 illustrate the relative rates of precipitation of the second phase θ' in the undeformed and explosive-formed condition. The micrographs are of rather low quality due to slight motion of the specimen during exposure of the photographic plate. This motion results from electrostatic charging of a thin ($\sim$15Å) oxide film on the surface of the foil. Appropriate changes were made to eliminate this problem and, thereby improve the quality of the plates. Figures 52a and 52b show the extent of precipitation of θ' in the undeformed condition after elapsed times at 325°F for 9 and 25 minutes, respectively. In Fig. 52a, the θ' has just nucleated and is starting to grow after 9 minutes. In Fig. 52b, the θ' is evenly dispersed (about 100A between θ' plates) and well developed on the (001) habit planes. Figure 52b is representative of the fully-aged condition; i.e., the alloy in this condition will exhibit the maximum ultimate tensile and yield strength. The over-aged condition of the undeformed specimen is shown in Fig. 53 where the phase θ is seen to be forming at the expense of the θ' and, thus, increasing the separation distance between precipitate plates.

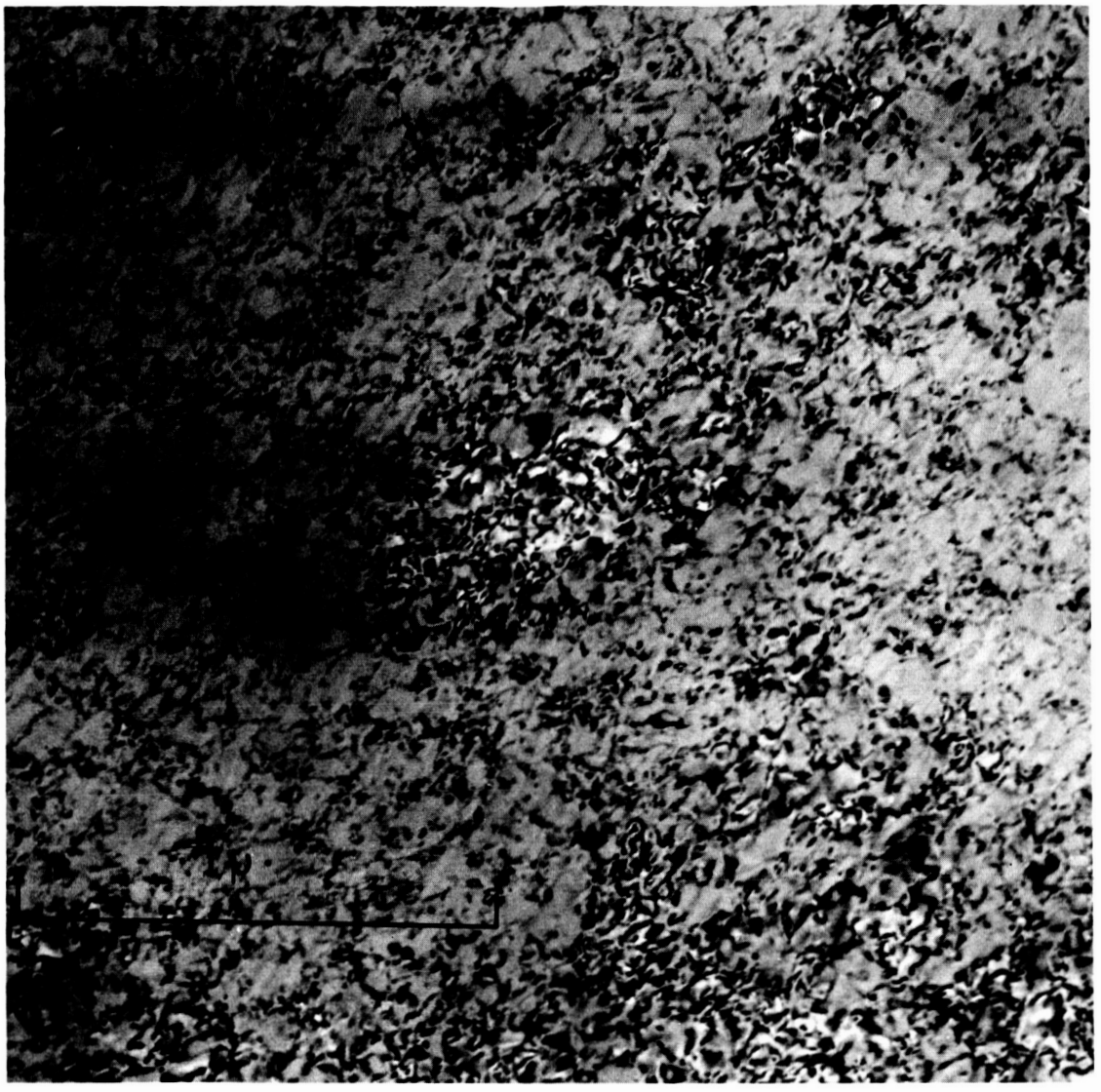

Note: The diffuseness of the dislocation image is believed to result from segregation of Cu atoms to the strain fields of the dislocations. Of particular note is the rather high dislocation density $\left(\sim 10^{11}/\text{cm}^2\right)$ but rather uniform distribution. The density and distribution of dislocations before explosive forming is similar since this temper condition is a result of solution heat treatment and cold working of about 8% reduction.

Fig. 51 Transmission Electron Micrograph of 2219-T37 Aluminum After Explosive Forming

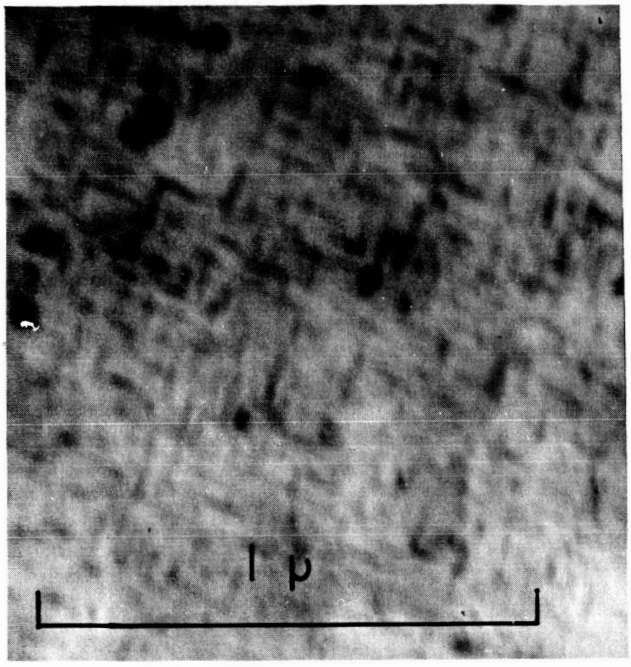

a. Undeformed, Heated at 325°F±10°F for 9 min

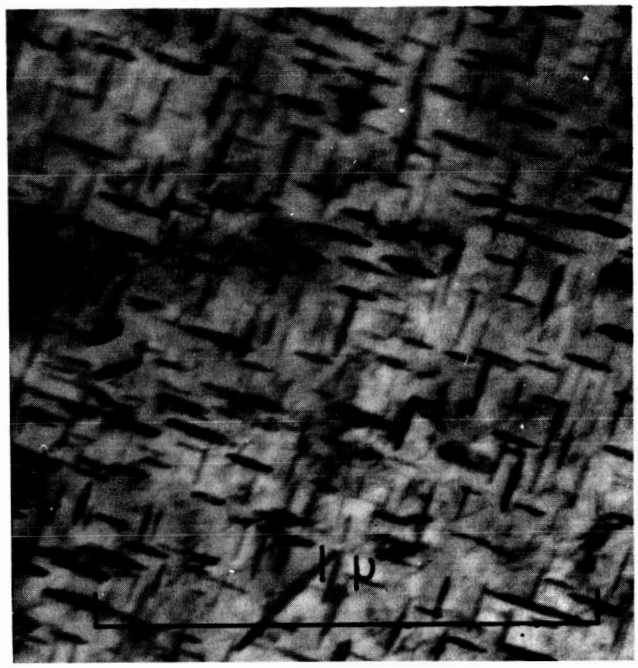

b. Undeformed, Heated at 325°F±10°F for 25 min

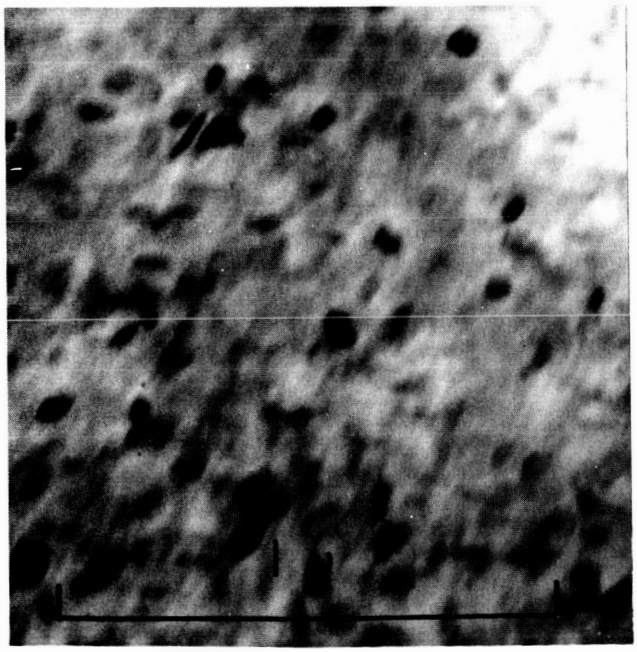

c. Explosively Formed, Heated at 325°F ±10°F for 5 min

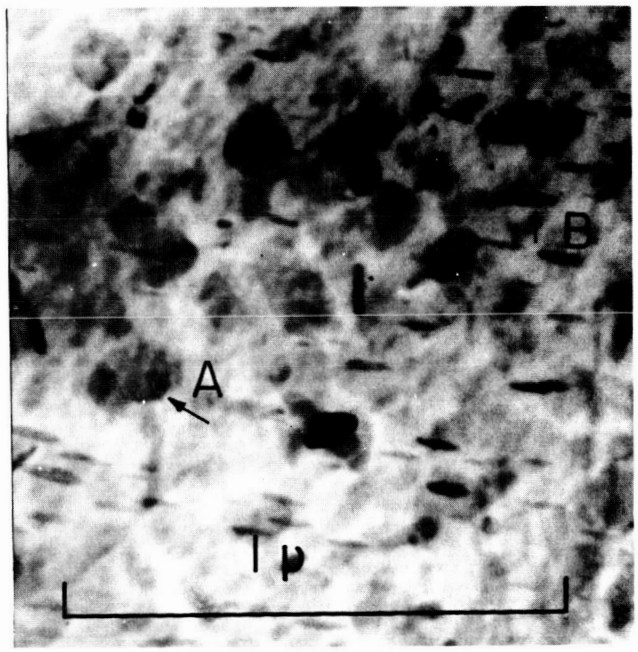

d. Explosively Formed, Heated at 325°F ±10°F for 15 min

Fig. 52 Micrographs of the Precipitation Process of 2219-T37 Aluminum as Observed Using the Heating Stage of the Electron Microscope

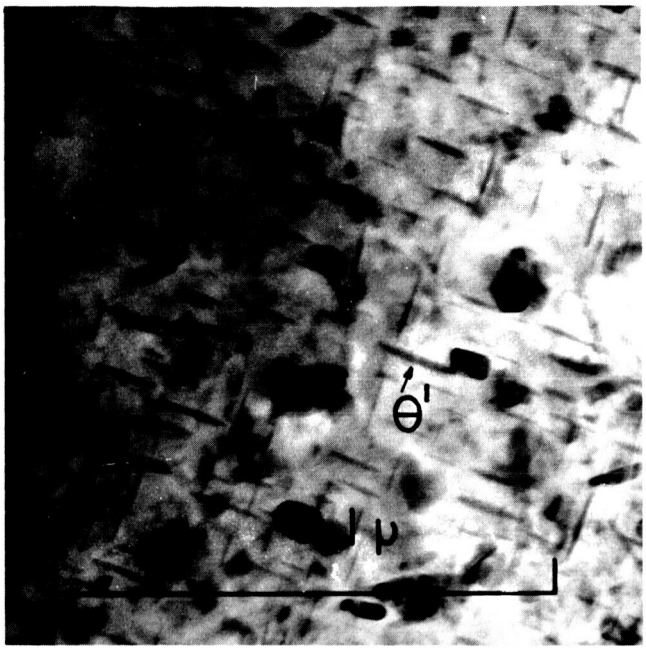

a. Undeformed, Heated at 325°F ±10°F for 38 min

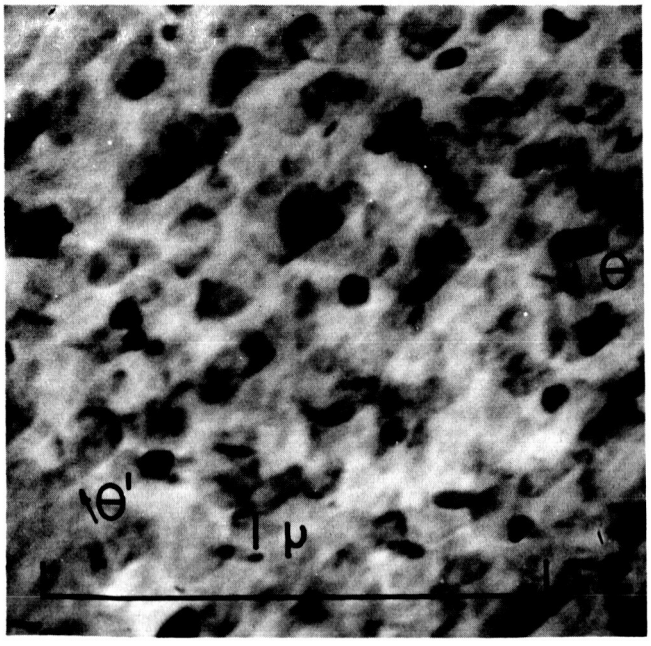

b. Explosively Formed, Heated at 325°F ±10°F for 22 min

Fig. 53 Micrographs of the Precipitation Process of 2219-T37 Aluminum as Observed Using the Heating Stage of the Electron Microscope

Figures 52c and 52d show the extent of precipitation of θ' in the explosive-formed condition after elapsed times of 5 and 15 minutes, respectively. The orientation of the foil in the explosive-formed specimen is different from that of the undeformed specimen. Therefore, the projected image of θ' appears differently in Fig. 52c, 52d, and 53b with regard to Fig. 52a, 52b, and 53a. This causes no difficulty, however, in comparing the two foils since the boundaries of the θ' in the explosively-formed specimen are still resolvable; e.g., at "A" in Fig. 52d.

In Fig. 52c, the nucleation and growth of θ' has occurred in the explosive-formed specimen in 5 minutes at 325°F. Further, the extent of growth of θ' after 5 minutes is greater than that in the undeformed condition (Fig. 52a) after 9 minutes. After 15 minutes the explosively-formed specimen is near the fully-aged condition as shown in Fig. 52d. The over-aged condition is being approached in Fig. 53b as indicated by a less uniform distribution of θ' and the disappearance of the θ' steeply inclined to the foil surface shown at "B" in Fig. 52d.

The results show that the rate of precipitation of θ' is increased by explosive forming by a factor of two. Therefore, it is recommended that the aging time for temper T37, which has been explosively formed, should be reduced to about 12 hours instead of the 24 hours given in the heat treatment specification.

2219-T81 - Specially handled specimens of undeformed 2219-T81 were examined after preparation from thin films. All of the areas examined contained θ' precipitate, a metastable form of $A\ell_2Cu$. The precipitate has a tetragonal unit cell with lattice constants of a = 4.04 Å and c = 5.80 Å.* Uniform distribution of precipitate is evident in Fig. 54 thru 58. The streaks in the selected area diffraction pattern indicate clearly that the platelets are too thin to diffract coherently. The large face of the platelets is not circular (Fig. 57). Platelets lying at right angles to each other have different orientations as shown in Fig. 58. However, crystallographic equivalency still exists.

*Pearson, W. B.: Handbook of Lattice Spacings and Structures of Metals and Alloys.

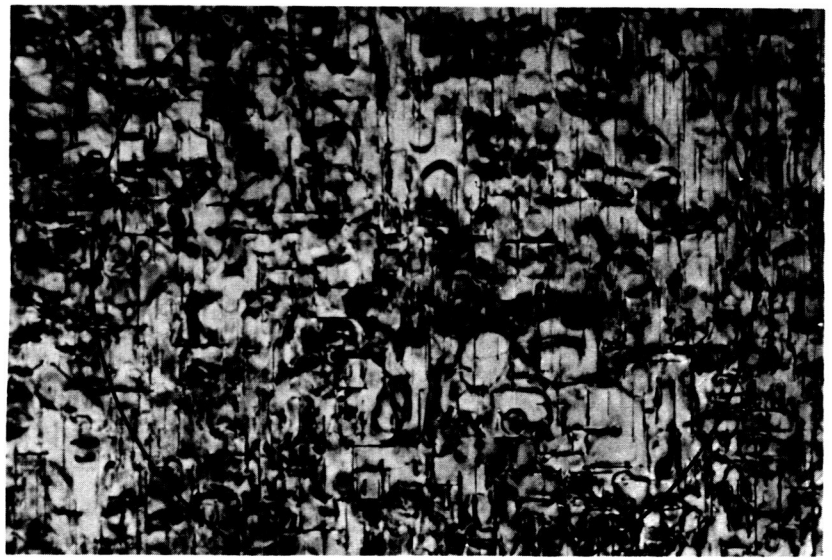

a. Platelets of θ' precipitate are perpendicular to the plane of the foil which is in [100] orientation. Since the platelets are parallel to $\{100\}$ planes in the matrix they produce traces at right angles to each other in the micrograph. Most of the curved dark bands are extinction contours, probably due to the strain fields set up in the matrix by the platelets. Contrast from dislocations is not readily recognizable. The circle indicates the size and location of the 50μ selected area from which the diffraction pattern was taken (x39,000).

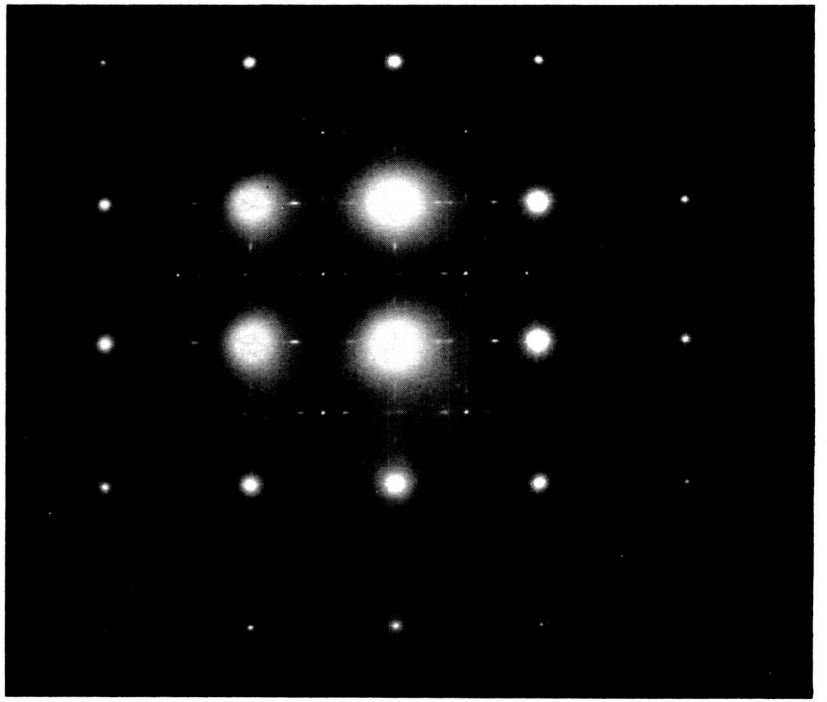

b. Selected area (50μ) diffraction pattern from central region of Fig. 54a. The pattern represents virtually an exact $\{100\}$ orientation of the matrix. The rectangular gridwork between the large spots is due to the platelets of θ' precipitate.

(Applicable camera constant λ L = 80.5).

Fig. 54 Platelets of θ' Precipitate and Diffraction Pattern

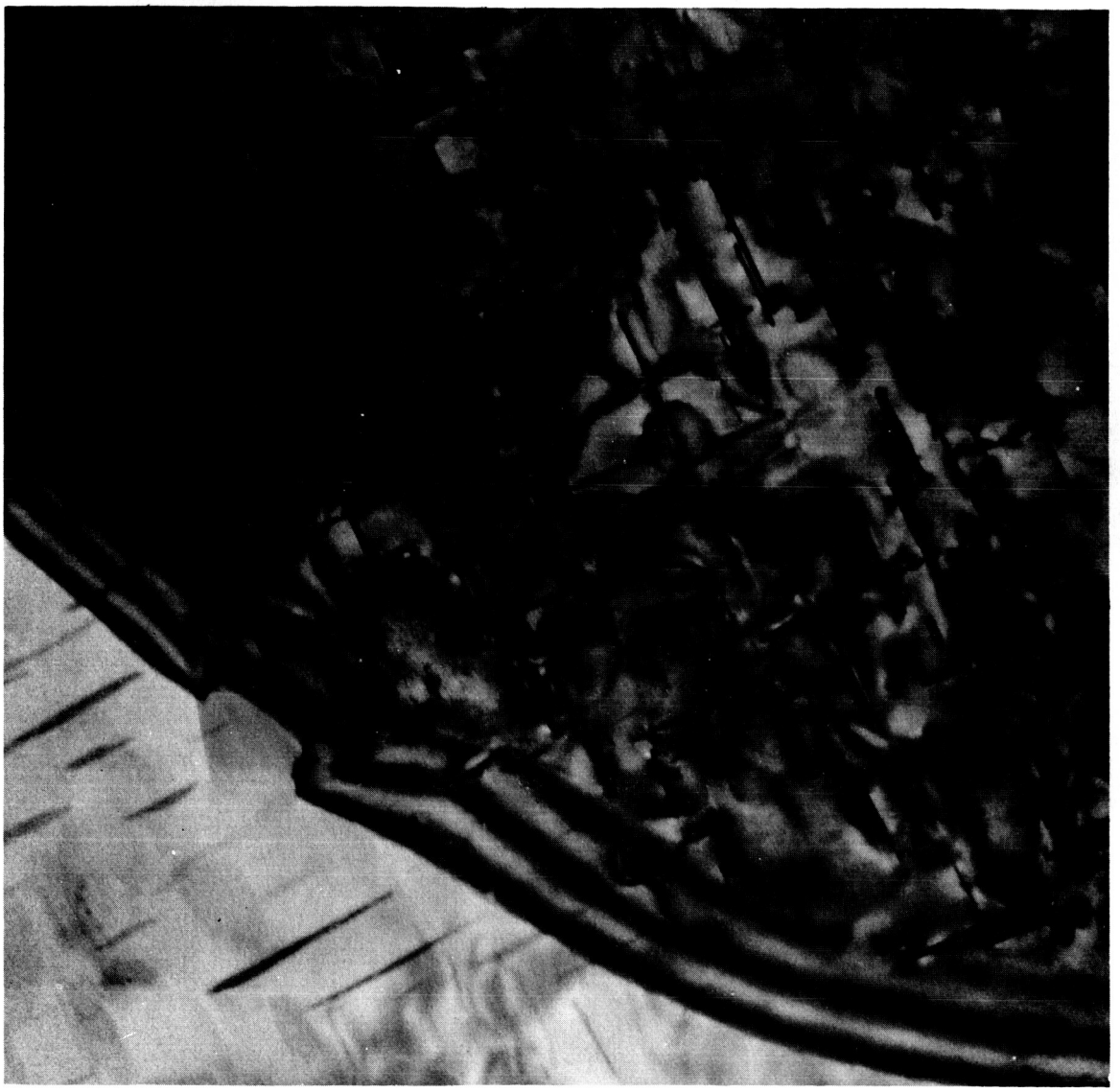

Note: The boundary between the two differently oriented grains gives rise to the interference fringes visible on the photograph. The difference in contrast between the two grains is due to difference in orientation, as is also apparent from the appearance of the θ' platelet precipitate. Although the magnification is considerably larger than in Fig. 54a, essentially no dislocations appear to be present. The mottling effect is due to the strain fields around the platelets (x143,000).

Fig. 55 Boundary between Two Differently Oriented Grains

Note: The platelets of θ' precipitate appear uniformly distributed in all three grains and extend essentially up to the grain boundaries. The four white patches are thought to have arisen during sample preparation, perhaps due to localized regions (probably θ' platelets on the third set of $\{100\}$ planes) where electrolytic polishing may have occurred more rapidly (x39,000).

Fig. 56 Comparison of Three Differently Oriented Grains

a. The orientation of the foil is well away from {100}, and the projected shape and size of the platelets of θ' precipitate is seen clearly. Note that in this orientation, the contrast due to the strain fields around the platelets is not obtained. Nonuniform electrolytic polishing is also evident (x39,000).

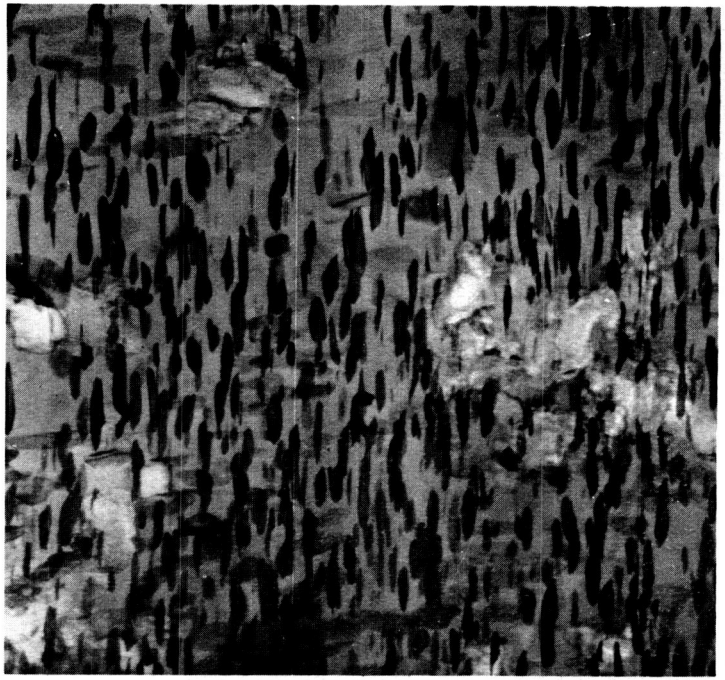

b. Same area as Fig. 57a, but with the foil tilted slightly so as to show the other set of θ' platelets in contrast. The foil has not been rotated in the plane of view (x39,000).

Fig. 57 Two Views of θ' Platelets

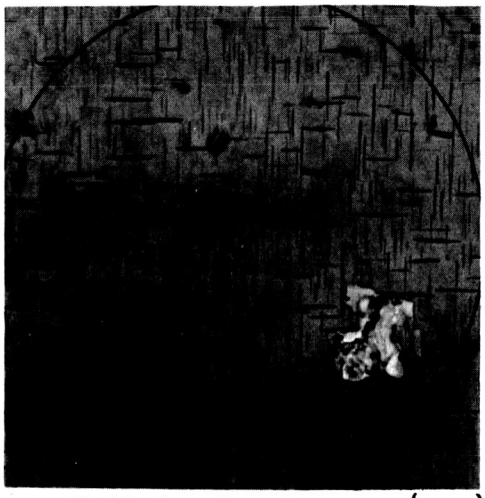

a. Foil fairly close to {100} orientation showing two orthogonal sets of θ' platelets. That parallel platelets are also similarly oriented can be shown by obtaining the dark field images, as in Fig. c and d. The circle indicates the size and location of the 50μ selected area from which the diffraction pattern was taken (x39,000).

b. Selected area (50μ) diffraction pattern from central region of Fig. a. The symmetry of the spots is the same as of those shown in Fig. 54b; their non-uniform distribution shows that the orientation is not exactly on {100}. The circled spots are those from which the dark field images, Fig. c and d, were obtained.

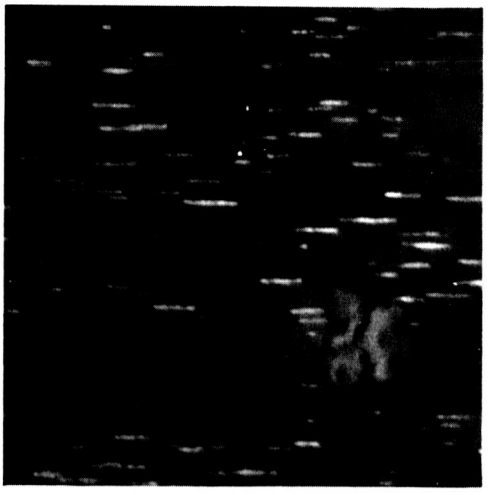

c. Dark field image from spot A, Fig. b. All platelets similarly oriented show up in the same constant (white); it can be seen that all such platelets are essentially parallel (x39,000).

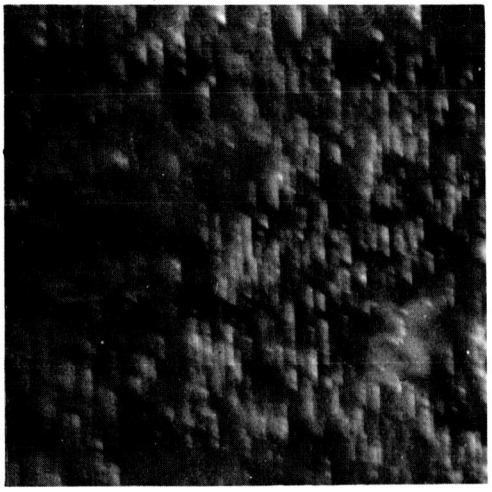

d. Dark field image from spot B, Fig. b. The other set of parallel platelets are now visible as white against a dark background and prove that they are similarly oriented and that this orientation is different from that of the set of platelets in Fig c. The photographs have not been rotated relative to each other (x39,000).

Fig. 58 Micrographs of Differently Oriented θ' Platelets

There was no evidence obtained to support the presence of dislocations even though the specimen was tilted through several degrees in order to be certain that they were not being overlooked for lack of contrast.

In summation there is clear evidence that explosive deformation modifies the rate at which precipitation from solid solution progresses. The rate is modified only slightly from 2219-0 and 2219-T42 but rather significant changes in precipitation rates were noted for 2219-T351 and 2219-T37. In fact, it was necessary to reduce the aging time at 325°F by 50% in order to effect full alloy response to the thermal treatment. It appears possible that by sufficient energy input into the alloy during the forming process one could develop a procedure whereby full properties might be achieved by natural aging or aging at a reduced temperature than that normally used.

It is not within the scope of the contract to determine optimum heat treating schedules but the development of such optimized thermal treatments would be a worthwhile endeavor.

d. X-ray Diffraction

X-ray measurements have been taken for three typical 2219 samples to compare the effects of thermal and mechanical treatments. Both outer surfaces have been examined while surface removal techniques enabled the simultaneous measurement at various selected depths below the original specimen surface. X-ray scans from 35 to 160 deg 2 θ produced a set of Debeye-Scherrer diffraction peaks that were analyzed for peak position and peak broadening. These raw data were then analyzed for various macroscopic and microscopic parameters that included extrapolated lattice parameters, residual stresses, x-ray particle sizes, and x-ray root mean squared strains.

The determination of residual surface stress in the preshocked and shocked material was made by comparing the extrapolated lattice parameters of the prestretched specimens with the specimens of material in the annealed state.

The surface strains as seen by the x-rays are computed from the relation

$$\bar{E} = \frac{a_{cw} - a^*}{a^*} = \frac{\Delta a}{a^*},$$

a_{cw} and a^* being the shocked (cold-worked) and annealed lattice parameters respectively; then the residual surface stress is

$$\bar{\sigma} = \frac{1}{K}\bar{E} = \frac{1}{\bar{K}} \times \frac{\Delta a}{a^*},$$

where $\bar{K}$ is a constant average stress-strain factor derivable from the elastic constants for the material. Since the elastic constants for 2219 were not available, those for pure aluminum were used. Although this would affect the absolute stress values somewhat, the relative values and trends will be unaffected. The value of $\bar{K}$ used was 1.87×10^{-8} in.^{2}/lb. Particle sizes and microscopic root mean squared strains were determined by an integral breadth analysis of broadened multiple order diffraction peaks. Specimens used in the analyses were extracted from explosively-formed panels near the part apex.

Extrapolated lattice parameters were determined by extrapolation procedures shown in Fig. 59. The intercept method is independent of random and systematic measurement errors but it does account for elastic effects (responsible for the apparent scatter of lattice parameters determined from each Debeye-Scherrer peak in a diffraction scan). The results are indicated in Table 5.

The annealed material (1-0-0) has the largest lattice parameter (a_o = 4.0579Å) approaching that of pure aluminum due to the precipitation reaction that occurs during the annealing process. The 2219-T37 material (1-37-0) has a lower lattice parameter (a_o = 4.0358Å) due to the solution heat treatment and quenching procedure that retains the alloying elements in the lattice. Note that both surfaces as well as some interior depths of these specimens have the same lattice parameters. On the other hand, the shock-loaded specimen (C1-3-37-1-1) had a gradual change in lattice parameter from one surface to the other; the extremum value at each surface bracketed the lattice parameter for the 2219-T37 samples. This effect was produced by macroscopic residual lattice stresses created by the explosive forming operation and will be discussed subsequently.

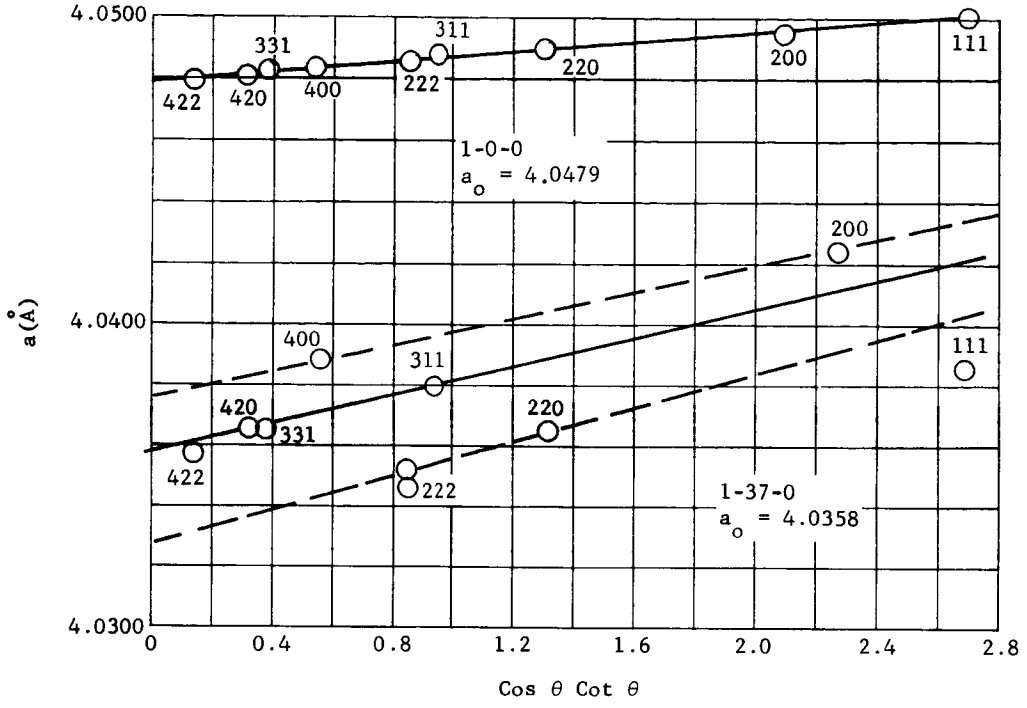

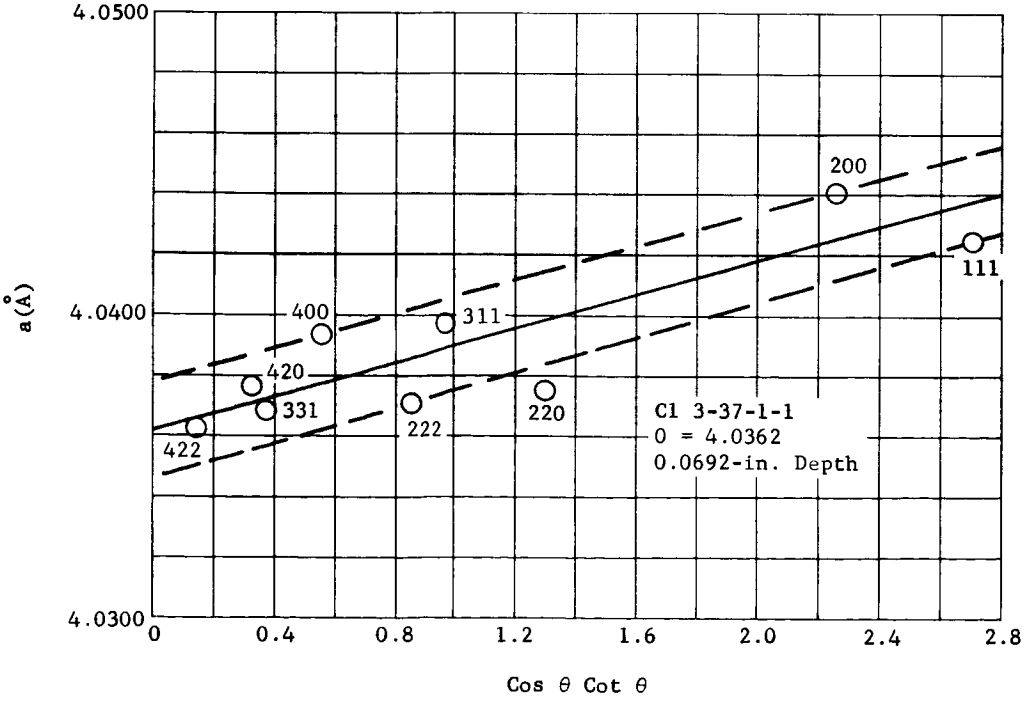

Fig. 59 Lattice Parameters

Table 5 Lattice Parameters for Formed and Unformed 2219 Aluminum Plate

Treatment	Depth from Shock Interface (in.)	Extrapolated Lattice Parameter, Angstroms
Annealed (2219-0)	0.0	4.0478
	0.0025	4.0479
	0.272	4.0479
Solution-treated and cold-worked (2219-737)	0.0	4.0358
	0.052	4.0356
	0.272	4.0358
Solution-treated, cold-worked, and explosively-formed (2219-T37, formed)	0.0	4.0396
	0.0614	4.0370
	0.069	4.0362
	0.0813	4.0360
	0.266	4.0352
	0.272	4.0352

Microscopic x-ray measurements were obtained by comparing the broadening of multiple order peaks. The annealed material exhibited little peak broadening indicating an annealed structure where the x-ray particle sizes were too large and the x-ray root mean squared strains (rmss) were too small to be measured reliably. The 2219-T37 material, however, had reduced isotropic x-ray particle sizes of approximately 1000Å and an isotropic rmss of $(0.23 \pm 0.02) \times 10^{-2}$. Of some significance is the fact that explosively-formed samples had virtually the same amount of peak broadening as a result of particle sizes of 1000Å and rmss of $(0.23 \pm 0.02) \times 10^{-2}$ indicating that no substantial microscopic changes were produced during explosive forming. Furthermore, the microscopic parameters (rmss and particle sizes) remained consistently within experimental accuracy for several depths below the surface at the dome apex indicating a uniform deformation mode normal to the cross sectional area of this element. These x-ray results are in agreement with electron microscopic observations that also indicate a substantial change between the specimen microstructure in the 2219-T37 and 2219-0 conditions but no significant change between the 2219-T37 and the shock-loaded condition.

Finally x-ray results have shown that a macroscopic residual stress system is produced by shock loading. This is shown in Fig. 60. After shock loading, the surface on the concave side of the part is in a compressive mode whose maximum value is 50,000 psi, a value very close to the tensile yield strength of 2219-T37. The opposite side is subjected to a surface tensile stress of 8,000 psi while the interior assumes intermediate values. Thus, the relative constancy of x-ray microscopic parameters with depth in conjunction with the variation in macroscopic residual stresses indicate that the principle effect of explosive forming is to produce macroscopic bending and flow of 2219-T37.

e. Mechanical Properties

Upper Gore Die - One of the objectives of the research program was to establish whether uniform mechanical properties could be obtained in explosively-formed gore segments of 2219 aluminum alloy and whether the subsequent thermal treatment of the alloy would result in full design properties. This would make it possible to explosively strain a low strength temper, uniformly, to a higher yield strength, and age the formed component to full strength using a conventional or modified heat treatment schedule.

The properties of the starting material used to form the 1/5-scale gore segment parts (Chap. II) varied somewhat from specification values. The annealed material that was supplied failed to meet either the ultimate or tensile yield strengths stipulated by applicable specifications, and measured elongation was significantly higher than required. All the other tempers that were supplied; that is, 2219-T42, 2219-T351, and 2219-T37, met or exceeded minimum specification values except for one marginal specimen of 2219-T42. Upon subsequent heat treatment, only the 2219-T37 responded fully. The 2219-T351 material was marginal while neither the 2219-0 or 2219-T42 stock responded.

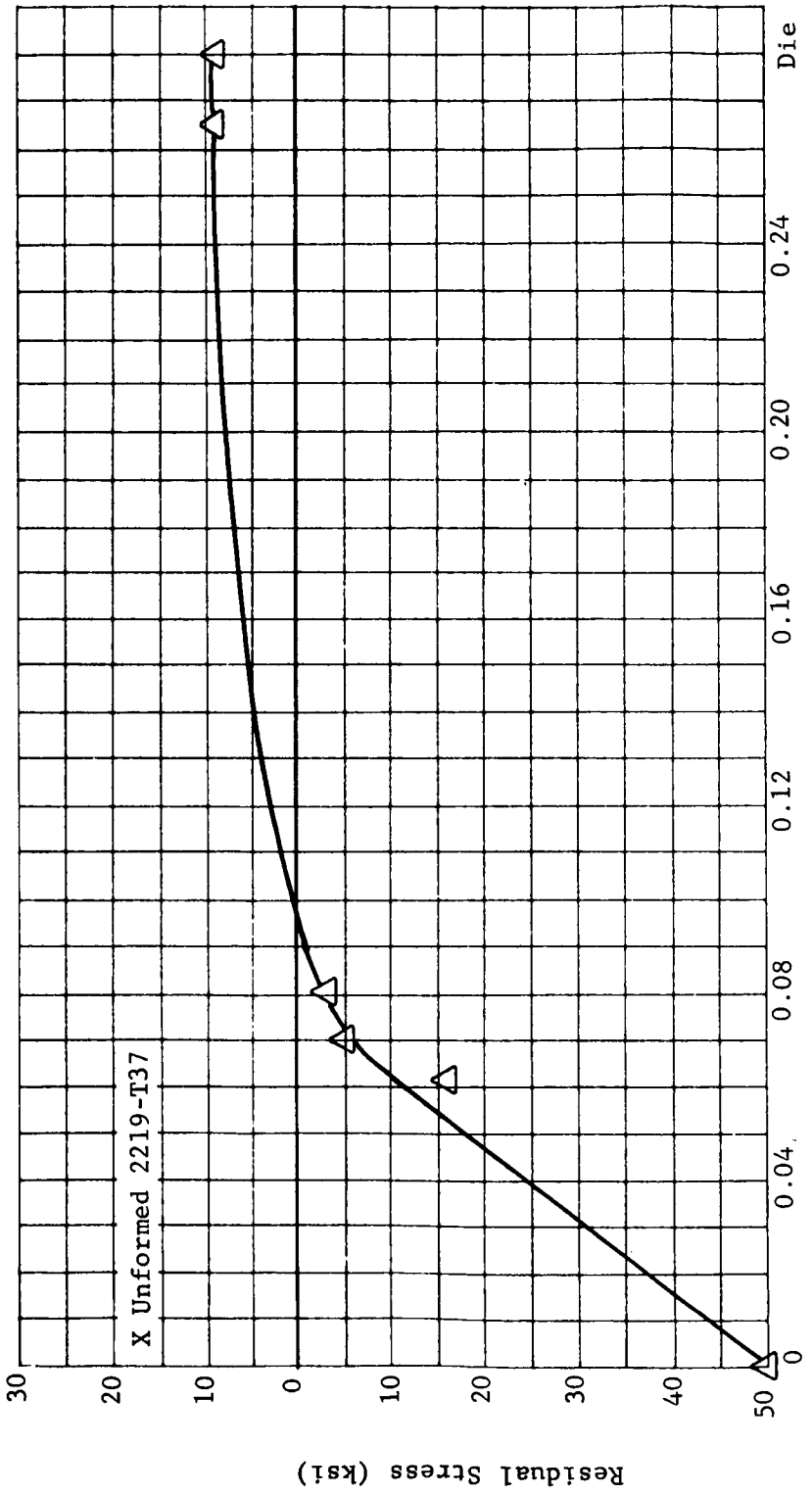

Fig. 60 Residual Stress vs Depth for Explosively Formed 2219-T37 Aluminum

A number of different forming sequences and forming parameters were used in early experiments to establish the conditions necessary to produce uniform mechanical properties across the blank contour. Central charges of either Cyadyn 3 or PETN bulk explosives did not produce this desired effect. However, the use of sheet explosive did permit the attainment of uniform properties for the 2219-T351 material. Figure 61 shows the properties obtained using the three explosive charge types. The variations of material properties across the blank using the different explosives can be seen in Fig. 62. It should be noted that for central bulk charges center properties come the closest to meeting specification values after heat treatment while the blank edges show lower tensile strengths. One anticipated result was the failure of explosively-formed 2219-T37 material to respond fully to heat treatment after forming. Premature precipitation occurred during the aging treatment resulting in a reduction of mechanical properties. Electron microscopy results revealed that the aging time at 325 $\pm$ 10°F should be reduced by about 50% to achieve maximum properties. Subsequent heat treatment of explosively-formed 2219-T37 using a modified time schedule yielded material with maximum properties. Figure 63 presents the results of heat treat studies on the 2219-T37 deformed blanks. The response of all the alloy tempers to heat treatment after explosive forming is shown in Fig. 64, and a summary of mechanical property evaluation is shown in Table 6.

The effect of material thickness on the mechanical properties of 2219-T31 was evaluated by forming specimens 0.032-, 0.132-, and 0.250-in. thick in the upper gore die. The results of mechanical tests performed on explosively-formed material are shown in Table 7. As evidenced from the table, generally higher ultimate strengths were achieved by forming 0.032-in. thick blanks; however, the yield strengths were not improved enough to exceed minimum properties specified in applicable specifications. More uniform properties were obtained by forming material 0.132-in. thick or greater.

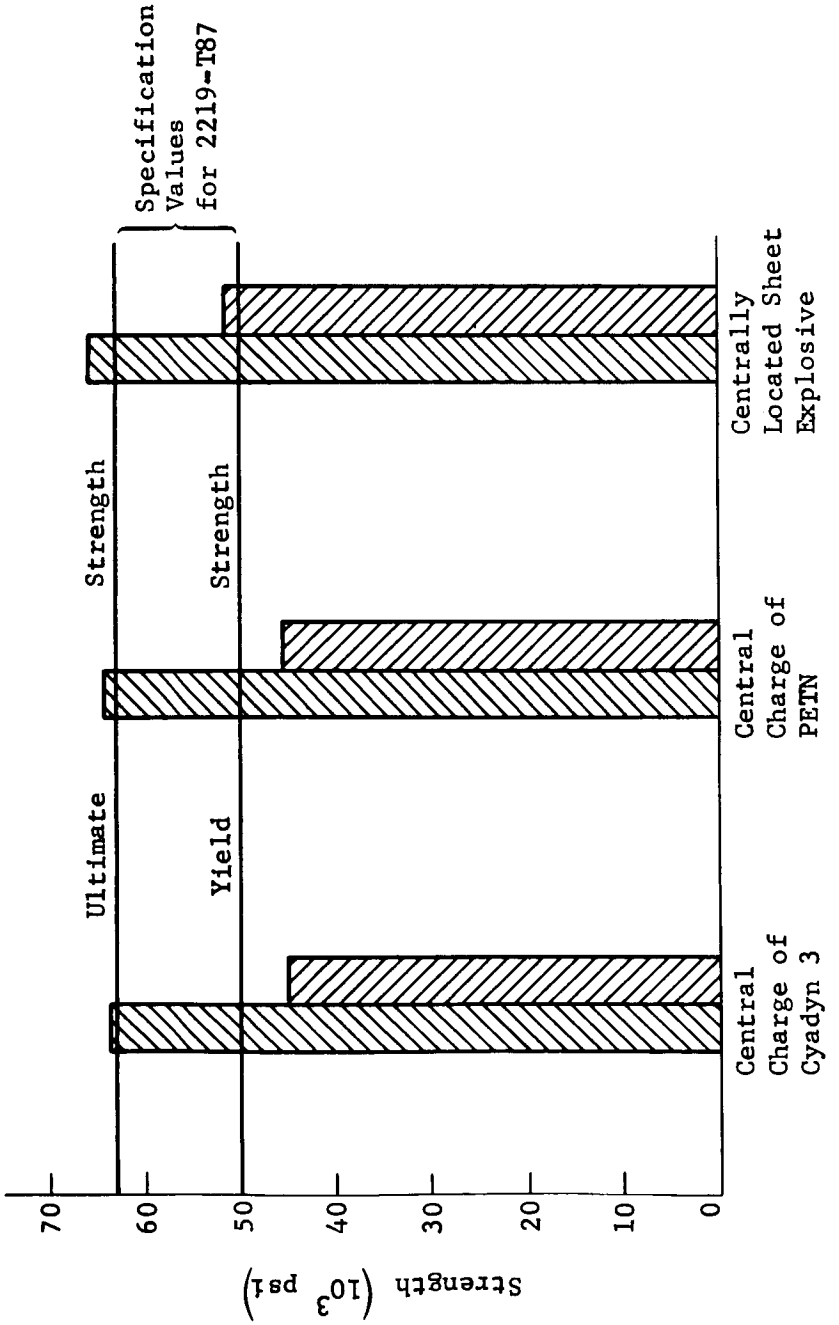

Fig. 61 Typical Mechanical Properties Obtained After Heat Treatment from the Use of Different Explosive Charge Types

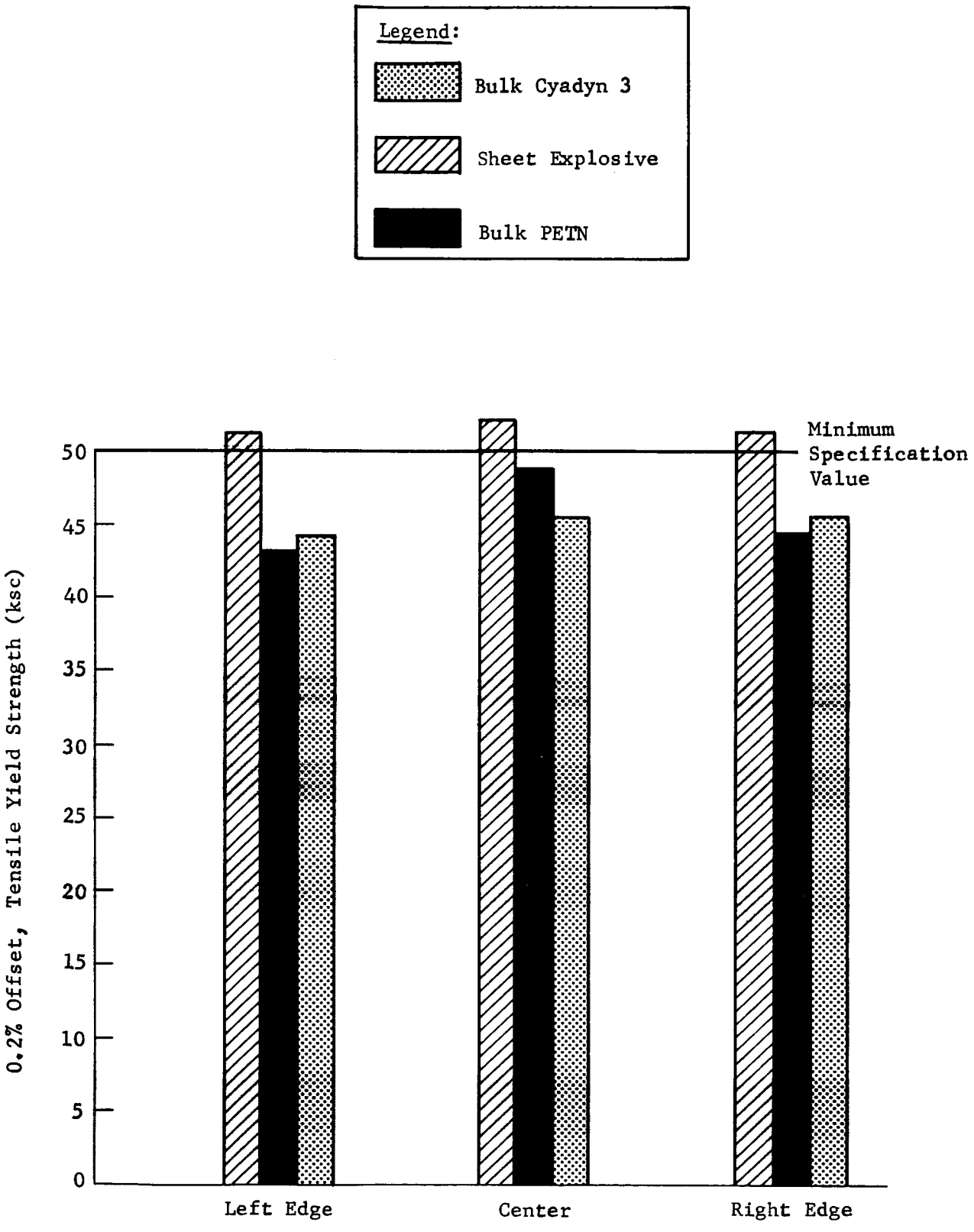

Fig. 62 Variation in Tensile Yield Strength of 2219-T351 Explosively Formed Blanks Using Different Explosive Types (After Heat Treatment)

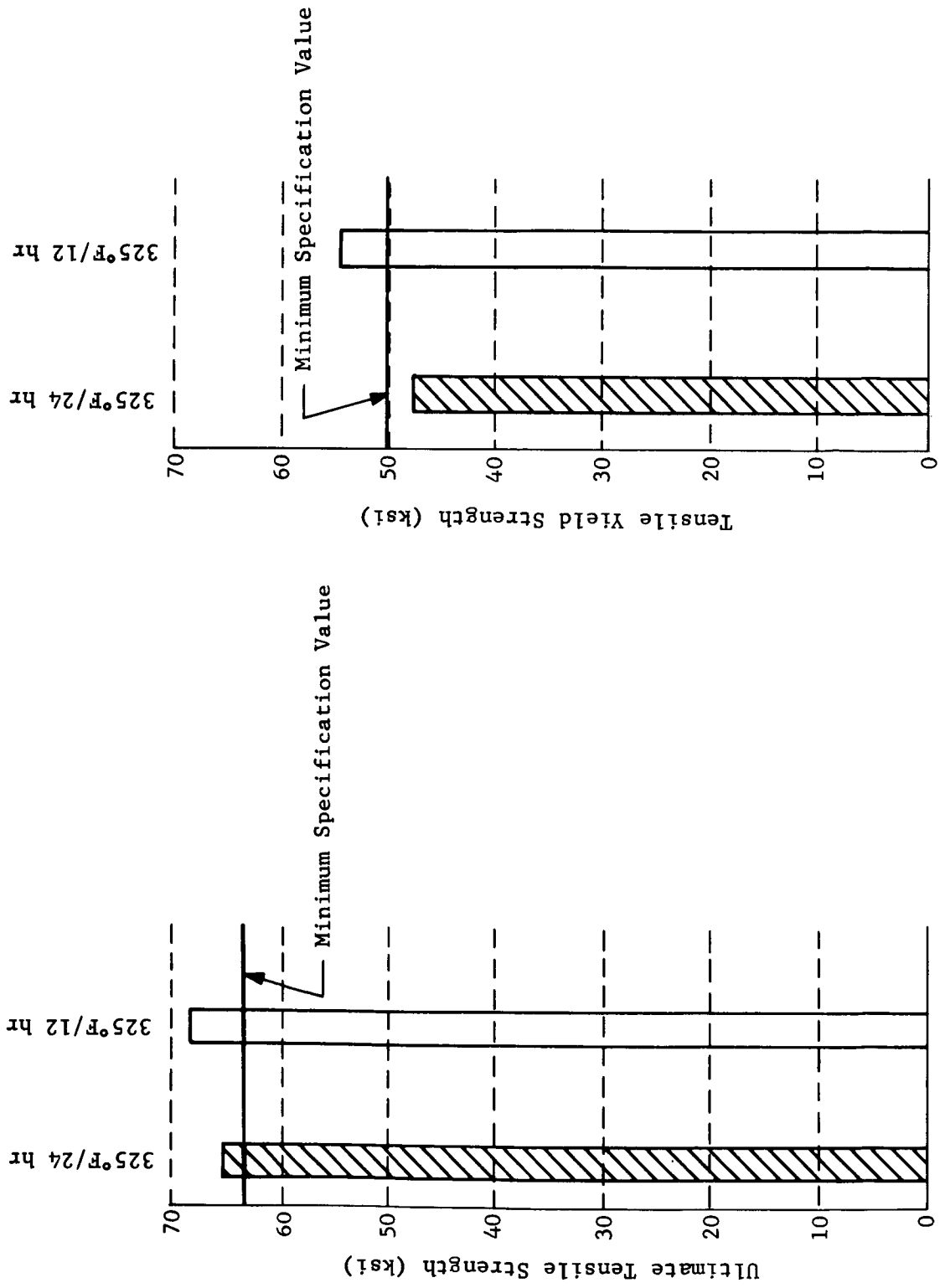

Fig. 63 Influence of a Modified Heat Treatment on the Response of Explosively Deformed 2219-T37 Aluminum Plate

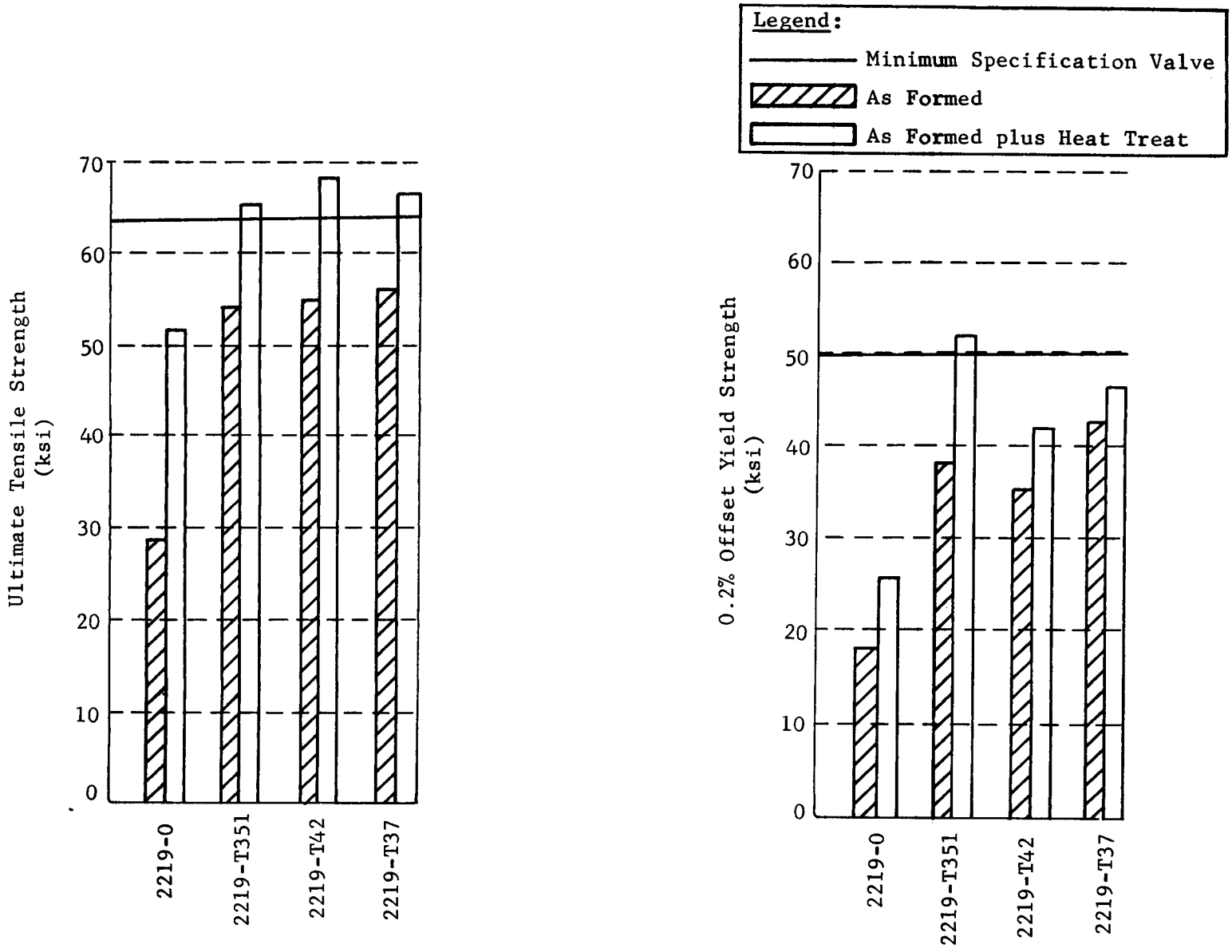

Fig. 64 Effect of Explosive Deformation on the Heat Treat Response of 2219 Aluminum, 0.250-in. Thick

Table 6 Summary of Mechanical Property Evaluation of 2219 Aluminum Plate

Alloy Temper	Mechanical Properties*											
	As-Received			Heat Treated			As Formed			Heat Treated		
	UTS	TYS	%E	UTS	TYS	%E	UTS	TYS	%E	UTS	TYS	%E
2219-0	29.0	13.6	23.7	47.5	28.7	12.7	29.5	18.9	20.0	48.9	27.7	12.3
2219-T42	49.6	23.1	23.3	50.7	29.3	12.2	55.1	34.5	19.7	69.1	43.1	10.7
2219-T351	55.0	40.1	22.7	61.0	43.4	12.3	55.4	39.3	15.8	65.6	51.6	10.4
2219-T37	58.7	43.5	16.2	65.4	52.0	10.5	56.2	42.5	19.5	65.4	47.3	11.1
Specification												
2219-T62	--	--	--	54	36	6	--	--	--	54	36	6
2219-T851	--	--	--	61	44	6	--	--	--	61	44	6
2219-T87	--	--	--	63	50	5	--	--	--	63	50	5

*All ultimate tensile strengths and tensile yield strengths are in thousands of pounds per square inch. Elongation is over 2 inches of measured gage length. Values listed are averages of at least three specimens.

Table 7 The Effect of Material Thickness on the Mechanical Properties of Explosively-Formed 2219-T31 Aluminum

Specimen	Location	Material Thickness (in.)	Mechanical Properties					
			As-Formed			As-Formed and Aged		
			UTS	TYS	%E	UTS	TYS	%E
1	Left Edge	0.032	57,800	36,300	17.5	--	--	--
2	Left Edge		--	--	--	68,200	45,500	13.0
3	Center		59,600	40,300	15.5	--	--	--
4	Center		--	--	--	68,800	50,500	12.0
5	Right Edge		57,500	37,400	17.5	--	--	--
6	Right Edge		--	--	--	68,200	48,200	12.5
7	Left Edge	0.132	54,600	35,000	19.0	--	--	--
8	Left Edge		--	--	--	65,300	51,500	13.0
9	Center		54,600	40,400	16.5	--	--	--
10	Center		--	--	--	64,700	53,800	8.5
11	Right Edge		54,300	35,000	19.0	--	--	--
12	Right Edge		--	--	--	65,600	51,900	12.5
13	Left Edge	0.250	55,700	37,000	17.0	--	--	--
14	Left Edge		--	--	--	65,200	51,200	11.0
15	Center		54,100	42,200	15.0	--	--	--
16	Center		--	--	--	65,200	52,100	10.5
17	Right Edge		55,800	38,600	15.5	--	--	--
18	Right Edge		--	--	--	66,300	51,600	10.0

This is probably due to the greater plastic strains in the thicker materials, which is evident by use of the relation:

$$E = \frac{h}{2R}$$

where

E = metal strain at the blank surfaces due to bending,

h = material thickness,

R = radius of curvature.

Thus, in the explosive forming of shallow gore segments it is necessary to use material at least 0.132-in. thick on a 1/5-scale to permit the development of uniform mechanical properties over the blank surface. This corresponds to a thickness of 0.660-in. for a full-scale part.

Lower Gore Die - Blanks formed explosively into the lower gore segment die (draw depth of 4.66 in.) were evaluated to establish the uniformity of properties as a result of explosive forming. Sheet explosive of 10 in. by 20 in. dimension (1196 grains of contained PETN) was used to form the parts. The consistency of results was excellent as shown in Table 8. Two separate blanks were sectioned to establish repeatability. Note that in both cases very uniform properties were produced over the blank surface, which exceeded minimum specification values after heat treatment. The more consistent properties of material formed in the deeper die as compared to the shallower upper gore die are undoubtedly a result of larger plastic strains produced by greater blank deformation.

Free-Formed Components - Several blanks were formed in a 24-in. diameter free-forming tool to determine the properties produced in an explosively-formed 1/5-scale dome cap and to evaluate the influence of draw depth on resulting mechanical properties. It can be seen from Table 9 that metal deformation during the forming of a 1/5-scale dome cap (1.35 in. draw depth) is not sufficient to produce uniform properties over the blank. In fact, the strengths acieved after explosive forming and heat treating do not meet specification minima. As the part is formed deeper the property uniformity improves and it is indicated from the data that a draw depth ratio of at least 0.21 is necessary to obtain strength and ductility greater than the required minimum design values.

Table 8 Mechanical Properties of 2219-T31 Aluminum Formed in the Lower Gore Die (4.66 in. of Draw)

Specimen	Location	Mechanical Properties					
		As-Formed			Formed and Heat Treated		
		UTS	TYS	%E	UTS	TYS	%E
1	Left Edge	57,600	46,700	14.5	--	--	--
2		57,100	45,500	15.5	--	--	--
3		--	--	--	67,600	52,700	10.5
4		--	--	--	67,600	52,900	10.0
5	Center	59,100	48,300	14.5	--	--	--
6		58,600	47,500	16.0	--	--	--
7		--	--	--	68,700	53,800	10.0
8		--	--	--	69,200	51,300	11.5
9	Right Edge	58,500	47,000	17.0	--	--	--
10		58,600	48,300	15.5	--	--	--
11		--	--	--	69,300	52,500	10.0
12		--	--	--	68,700	50,800	Failed on gage mark
13	Left Edge	58,000	45,300	14.5	--	--	--
14		58,000	42,100	Failed on gage mark	--	--	--
15		--	--	--	68,800	53,600	10.0
16		--	--	--	68,800	51,300	11.0
17	Center	58,100	43,500	17.0	--	--	--
18		57,800	43,600	14.5	--	--	--
19		--	--	--	68,800	51,900	10.5
20		--	--	--	68,400	51,900	10.5
21	Right Edge	57,400	43,800	19.5	--	--	--
22		57,100	42,600	16.0	--	--	--
23		--	--	--	68,000	56,400	11.0
24		--	--	--	68,000	50,300	10.0

Table 9 Mechanical Properties of 2219-T31 Aluminum Free-Formed in a 24-in.-Diameter Tool

Specimen	Location	Mechanical Properties						Draw Depth (in.)
		As-Formed			Formed and Heat Treated			
		UTS	TYS	%E	UTS	TYS	%E	
1	Left Edge	55,600	34,600	20.0	--	--	--	1.35
2		56,000	39,700	21.0	--	--	--	1.35
3		--	--	--	68,600	48,000	13.5	1.35
4		--	--	--	68,500	48,200	14.0	1.35
5	Center	55,600	39,400	22.5	--	--	--	1.35
6		55,500	40,000	21.5	--	--	--	1.35
7		--	--	--	68,300	53,400	14.0	1.35
8		--	--	--	68,400	54,300	13.5	1.35
9	Right Edge	54,900	36,700	22.0	--	--	--	1.35
10		55,200	39,700	23.0	--	--	--	1.35
11		--	--	--	67,900	49,200	13.5	1.35
12		--	--	--	67,600	45,400	14.5	1.35
13	Left Edge	56,100	41,200	19.5	--	--	--	3.08
14		55,800	39,100	20.5	--	--	--	3.08
15		--	--	--	68,200	49,700	11.5	
16		--	--	--	68,200	52,300	11.0	
17	Center	56,000	42,000	21.0	--	--	--	
18		56,300	42,200	20.5	--	--	--	
19		--	--	--	67,600	51,500	12.5	
20		--	--	--	67,900	50,200	14.0	
21	Right Edge	58,000	41,300	20.0	--	--	--	
22		56,300	41,900	20.0	--	--	--	
23		--	--	--	68,000	43,400	12.0	
24		--	--	--	67,700	49,400	12.0	3.08
25	Left Edge	58,100	46,300	16.5	--	--	--	5.22
26		58,100	45,700	16.5	--	--	--	
27		--	--	--	68,700	52,400	10.0	
28		--	--	--	68,600	50,000	10.0	
29	Center	58,600	47,400	16.0	--	--	--	
30		58,500	44,300	17.0	--	--	--	
31		--	--	--	66,400	51,300	12.0	
32		--	--	--	72,500	57,600	10.5	
33	Right Edge	57,800	46,800	17.5	--	--	--	
34		57,800	46,500	14.5	--	--	--	
35		--	--	--	69,000	51,800	10.0	
36		--	--	--	68,700	48,900	10.5	5.22

C. SPECIAL EFFECTS

1. Surface Pitting

A phenomenon was observed during the experimental effort that might cause problems in subsequent processing of full-scale explosively-formed components. Surface pits in a concentric ring between the edge of the blank and the blank apex were present regardless of the shape and type of explosive used. The nature of the pits is shown in Fig. 65. Ti appeared to make little change in the diameter of the ring whether central charges of either Cyadyn 3 or PETN were used or sheet explosive of various sizes. There was evidence of the surface pits even at charges down to 100 grains of PETN. Below 100 grain charges, it was difficult to see any evidence of pitting although an occasional pit was observed at random points on the surface. Raising the explosive standoff had the effect of decreasing the diameter of the pit ring. It was not possible to eliminate the pits by lowering the standoff since one would have to be very close to the blank to remove the pits.

The two possible causes of the surface pitting are shock wave intersection and surface bubble collapse. Shock wave intersection caused by reflected waves from the die surface can cause surface pitting due to locally high pressures. We did not observe any change in the position of the pits using centrally located charges even though explosives of different shapes and detonation velocities were used. It seems unlikely that a change in shape and type of charge would produce no change in the pattern of intersecting shock waves.

It was observed during a NASA contract (Ref 1) that air bubbles adhering to the blank surface could collapse under the force of local, high pressures similar to the cavitation experienced on ship propellers. The intense pressure caused by the collapsing bubbles produced surface pits in the blank being formed. It was found that by using certain wetting agents on the blank surface before immersion of the die into the forming pool that pitting could be eliminated. This was not confirmed during this study due to limitations in time and funding; however, the presence of bubbles on the blank before forming is a plausible explanation for the observed effect.

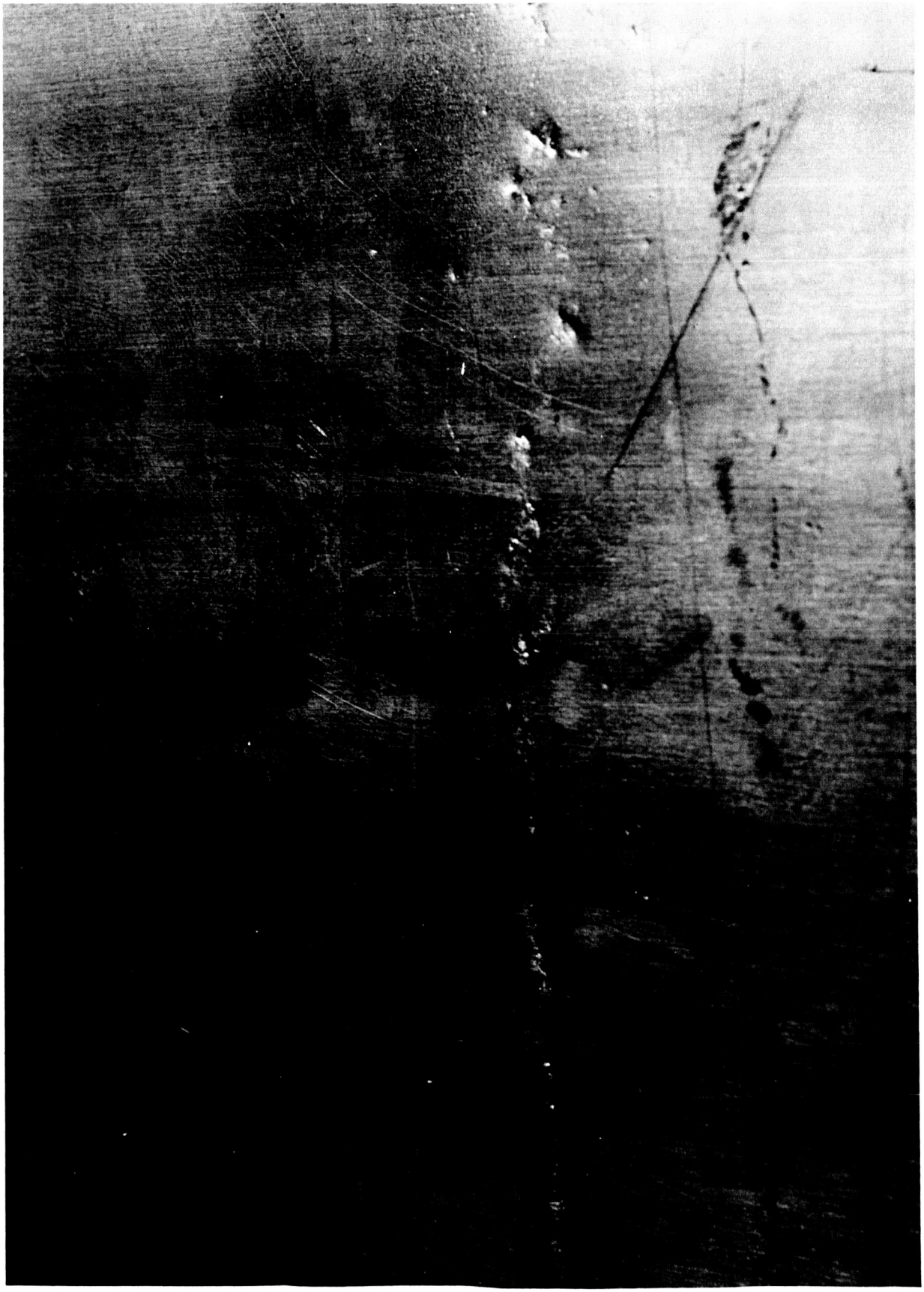

Fig. 65 Surface Pits Resulting from High-Energy Deformation of 2219 Aluminum

2. Multiple Forming Sequences

The scope of the present contract precluded extensive research into the value of multiple forming operations in the reduction of springback and the effect of such operations on the residual mechanical properties. Economically it is desirable to form a particular component in as few operations as possible. Often it is necessary to compromise with respect to economics in order to achieve certain tolerances or properties in the formed part that might facilitate fabrication or processing downstream.

A trial experiment was conducted during the latter stages of the contract to ascertain the influence of subsequent sizing shots on resulting metal springback. Using optimum conditions of explosive standoff, holddown pressure, and explosive size, a 2219-T351 blank was formed into the upper gore die cavity using a previously established sequence. Subsequent measurements revealed high springback. The formed blank was replaced in the die and a sizing shot made using conditions identical to the first operation. Upon subsequent measurement it was found that the springback was reduced by over 50%. The results are shown in Fig. 66. The preliminary tests indicate the value of using multiple forming sequences in reducing metal springback. More research is needed to optimize the forming sequences to produce minimum springback, shorter heat treatment cycles, and improved mechanical properties.

3. Effect of Edge Restraint on Springback

Using a die without complete edge restraint on the blank allows the metal to flow freely into the die cavity. This "free flow" of metal causes a modification in the springback characteristics of the blank. This effect was not apparent during the fabrication of parts in the 1/5-scale upper gore die. However, modification of the die to permit the evaluation of the effect of deeper draws on springback resulted in more springback, contrary to expectation. Due to the use of magnesium inserts, the coefficient of friction between blank and insert was lowered. This provided less restraint against pull-in, hence decreasing the strain even though the draw depth was greater. This probably caused the increased springback. Experience has shown that complete edge restraint causes more plastic strain and hence less springback. It is indicated, therefore, that in the forming of shallow parts one must provide complete blank restraint to effect maximum plastic deformation and thus minimize springback. Some answers will undoubtedly be provided with respect to edge restraint during a present NASA contract now underway (Ref 25). However, additional research is required to effect a complete understanding of blank restraint on metal springback.

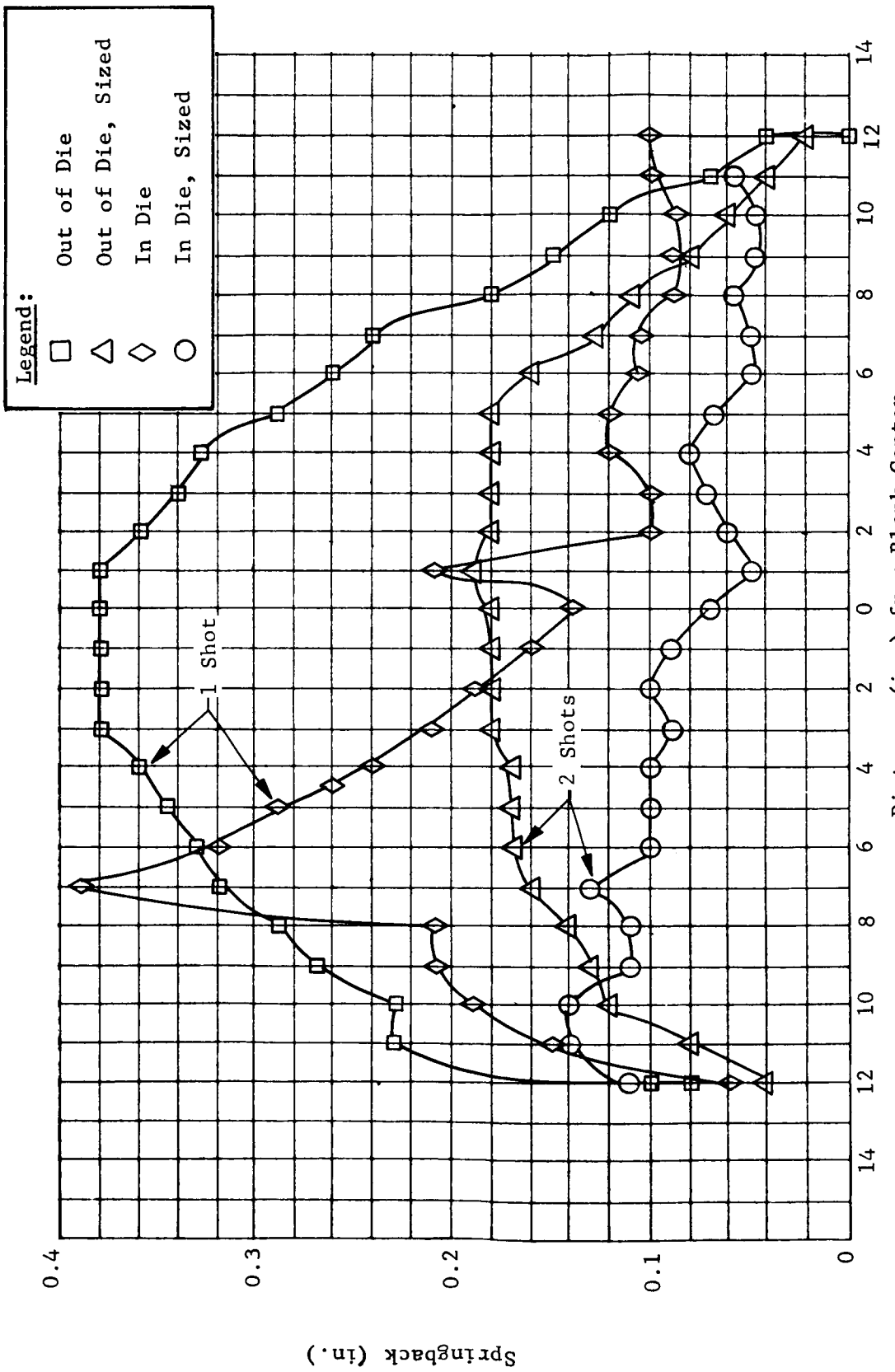

Fig. 66 Influence of Multiple Forming Shots on the Springback of 2219-T31 Aluminum Plate

4. Flange Distortion After Forming

One aspect of metal springback that is difficult to control is the flange distortion observed when holddown pressure is released after forming. Techniques were developed whereby contour variations were measured using the draw radius position of the die as a reference plane. Thus, any flange distortion occurring as a result of explosive forming did not influence measurements of the formed part. However, distortion in flange areas can be of real significance when subsequent processing of the part is attempted. Although specific measurements of flange movement were not made during the program, visual observations showed that the flange distortion was, in general, a function of alloy temper; i.e., distortion was least for 2219-0 and greatest for 2219-T37. In addition, with unrestrained edges the blanks formed using die inserts for greater depth showed severe flange distortion, the distortion increasing with draw depth. Thus another justification appears evident for the use of complete blank restraint in the explosive forming of shallow gore-shaped parts.

D. SCALING CRITERIA

During the course of the program the requirements for the explosive forming of full-scale components was kept in mind so at the conclusion of the program recommendations could be made relative to forming conditions necessary for the fabrication of full-scale hardware. Based on the criteria established during this contract the following scaling criteria are presented.

These results show that a lower springback can only be obtained by the provision for complete edge restraint of the blanks.

Item	1/5-Scale	Full-Scale
Blank Thickness	0.250 in.	1.250 in.
Initial Blank Temper	2219-T31 (-T351)	2219-T31 (-T351)
Blank Dimension		
Upper Gore	25 in. x 30 in.	125 in. x 150 in.
Lower Gore	32 in. x 32 in.	160 in. x 160 in.
Dome Cap	33.6 in. dia	168 in. dia
Explosive		
Type	Deta Sheet C	Deta Sheet C
Upper Gore	10 in. x 13 in. x 0.025 in. thick (778 grains)	50 in. x 65 in. x 0.125 in. (97,250 grains)
Lower Gore	10 in. x 20 in. x 0.025 in. thick (1196 grains)	50 in. x 100 in. x 0.125 in. thick (149,500 grains)
Dome Cap (Central Charge PETN)	100 grains	12,500 grains
Standoff	3.54 in.	17.70 in.
Clamping Pressure (Knurled Holddown Rings)	100 psi	100 psi
Predicted Springback		
Upper Gore	0.10 in.	0.50 in.
Minimum*	0.04 in.	0.20 in.
Lower Gore	0.20 in.	1.00 in.
Dome Cap	--	--

*Springback with nonuniform properties.

IV. CONCLUSIONS AND RECOMMENDATIONS

A. CONCLUSIONS

Based on the technical information developed under NASA contract NAS8-11794 the following conclusions have been reached:

1) The minimum springback from explosive forming with attendant uniform mechanical properties results from deformation of 2219-T31 (or 2219-T351);

2) Lubrication of the die draw radius during forming causes an increase in springback;

3) Springback decreases as the metal thickness being formed is increased;

4) Very little influence was observed in changes in die material, draw radius, or draw depth on metal springback under the conditions used for experimentation;

5) Contrary to expectations, elevation of the charge standoff causes more severe springback. Optimum standoff was found to be 3.54 in. for the size of part formed;

6) Sheet explosive was more consistent than central bulk charges in producing lowered springback;

7) Knurling the holddown rings caused reduced springback after forming;

8) Reduction of edge restraint causes an increased springback;

9) Complete edge restraint is required to minimize springback and to produce more consistent properties;

10) Multiple forming operations appear to significantly reduce springback when compared to a single operation;

11) Explosive forming reduces the residual stresses present in the as-received material as shown by x-ray diffraction;

12) Lattice parameters for 2219 aluminum are significantly reduced as a result of explosive deformation;

13) Sheet explosive was found to produce uniform properties across the blank surface;

14) Explosive forming modifies the heat treat response of 2219-T37, 2219-T31 (-T351), and 2219-T42. Electron microscopy observations indicate acceleration of aging time by factors of 0.5, 0.7, and 0.9 times as fast as normal aging times, respectively;

15) Copious amounts of dislocations (dislocation densities in the range 10^{11} to 10^{12} lines /cm^2) are introduced by explosive forming;

16) Excess concentrations of vacancies are produced by stress induced climb of jogs on screw dislocations;

17) Crystallographic imperfections such as stacking faults, micro and macroscopic twins, and microcracks were not observed in any of the more than 300 transmission electron micrographs prepared from explosively formed material.

B. RECOMMENDATIONS

Several areas of endeavor were uncovered during the course of the contract, which could form the basis for another research program of importance in the understanding of metal springback and the factors affecting metal behavior during explosive forming. Therefore, the following recommendations are presented for future work:

1) Optimization of multiple forming sequences should be accomplished with attendant studies of high energy effects on metal behavior. These studies should be conducted using both the upper and lower gore dies;

2) The influence of complete blank restraint on metal springback and subsequent metal properties should be established;

3) The stress-corrosion behavior of explosively formed 2219 aluminum should be evaluated and compared with results from conventionally formed material to establish any detrimental effects resulting from high energy deformation;

4) Bulk aging studies are necessary, using the electron microscope, to determine whether the behavior of bulk material during heat treatment is similar to that observed using thin films;

5) More complete residual stress measurements are required to exploit the observations made in this program that explosive forming reduces the residual stress initially present in the blank;

6) The causes for observed surface pitting during explosive forming should be determined;

7) A more thorough study of the integral blanket concept should be made to establish conditions under which a reduction in springback is produced.

V. REFERENCES

1. H. F. Wallen and K. D. Hawkins: Explosive Forming Development Program. No. 64B080A (NASA Contract NAS8-5129), Ryan Aeronautical Company, 5 June 1964.

2. E. L. Fowler and J. J. Moran: "Controlling Springback in Forming Stainless." Metal Progress, pp 111-114, August 1964.

3. F. Strasser: "Correcting for Springback in Sheet Metal Bending: Sound Design Principle." Design Engineering, pp 22-25, January 1962.

4. F. Strasser: "Precision Bending with Dies." Iron and Steel, Vol 33, No. 2, pp 65-68, February 1960.

5. F. B. Chapman, et al.: "Springback in Flanging." Product Engineering, Vol 13, pp 382-383, 1942.

6. F. Strasser: "Springback Problem in Metal Forming." Steel, Vol 131, No. 5, pp 90-91, 4 August 1952.

7. Strohecker, et al.: Explosive Forming of Metals. DMIC Report 203, 8 May 1964.

8. J. M. Alexander: "An Analysis of Plastic Bending of Wide Plate and Effect of Stretching on Transverse Residual Stress." Proceedings of the Institute of Mechanical Engineers, Vol 173, p 73, 1959.

9. B. W. Shaffer and E. E. Angar: "Mechanics of the Sheet Bending Process." ASME Transactions, J. Applied Mechanics, Vol 27, Series E, No. 1, pp 34-40, March 1960.

10. J. P. Orr: "High Energy Forming, New Manufacturing Techniques." SAE Paper No. 340A, National SAE Meeting, New York, 1961.

11. J. Pearson: "The Explosive Working of Metals." National Meeting of SAMPE, Dayton, Ohio, 9-10 March 1960.

12. G. W. Gipe: "New Manufacturing Techniques, High Energy Forming." National Aeronautic Production Forum, Los Angeles, California, 10 October 1960.

13. W. K. Beyer: Behavior of Materials Under Conditions of Explosive Stressing. Report AN61AMR8024, General Dynamics, December 1961.

14. B. J. Bryan: "Epoxy Dies for Explosive Forming." The Tool Engineer, February 1960.

15. W. W. Wood, et al.: Metal Formability Limits. Report ASD-TDR-63-7-871. [Contract AF33(657)-7314], Ling-Tempco-Vought Company. July 1963.

16. E. K. Henriksen: "Residual Stresses from Explosive Forming." American Society of Mechanical Engineers, Los Angeles, California, 11-14 June 1961.

17. J. M. Silverman, et al.: Effect of Shock-Induced High Dynamic Pressures on Iron Base Alloys. Report ASD-TDR-62-442 [Contract AF33(616)-8190], Pratt and Whitney, August 1962.

18. B. G. Koepke, et al.: Strengthening Iron-Base Alloys by Shock Waves. Report ML-TDR-64-282 [Contract AF33(657)-11250], Rocketdyne Division of NAA, October 1964.

19. J. M. Walsh, et al.: "Shock-Wave Compressions of Twenty-Seven Metals. Equations of State of Metals." Physical Review Vol 108, No. 2, pp 196-216, 15 October 1957.

20. N. Ida and J. Burkhart: Metallurgical Effects on Residual Properties of Explosively Formed 2014 Aluminum Alloy. R-61-7, Martin Company, Denver, Colorado, May 1962.

21. J. F. Wilkin, et al.: Metallurgical Effects of Explosive Strain Rates on Metal Alloys. 0513-01(02)FP (Contract NAS8-2416), Aerojet General Corp, 26 July 1963.

22. A. W. Hall, et al.: Investigate the Effect of High Dynamic Pressures Upon the Metallurgical Properties of Iron and Titanium Base Alloys. ASD-TDR-62-534. [Contract AF33(616)-8191], February 1963.

23. L. J. Effenberger and K. R. Agricola: Explosive Cold-Forming of Titanium Alloy Sheet and Foil. Martin-Sponsored Research Program, April 1965 (to be published).

24. A. Ezra, N. Ida, R. Agricola, and N. Burningham: "Explosive Forming and Welding of Honeycomb Sandwich Material." NASA-CR-64-36 NASA (Contract NAS8-5463). Martin Company, Denver, Colorado, October 1964.

25. K. R. Agricola and I. K. Sheffield: Explosive Forming of Saturn V Components. (Contract NAS8-11616). Marshall Space Flight Center, Huntsville, Alabama, 1965 (to be published).

DISTRIBUTION

Copies	To
1 thru 10 (plus one set of reproducibles)	National Aeronautics and Space Administration George C. Marshall Space Flight Center Huntsville, Alabama 35812 Attn: PR-RC
Remaining Copies	Martin Company Denver Division Denver, Colorado 80201 Attn: Libraries Section